Chapter 7

VIBRATIONAL SPECTRA AND STRUCTURE OF CONJUGATED AND CONDUCTING POLYMERS

Issei Harada and Yukio Furukawa

Pharmaceutical Institute
Tohoku University
Aobayama, Sendai, 980 Japan

I. INTRODUCTION

Polyacetylene is the first conjugated polymer that was found (in 1977) to show high electrical conductivity upon doping with iodine, AsF_5, sodium, etc. [1,2]. During the following decade the conductivity improved three orders of magnitude: a recent value is 1.7×10^5 Scm^{-1} ($S = \Omega^{-1}$) exceeding that of cobalt. Many other doped polymers have turned out to be conductive, including polythiophene, polypyrrole, polypara-phenylene, polypara-phenylene-sulfide, polypara-phenylenevinylene, etc. [3]. Among them, polyaniline is the first commercialized conducting polymer (September, 1987) as the positive electrode of a rechargeable battery. Since doping is essentially transfer of electrons from or to the polymer leaving mobile charges on it, a drastic spectroscopic change is observed upon doping, concomitant with an increase of electrical conductivity by many orders of magnitude. It is not proper to simply correlate the conductivity, a macroscopic property, with the spectroscopic observations which are merely manifestations of electronic and nuclear configurations of individual polymer molecules. This can be easily understood if one looks at the electron micrographs of polyacetylene (Fig. 1). A film consists of fibrils of about 200 Å diameter entangled with one another like spaghetti, and the overall conductivity must be a function of intra-polymer conductivity, inter-polymer conductivity within each fibril, and inter-fibril conductivity, the last being the determinant. (In fact, the well-aligned film (Fig. 1b) conducts electricity much better than the spaghetti-like film (Fig. 1a) upon doping.) However, there do exist some correlations between the vibrational spectra of undoped precursor polymers and the electrical property after doping them. For instance, in Fig. 2 are shown the infrared spectra of two films of trans-polyacetylene obtained from the same cis-polyacetylene film through different thermal isomerization processes. The spectra may look similar to each other, but there are some differences between them, e.g., the shapes and intensities of the bands around 1630-1460 cm^{-1} and 2900 cm^{-1}, and from such differences it is possible to predict with reason that film A would show an electrical conductivity much higher than that of film B upon maximum doping. The prediction is possible if one interprets the vibrational spectra properly. It must be noted that the structure and property of the polymers depend very much on the synthetic conditions and the treatments after the syntheses, and that contradicting conclusions obtained by different physico-chemical methods or even by the same method from different studies have often turned out to be due to the difference in the samples.

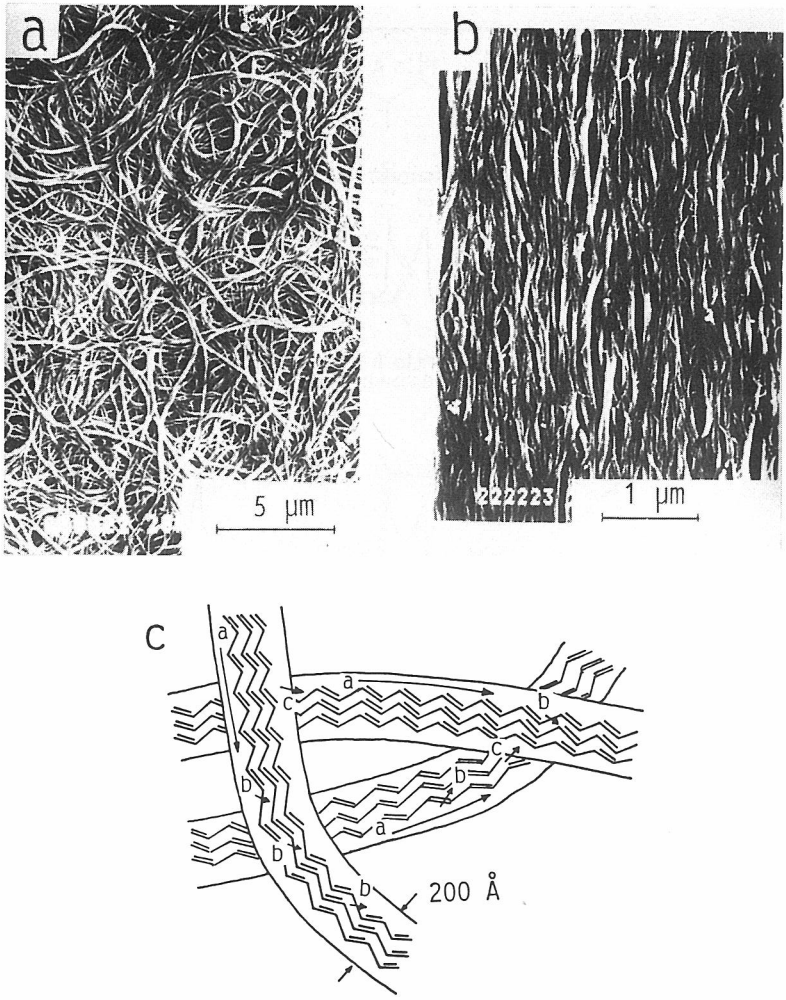

FIG. 1. Scanning electron micrographs of polyacetylene and possible carrier transport. (a) As-polymerized film (ZNS method), (b) as-polymerized oriented film on oriented liquid crystal, and (c) scheme of electrical conduction: a, intra-molecular transport; b, inter-molecular transport; c, inter-fibrillar transport. (Figures 1a and b, courtesy of Professor H. Shirakawa, University of Tsukuba.)

In this chapter, vibrational spectra and their interpretations are described on polyacetylene in detail because this polymer has been studied most extensively and yet there have been various arguments concerning the interpretations. Polythiophene is a conjugated heterocyclic polymer which becomes a radical cation and/or dication upon doping. The vibrational spectra are analyzed by comparing the data with those of isotopically sub-

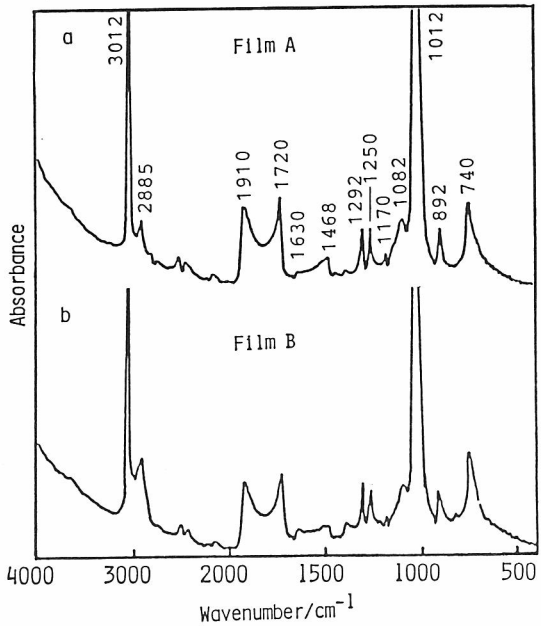

FIG. 2. Infrared spectra of two trans-polyacetylene films obtained from the same cis-polyacetylene through different thermal isomerization processes. (a) Film A (isomerization condition; 190°C, 15 min.) and (b) Film B (230°C, 180 min.).

stituted analogs and model compounds, and the electrical property is discussed in relation to the structure. Vibrations arising from the dication and radical cation are clearly observed for doped polypyrrole, and the optical absorption spectra are assigned on the basis of the resonance Raman characteristics. Polyaniline takes various forms by acid/base treatment, reduction/oxidation, and the combinations. The structures determined by vibrational analyses are shown and the relation between structure and electrical conductivity is explained. Spectroscopic studies on some other polymers including polypara-phenylene are reviewed briefly.

II. POLYACETYLENE

Polyacetylene [poly(vinylene), $(CH=CH)_x$, or $(CH)_x$] is the simplest conjugated polymer with the structural unit consisting of one carbon and one hydrogen. Film of polyacetylene is instantaneously developed on the surface of concentrated solution of $Ti(O\text{-}n\text{-}Bu)_4\text{-}AlEt_3$ (a Ziegler-Natta catalyst),

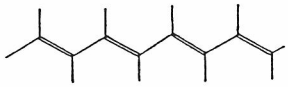

trans-transoid

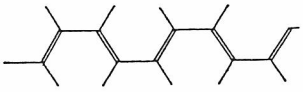

trans-cisoid

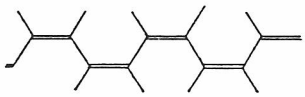

cis-transoid

FIG. 3. Three possible planar structures of polyacetylene.

e.g., on the inside wall of a flask wetted with the solution, when gaseous acetylene is introduced to the system [4,5]. [Ziegler-Natta-Shirakawa (ZNS) method. Hereafter, the physical and chemical properties of ZNS films are described unless otherwise mentioned.] By low-temperature polymerization (-78°C) a film consisting mainly (85-90%) of a thermally unstable configuration around the double bond is obtained [4,5] and the unstable form is converted to a thermally stable form through heat treatment [6]. The latter is the trans-transoid (to be termed trans) structure (Fig. 3) on the basis of two very strong infrared bands at 3012 and 1012 cm^{-1} assignable respectively to the CH antisymmetric stretch and the CH out-of-plane bend of the trans -C=C- double bond [5]. The structure of the unstable form has been concluded to be cis-transoid (cis) since one C=C double bond stretching band is observed in the Raman spectrum as expected for this structure [7]. (Trans-cisoid would give two such bands.) Polyacetylene does not melt nor is soluble in any solvent. The chain length in terms of the number of double bonds determined by indirect methods on modified (hydrogenated [8,9] or chlorinated [10-12]) polyacetylene is reported to be 200-400. It is 2-3 times larger when ^{3}H or ^{14}C labelling method is used [13-16].

The macroscopic structural unit of polyacetylene is a crystalline fibril of 200-1000 Å diameter [4,17-21] (1000 Å for material by liquid crystal polymerization under magnetic field [21]). The bulk density obtained from the

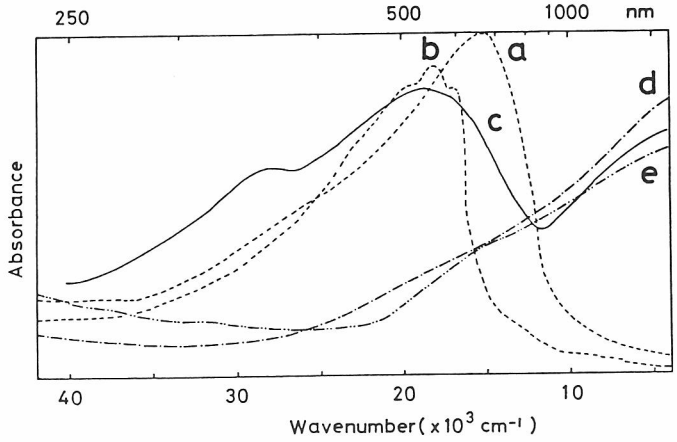

FIG. 4. Optical absorption spectra of intact and doped polyacetylenes. (a) trans-polyacetylene, (b) cis-polyacetylene, (c) iodine-doped trans-polyacetylene (the broad absorption in the visible-ultraviolet region being due to polyiodides, I_5^-, $(I_3^-)_x$, I_3^-, etc. as are evident by resonance Raman scattering from the species), (d) AsF_5-doped trans-polyacetylene, and (e) SO_3-doped trans-polyacetylene. Used by permission, Ref. [62].

dimensions and weight of the films is in the range 0.3-0.6 gcm^{-3} compared with 1.154 gcm^{-3} obtained by the floating technique, indicating that the films are porous [22]. The microcrystallinity can be high (>80% [23]) depending on the catalyst used. Cis film can be stretched by 3 - 3.5 times through thermo-mechanical stretching to give uniaxially oriented trans film [18]. The molecular axis also is oriented along the fibril axis as evidenced by the electrical [19], optical [24], and magnetic [25,26] anisotropy. Oriented films can be obtained by Meyer's method [27], Durham-route [28-30], epitaxial polymerization [31-33], and the liquid crystal method [21,34-37].

The crystal structure has been studied by X-ray [20,38-42], electron [11,31,33,43-49], and neutron [50,51] diffraction: for example, cis form, orthorhombic (P_{nma}) with a = 7.61, b = 4.47 (molecular axis), and c = 4.39 Å [38]; and trans form, monoclinic ($P2_1/n$) with a = 4.24, b = 7.32, c = 2.46 Å (molecular axis), and β = 91.5° [20,40] (ZNS material) or monoclinic ($P2_1/a$) with a = 4.18, b = 7.34, c = 2.455 Å, and β = 90.5° [42] (highly oriented Durham material). The difference in the lengths of the single and double bonds in the trans form is 0.06 Å [20,40] or 0.09 Å ($r_{C=C}$ = 1.36 and r_{C-C} = 1.45 Å [25]). A similar value, 0.08 Å, has been obtained by a nutation NMR spectroscopic study on ^{13}C labelled sample [52]. It must be noted that bond alternation persists even in very long polyene chains.

The π-π^* absorption spectrum of thin trans film (Fig. 4) ranges from red to ultraviolet without vibrational fine structures [λ_{max} = 14,800 cm^{-1} (675 nm)]. The peak wavenumber and the band shape depend on the isomerization conditions. In polyene molecules, the optical absorption is known to have vibronic fine structures and to show systematic bathochromic shifts as the number of conjugated double bonds ($N_{C=C}$) increases [53]. Since the transition energy converges to a constant value as $N_{C=C}$ reaches a certain high value, estimation of $N_{C=C}$ for a long polymer from the absorption maximum is impracticable. However, if the mean $N_{C=C}$ value in the trans film is high, the vibrational fine structure would be observed because of the convergent nature. The broad structureless absorption is indicative of the presence of chains of shorter conjugation lengths absorbing at higher energy and washing out the vibrational structure. In fact, the reflection spectrum of carefully isomerized thick film exhibits two peaks at 12,000 cm^{-1} (833 nm) and 13,000 cm^{-1}, indicating that the film is composed largely of chains of effectively "infinite" conjugation length [54].

As-prepared thin cis film, on the other hand, gives the absorption spectrum with three peaks whose frequencies and relative intensities are reported differently depending on synthetic conditions (Fig. 4). The value of the first maximum for low-temperature ZNS material at 16,830 cm^{-1} (594 nm) is lower than that for Luttinger material (16,950 cm^{-1}), implying a slightly longer chain length for the former [55]. The relatively well-resolved vibrational structure indicates a high mean value of $N_{C=C}$ and the absence of low $N_{C=C}$ sequences in the cis-rich films. The reflection spectrum of thick cis film is similar in shape to the absorption spectrum of the thin cis film [54]. One reason for the different behavior of thin and thick trans films has been ascribed to a difference in diameter of the fibril making up the film (100 Å versus 800 Å) [54]. It has been suggested that the formation of conjugation length limiting chemical defects during cis → trans isomerization is more likely in the structurally disordered surface region of the fibril [54].

Since CH bonds in the trans and cis parts in polyacetylene give strong infrared CH out-of-plane bending bands at characteristic frequencies, the intensities are useful in estimating the contents of the trans and cis parts in a film [4,56,57]. In the Raman spectrum of trans-polyacetylene two strong bands are observed (in the 1590-1450 and 1150-1050 cm^{-1} region) whose frequencies and shapes depend on the excitation wavelength [58-66], though such behavior is not observed for cis-polyacetylene [58-64,67]. Studies on trans oligoenes have indicated that these frequencies reflect the number of conjugated trans double bonds [58,68-70], and equations expressing the relationship between them have been obtained [60,61,70,71]. The Raman

spectral behavior is a result of coexistence of segments of various conjugation lengths: a very long segment gives rise to resonance Raman peaks at low frequencies with red light excitation and a shorter segment gives rise to those at higher frequencies with excitation at a shorter wavelength.

According to ESR studies, neutral radicals are detectable in trans-polyacetylene [72-74] but not in cis-polyacetylene [75-77]. These radicals are mobile [78-80]. They are called "phase kink", "domain wall", or "neutral soliton" [81-84] (see below).

Excited states of trans- and cis-polyacetylenes have been studied by absorption spectroscopy from the visible to infrared region [85-95] and ESR [96-98] with laser excitation.

Room temperature conductivities of undoped cis- and trans-polyacetylenes are 10^{-9} and 10^{-5} Scm^{-1}, respectively [74]. Upon doping, the conductivity increases by orders of magnitude: stretched ZNS material, 10^{3} Scm^{-1} at y = 0.1 for $[(CH)^{+y}A^{-}_{y}]_{x}$ or $[(CH)^{-y}D^{+}_{y}]_{x}$ where A and D stand for acceptor and donor, respectively [19]; material by liquid crystal polymerization under magnetic field, 10^{4} Scm^{-1} [21,37]; and Naarmann polymer, 1.7×10^{5} Scm^{-1} [99].

The temperature dependence of conductivity shows an activation energy even at a heavily doped state [100]. However, small thermopower and its temperature dependence [101-103], appearance of Pauli susceptibility [104-106], and optical absorption and reflection [107-111] have suggested that the individual segments are metallic at the heavily doped state.

X-ray diffraction studies of iodine-doped films have indicated the intercalation of iodine species (I_3^- and/or I_5^-) [46,112,113]. In alkali-metal doped polyacetylene, alkali metals except lithium (Na, K, Rb, and Cs) are reported to be present in channels [114].

Acceptor-doping induces three characteristic absorptions in the infrared region for trans- and cis-polyacetylenes [62,115-118]. Similar spectral patterns with different peak frequencies are observed for donor-doped polyacetylenes [119,120]. Since these spectral patterns are quite different from those of pristine films, drastic changes in chain structure occur upon doping. Raman spectra of polyacetylenes doped heavily with acceptors [61,62] or donors [121-126] are also different from those of pristine polyacetylenes. These observations can be interpreted by the formation of charged domains whose structure is significantly different from those of neutral chains. Possible species of charged domains are cations (or charged solitons by physicists) and radical cations (polarons), or anions (charged solitons) and radical anions (polarons). The cis configuration is transformed to trans configuration upon doping [119,127-132].

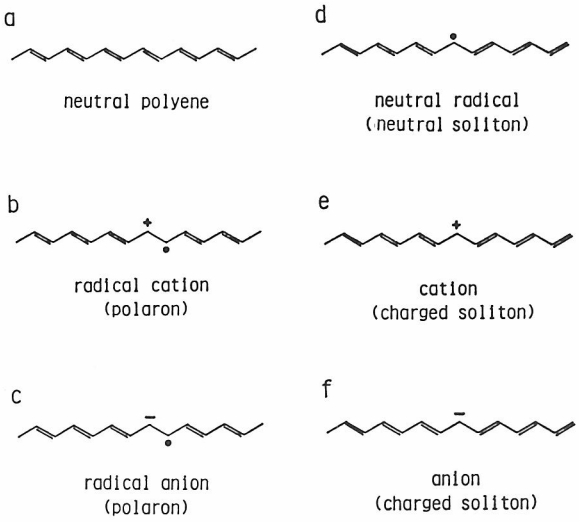

FIG. 5. Notations of neutral and doped trans-polyenes.

ESR studies of doped polyacetylenes are discussed from the viewpoint of soliton doping [105] and other mechanisms [133] and they are controversial.

It may be appropriate to compare here the structural notations by physicists and chemists. The majority of the polymers in a neutral trans film take the structure shown in Fig. 5a. Each polymer contains 200 - 1200 double bonds and the bond alternation persists even in such a long polyene as suggested by the diffraction and NMR results. The terminal groups are most likely CH_3CH_2- from the catalyst, -CH=CH_2, and -C≡CH. Not all the double bonds are conjugated from one end to the other end of a polymer chain but the conjugation is interrupted by some reasons like distortion of the single or double bond, remaining cis bond, a hydrogenated carbon, an oxidized carbon, a cross link, etc., to yield segments of various conjugation lengths as proven by Raman observations. Each segment like the one shown in Fig. 5a contains $2N_{C=C}$ π electrons. When this segment is doped by an electron acceptor, one electron is removed from the segment and it becomes a radical cation (Fig. 5b). This species is called a polaron by physicists. The remaining unpaired electron is not localized at the carbon near which the acceptor exists, but can be delocalized among nearby carbons up to 15 if the size of the segment is beyond that. If it is doped by an electron donor, it becomes a radical anion (a polaron). As the doping continues, a long segment is doped at many sites and two nearby radical cations may combine to form a cation pair (a charged soliton pair) while some radical cations may

remain as they are, depending on the micro-environmental conditions. By some unusual reasons, a segment may contain odd number electrons (a neutral radical, Fig. 5d). This minor species, called a neutral soliton by physicists, forms a domain wall consisting of about 15 carbons which is considered to give the ESR signal in pristine trans-polyacetylene. Since the neutral radical is very unstable, this would become one of the first targets by the dopants. Then it becomes a cation (Fig. 5e, a charged soliton) or an anion (Fig. 5f) and may contribute to an increase in electrical conductivity at the beginning of doping.

A. trans-Polyacetylene

In order to analyze the vibrational spectra of trans-polyacetylene, we first consider an infinite trans planar zig-zag polyene. Such a polymer belongs to a factor group isomorphous to C_{2h} point group and five Raman active and three infrared active vibrations are expected to be observed. The basis modes belonging to the symmetry species are: A_g, s_1 (C=C stretch), s_2 (C-C stretch), s_3 (CH in-plane bend), and s_{11} (CH stretch); B_g, s_8 (CH out-of-plane bend) and s_{10} (the acoustic mode due to rotation around the molecular long axis, z); A_u, s_7 (CH out-of-plane bend) and s_9 (the acoustic mode due to translation along the axis y, perpendicular to the molecular plane); B_u, s_4 (CH in-plane bend), s_{12} (CH stretch), s_5 (the acoustic mode due to translation along z), and s_6 (the acoustic mode due to translation along the in-plane x axis). The ν_i's are used for normal modes which are the coupled modes of s_i's belonging to the same symmetry species.

1. Raman Spectra

Raman spectra of trans film with excitation at three wavelengths are shown in Fig. 6 [62]. The bands at 1462, 1292, and 1072 cm^{-1} with 647.1 nm excitation are termed ν_1, ν_2, and ν_3 in that order. The frequency shifts upon ^{13}C and deuterium substitution [$\Delta\nu(^{13}C)$ and $\Delta\nu(D)$] are, -27 and -105 cm^{-1} for ν_1, -35 and -92 cm^{-1} for ν_2, and -25 and -224 cm^{-1} for ν_3. On this basis, they are roughly the C=C stretch, the C-C stretch and a mixed mode of the CH in-plane bend and the C=C stretch, correspondingly (see Sec. II.A.3). The assignment of ν_1 and ν_3 to the in-plane A_g mode is supported by the polarized Raman spectral measurements on highly stretch-oriented films [134,135]. Since the trans film is black and absorbs red through ultraviolet, we are observing the resonance Raman spectra at the three wavelengths (Fig. 6). Apparently, the spectra are considerably different from one another,

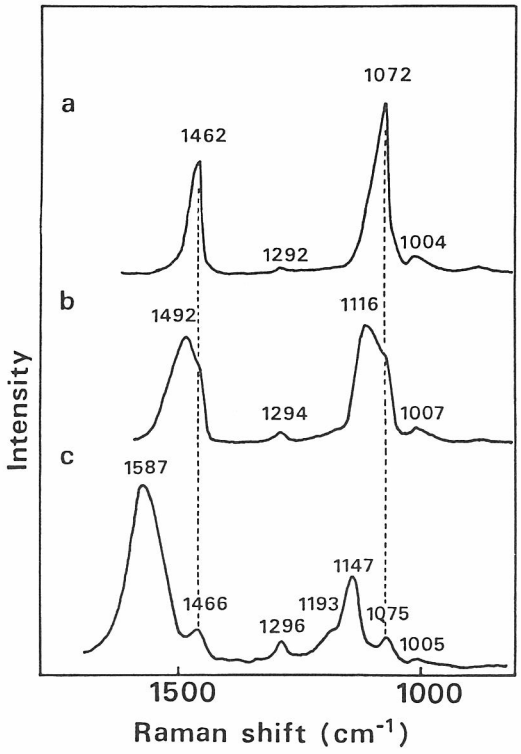

FIG. 6. Raman spectra of a thick trans-polyacetylene film excited at (a) 647.1 nm, (b) 488.0 nm, and (c) 350.7 nm. Used by permission, Ref. [62].

which can not be explained if the film is composed solely of infinitely long trans polyene because only four Raman active in-phase modes are expected in the frequency region.

Besides polyacetylene, there are many molecules in nature which contain trans polyenes and their vibrational spectra have been studied. Raman spectra of some of them are shown in Fig. 7. Amphotericin B is an antibiotic macrocyclic molecule containing seven conjugated double bonds with the absorption maximum at 414 nm [136]. With 514.5 nm excitation the Raman bands of the conjugated part are far more stronger than those of the other part of the molecule because the visible absorption arises from a π-π^* transition in the conjugated part and vibrations in that part are preresonantly enhanced. The spectral pattern (Fig. 7a) is similar to that of trans-polyacetylene with red light excitation (Fig. 7d) except the different peak frequencies of the major two bands, ν_1 and ν_3. Desmethyl β-carotene contains nine trans conjugated double bonds with the absorption maximum at 455 nm and the Raman pattern (Fig. 7c) [137] is similar to those of

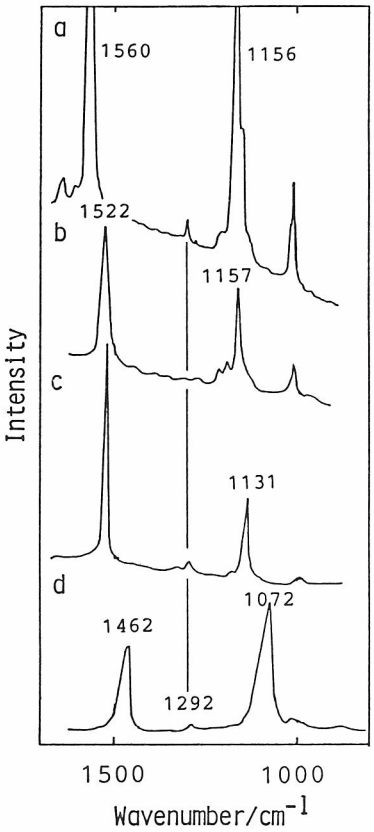

FIG. 7. Raman spectra of trans-polyene molecules. (a) Amphotericin B (514.5 nm excitation) [136], (b) β-carotene (488.0 nm), (c) desmethyl β-carotene (488.0 nm) [137], and (d) trans-polyacetylene (647.1 nm) [62].

amphotericin B and trans-polyacetylene (Fig. 7d) except that the ν_1 and ν_3 frequencies are between those of the two. The ν_2 frequencies are almost constant for the three. In β-carotene (λ_{max} = 475 nm), the vibrations of the methyl groups attached to the polyene chain couple more with the s_2 and s_3 modes than with the s_1 mode causing an upshift of ν_3 and obscuring the ν_2 peak (Fig. 7b).

What will be observed if one mixes amphotericin B with β-carotene? In short, Raman spectra of the mixture depend not only on the composition but also on the excitation wavelength (Fig. 8) because the resonance or preresonance Raman intensities depend significantly on the excitation wavelength. It is to be noted that the ν_1 band of amphotericin B relative to that of β-carotene is greater with 632.8 nm excitation (Fig. 8d) than with 514.5 nm excitation (Fig. 8c right). This is because the excitation wavelength 632.8 nm is far enough from the absorption maxima of both molecules to diminish the difference in the preresonance effects for the two.

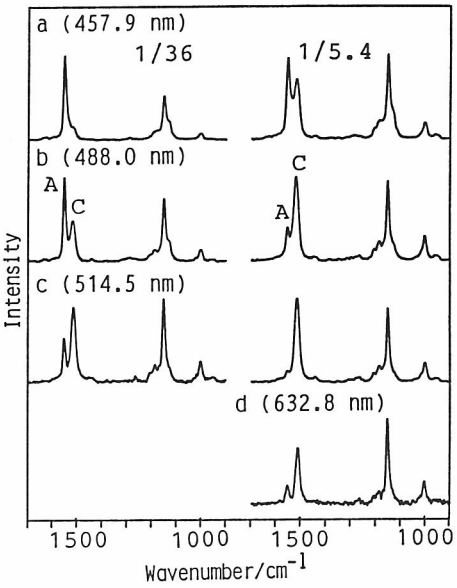

FIG. 8. Raman spectra of mixtures of β-carotene and amphotericin B in the ratio of 1/36 (left) and 1/5.4 (right) excited at (a) 457.9 nm, (b) 488.0 nm, (c) 514.5 nm, and (d) 632.8 nm. A and C indicate the ν_1 peaks of amphotericin B and β-carotene, respectively.

The Raman spectra of polyacetylene can be explained in a similar manner. A film consists of various chromophores, i.e., various polyene segments, and the Raman spectral pattern depends on the composition of the chromophores and the excitation wavelength. In Fig. 6c the peaks at 1466 and 1075 cm^{-1} due to long segments are observed even at a far off resonant condition because of their high contents in the film.

It is worth mentioning that the hot luminescence model makes no significant contribution to this variation in the Raman bandshapes with the excitation wavelength as evident by the anti-Stokes spectrum which is the mirror image of the Stokes spectrum contrary to the expectation from the hot luminescence model [138,139].

Raman spectra of many conjugated molecules have been studied and correlations are known among $N_{C=C}$, the frequencies of ν_1 and ν_3, and the wavelength of absorption maximum [58,68-70]. In Fig. 9 the ν_1 and ν_3 frequencies are plotted against $(N_{C=C} + 1)^{-1}$ [70]. (In general, strong infrared or Raman bands of a long straight-chain molecule composed of translational repeating units are attributable to the vibrations with the smallest phase difference [140,141]. In the present case, the repeating unit is a conjugated C=C bond and the smallest phase difference is $(N_{C=C} + 1)^{-1}$.) A linear relationship between the ν_1 frequency and $(N_{C=C} + 1)^{-1}$ holds for $N_{C=C} \geq 4$, viz.,

$$\nu_1(cm^{-1}) = 1454 + A(N_{C=C} + 1)^{-1}, \quad (N_{C=C} \geq 4), \tag{1}$$

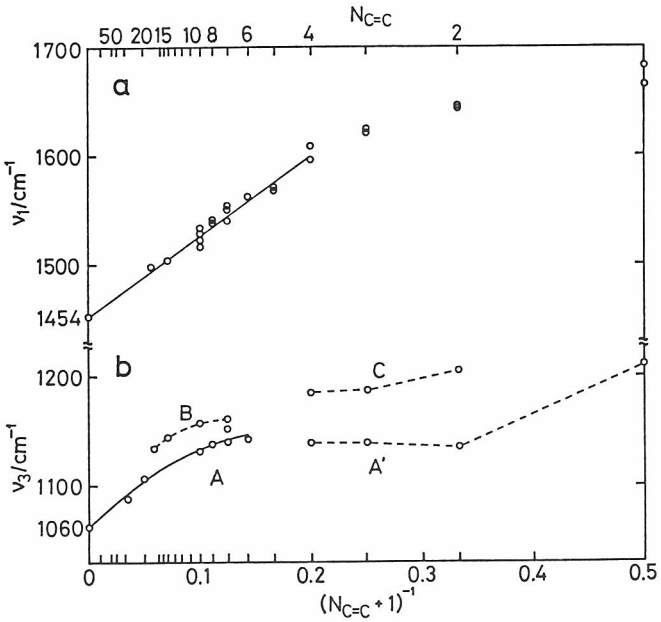

FIG. 9. $N_{C=C}$ - ν relationships. (a) Relation between ν_1 and $(N_{C=C} + 1)^{-1}$. The straight line represents Eq. (1). (b) Relation between ν_3 and $(N_{C=C} + 1)^{-1}$. Curve A represents Eq. (2): curve A' for $C_2H_5COO-(CH=CH)_n-COOC_2H_5$, (n=1-4); curve B, isoprenoid; curve C, data of 1,3-butadiene, 1,3,5-hexatriene, and 1,3,5,7-octatetraene. Used by permission, Ref. [70].

where A = 727 (standard deviation is 12). This relation is good for isoprenoids as well as for polyvinylenes. On the other hand, the series of ν_3 frequencies of isoprenoid compounds (curve B in Fig. 9) is different from that of polyvinylenes (curve A). This is because the coupling of the CH in-plane bend and the C=C stretch in polyenes without side chains is disrupted by methyl substitution in the isoprenoid compounds. Curve A is expressed in the following form:

$$\nu_3(cm^{-1}) = 1060 + B(N_{C=C} + 1)^{-1} + C(N_{C=C} + 1)^{-2}, \quad (N_{C=C} \geq 6), \qquad (2)$$

where B = 1020 (100) and C = -2910 (810) [70].

By using Eq. (1) conjugation lengths of the segments in polyacetylene can be estimated. In Fig. 6 the peak at 1587 cm^{-1} arises from segments of four conjugated double bonds absorbing ultraviolet light (350.7 nm), that at 1492 cm^{-1} from those of eighteen conjugated double bonds absorbing blue light (488.0 nm), and that at 1462 cm^{-1} from those of about ninety conjugated

double bonds absorbing red light (647.1 nm). (It must be mentioned here that the spectra in Fig. 6 were taken in the early days (1979) when the optimum thermal isomerization condition was not established yet. Films with the ν_1 frequency of 1454 cm^{-1} with 632.8 nm excitation can be obtained now.) Similar figures are estimated from Eq. (2). The peak frequencies are different for slightly different excitation wavelengths, indicating coexistence of segments of various conjugation lengths. The presence of short segments does not necessarily mean the presence of polyenes of small molecular weights. They must be parts of long polymers connected by certain breaks of conjugation, like a twisted double or single bond, sp^3 carbons, etc.

However, the Raman spectra must be interpreted as an overlap of excitation wavelength-sensitive Raman spectra of various polyenes whose compositions depend on the preparation conditions. Then the selection rule for the finite trans polyenes (point group C_{2h} if the polyenes are planar with the inversion symmetry) must be applied in assigning the vibrational bands. The modes corresponding to the acoustic modes in infinite polyene have some finite frequencies and any gerade or ungerade mode is Raman or infrared active, respectively. In fact, weak bands in addition to ν_1, ν_2, and ν_3 are observed clearly in high gain spectra as illustrated in Fig. 10. Assignments of these weak bands including the ν_8 fundamental (in infinite polyene approximation) will be shown in Sec. II.A.3 and II.A.4.

2. Infrared Spectra

The infrared spectrum of a thin trans film is dominated by two peaks at 3012 (ν_{12}, CH antisym. str., $\Delta\nu(^{13}C)$ = -11 cm^{-1}, $\Delta\nu(D)$ = -793 cm^{-1}) and 1012 cm^{-1} (ν_7, CH out-of-plane bend, $\Delta\nu(^{13}C)$ = -2 cm^{-1}, $\Delta\nu(D)$ = -266 cm^{-1}). Many weak bands are observed for thick films (Fig. 2) and the shapes and intensities of some bands are different for different films as mentioned in the introduction. Most of them (except the bands due to defects and impurities) must arise from vibrations in segments of finite lengths. In interpreting these spectral observations, knowledge on frequency dispersion of each vibrational branch (in infinite chain) is useful and for such purpose it is necessary to obtain a suitable force field applicable generally to short as well as long trans polyene chains. Assignments of the observed bands including the ν_4 fundamental (in infinite polyene) will be shown in Sec. II.A.3 and II.A.4.

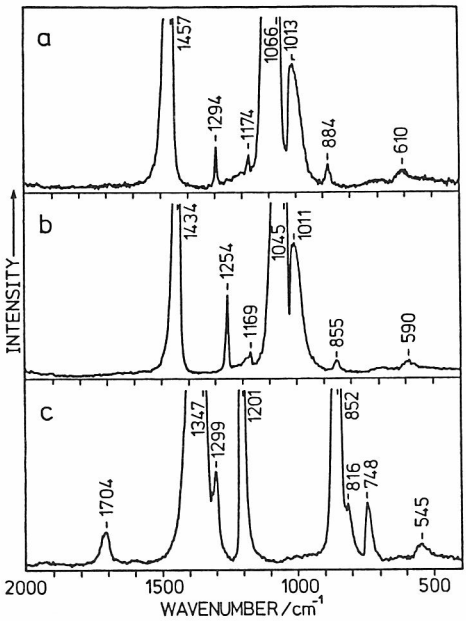

FIG. 10. High-gain Raman spectra of trans-polyacetylenes (632.8 nm, 77K). (a) $(CH)_x$, (b) $(^{13}CH)_x$, and (c) $(CD)_x$. Used by permission, Ref. [142].

3. Normal Vibrations

Several model calculations have been reported of the frequency dispersion curves for the in-plane vibrations in the infinite polyene chain [143-147]. Here, however, are shown the results by Takeuchi et al. in some detail [142,148-150].

Normal coordinate calculations have been performed for the in-plane [149] and out-of-plane [142] vibrations of several trans-polyene chains from butadiene to polyacetylene. The force field finally obtained consists of short range forces, which are primarily determined by the frequency data on small molecules, and long range interactions which are important in explaining the data on polyacetylene. The long range interactions between the C=C stretching coordinates are known to be important in the sp^2 π-electron conjugated system like benzene [151,152] and those as far as the fifth neighbor have turned out to have significant effects on the dynamical properties of the infinite polyene chain [149]. Some force constants related to the CC stretching coordinates are listed in Table 1 together with those of polyethylene and benzene.

The calculated $\delta = 0$ frequencies (δ being phase difference) below 2000 cm^{-1} of the infinite polyene chain are compared with experimental frequencies of polyacetylene in Table 2. Here, the infrared band at 1250 cm^{-1} and the Raman band at 884 cm^{-1} are assigned to ν_4 and ν_8 based on the isotopic shifts consistent with the calculated. The normal modes of ν_1, ν_2, and ν_3 are

TABLE 1

CC Stretching Force Constants of Polyethylene, Benzene, and Polyvinylenes

Molecule	Ref.	Coordinate[a]	Value (md/Å)
Polyethylene	[153]	C-C	4.453
		C-C/C-C	0.199
Benzene	[154]	CC	6.4153
		CC/CC ortho	0.7716
		CC/CC meta	-0.3189
		CC/CC para	0.2895
Polyvinylenes	[149]	C=C	7.751
		C-C	5.401
		C-C/C=C	0.407
		$C=C_n/C=C_{n+1}$	-0.730
		$C=C_n/C=C_{n+2}$	-0.266
		$C=C_n/C=C_{n+3}$	-0.200
		$C=C_n/C=C_{n+4}$	-0.150
		$C=C_n/C=C_{n+5}$	-0.100
		$C-C_n/C-C_{n+1}$	-0.130

[a]The symbol / denotes the interaction between two coordinates given on both sides.

TABLE 2

Comparison of Raman and Infrared Frequencies (in cm^{-1}) of trans-polyacetylene with the Calculated Frequencies at $\delta = 0$

		$(C_2H_2)_x$		$(^{13}C_2H_2)_x$		$(C_2D_2)_x$	
Symmetry	Mode	Obs.[a]	Calc.	Obs.[b]	Calc.	Obs.	Calc.
A_g	ν_1	1464	1470	1442	1447	1357	1352
	ν_2	1294	1302	1256	1256	1200	1191
	ν_3	1072	1079	1054	1054	855	854
B_u	ν_4	1250	1235	1231	1231	916	908
A_u	ν_7	1012	1014	1010	1011	746	744
B_g	ν_8	884	887	855	866	816	795

[a]Refs. [5,148].
[b]Ref. [62].

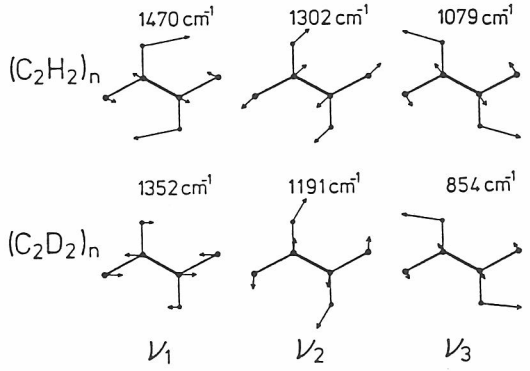

FIG. 11. Normal coordinates of the Raman active ν_1, ν_2, and ν_3 modes in trans-$(C_2H_2)_n$ and trans-$(C_2D_2)_n$. The arrows indicate the calculated atomic Cartesian displacement vectors multiplied by three. Used by permission, Ref. [149].

shown in Fig. 11. As expected from the observed isotopic shifts (Table 2), ν_3 is a mixed mode of the C=C stretch and the CH bend with a large contribution from the latter, contrary to its widely believed assignment to the C-C stretch. The ν_2 mode instead, predominantly involves the C-C stretch and the contribution of the C=C stretch to this mode is very small. The ν_1 mode is another mixed mode of the C=C stretch and the CH bend with a large contribution from the former. In $(C_2D_2)_n$, the C=C stretch mixes with the C-C stretch as well as the CD bend and the atomic movements of ν_1 and ν_2 are nearly parallel and perpendicular to the chain axis, respectively. The increased contribution of the C=C stretch to ν_2 in $(C_2D_2)_n$ accounts for the enhancement of the ν_2 Raman intensity on deuteration (Fig. 10c).

Frequencies of ν_1 and ν_3 are greatly lowered by the long range terms to become comparable with the experimental frequencies of polyacetylene with red light excitation (Table 2). These vibrations shift to higher frequencies steeply as the phase difference between adjacent HC=CH units increases from zero (Fig. 12). In Sec. II.A.1, relations between $(N_{C=C} + 1)^{-1}$ and the ν_1 and ν_3 frequencies are described. Such correlation between the frequency and the chain length should be connected with the dispersion curves in the infinite chain, if we assume substantially the same force field both for finite and infinite chains. In fact, the ν_1 and ν_3 dispersion curves agree fairly well with the observed frequencies of molecules of finite lengths (Fig. 13, see Fig. 9 also). The agreement between the calculated and the observed can be improved by systematic modifications of the long range forces [150] according to the formalism of Coulson and Longuet-Higgins [155].

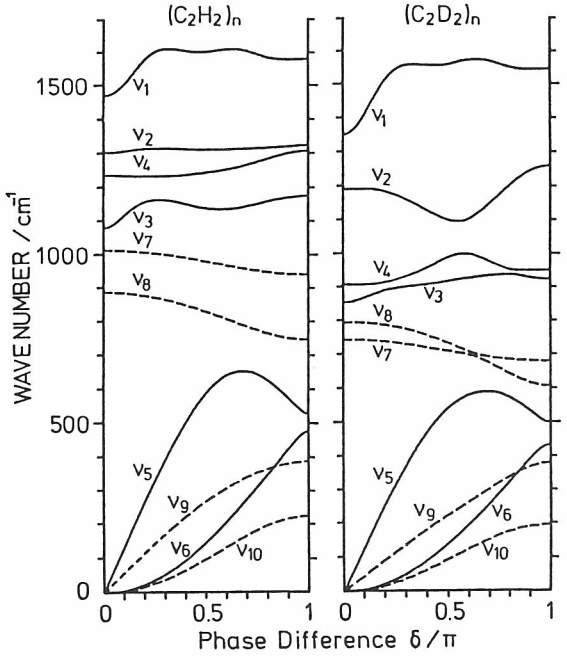

FIG. 12. Frequency dispersion curves (below 1700 cm^{-1}) calculated for the in-plane (solid line) and out-of-plane (dotted line) vibrations of trans-$(C_2H_2)_n$ and trans-$(C_2D_2)_n$. Used by permission, Ref. [142].

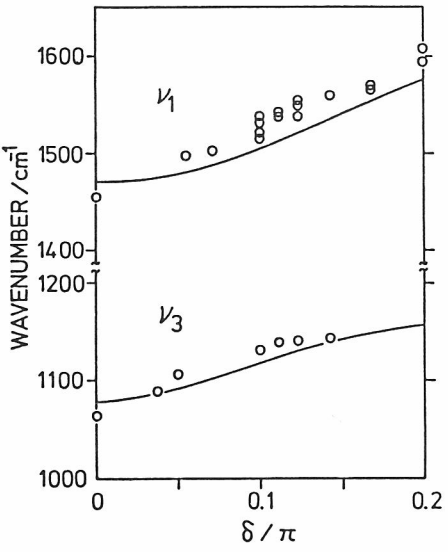

FIG. 13. Comparison of the Raman frequencies in finite polyene with the dispersion curves calculated for ν_1 and ν_3 in trans-$(C_2H_2)_n$. The experimental data are the same as those in Fig. 9. $\delta = \pi(N_{C=C}+1)^{-1}$. Used by permission, Ref. [149].

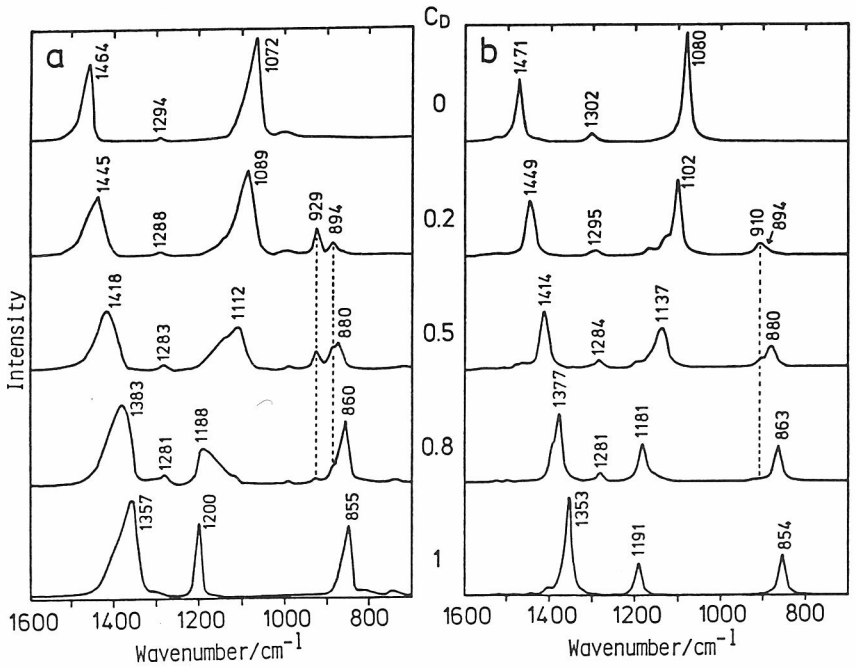

FIG. 14. Comparison of (a) the experimental Raman spectra excited at 632.8 nm and (b) the calculated Raman spectra for trans-$(C_2H_2)_n$ (C =0), trans-$(C_2D_2)_n$ (C =1), and copolymers (C = 0.2, 0.5, and 0.8). ^nC is the concentration of C_2D_2 relative to the total amount of acetylene. Used by permission, Ref. [149].

The greater dispersion of the ν_1 branch in $(C_2D_2)_n$ than in $(C_2H_2)_n$ (Fig. 12) accounts for the relative broadness of the ν_1 Raman band in deuterated trans-polyacetylene [62,148] because the ν_1 frequency is more dependent on the chain length in deuterated polyene than in the hydrogenated one and the band shape reflects the distribution of the chain length more sensitively [149].

Validity of the dispersion curves can be tested by comparing the observed and calculated spectra of copoly $(C_2H_2 + C_2D_2)$. Experimental Raman spectra of $(C_2H_2)_x$, $(C_2D_2)_x$, and copoly $(C_2H_2 + C_2D_2)$ are shown in Fig. 14a. The excitation wavelength of these spectra is 632.8 nm, which gives the spectra of very long polyene components. In Fig. 14b are shown the theoretical spectra for in-plane A_g vibrations in model polyene chains ($N_{C=C}$ = 50) assuming some geometrical change upon π-π^* excitation and an approximate equation of resonance Raman intensity [149]. Although some peak positions do not coincide with the experimental ones precisely, the calculated spectra reproduce the behavior of all the ν_1, ν_2, and ν_3 bands

upon introduction of isotopic species. For example, the ν_1 frequency shows a monotonical downshift as the concentration of C_2D_2 increases (one-mode behavior), which is characteristic of the vibration whose densities of states in two isotopically pure crystal (one-dimensional in this case) overlap each other [156], and the same shift is evident in the calculated spectra. In contrast, two-mode behavior is observed for ν_2 and ν_3 [149,156]. Mixing of isotopic species gives rise to the split bands as is clearly seen for ν_3. The two-mode behavior indicates that the densities of states of ν_3 in $(C_2H_2)_x$ and $(C_2D_2)_x$ do not overlap and the interaction between the ν_3 vibrations at C_2H_2 and C_2D_2 sites is negligible. Such behavior is also reproduced consistently in the calculated spectra.

4. Assignments of Infrared and Raman Bands

Each dispersion curve in Fig. 12 has at least two points of δ where the inclination of the curve is zero (critical points). The density of states at the corresponding frequencies are particularly high compared with the other frequency regions.

As mentioned previously, in the infinite polyene chain only the ν_4 and ν_7 fundamentals with $\delta=0$ are allowed in the infrared spectrum below 2000 cm^{-1}. For chains of finite length, more vibrations become infrared-active as a result of the lack of translational symmetry and they are correlated with the vibrations of $\delta \neq 0$ in the infinite chain. Since trans-polyacetylene contains polyene chains of various lengths as stated in Sec. II.A.1, the $\delta \neq 0$ vibrations, particularly at the critical points, are likely to appear in the infrared spectrum. The calculated density of states [$G(\nu)$] spectrum and the infrared spectrum are compared in Figs. 15 and 16 [142]. It is apparent that most of the infrared bands correspond to the high density points in the $G(\nu)$ spectra. Assignments of the infrared bands based on the calculated $G(\nu)$ spectra are summarized in Table 3 together with those of some bands due to minor structural components in the polymer films. Some assignments need explanations.

In the infrared spectrum of trans-$(CH)_x$ the broad absorption contour, with two peaks at 1630 and 1468 cm^{-1} mentioned in the introduction, is ascribed to the ν_1 vibrations which are calculated in the 1610-1470 cm^{-1} range (Fig. 15). The intensity distribution in this frequency range is sensitive to the distribution of trans conjugation lengths [70]: the peak on the low frequency side is strong for a film with a high content of very long segments and it is weak for a film with a low content of such segments. Since a film which is rich in long segments generally shows high electrical conductivity

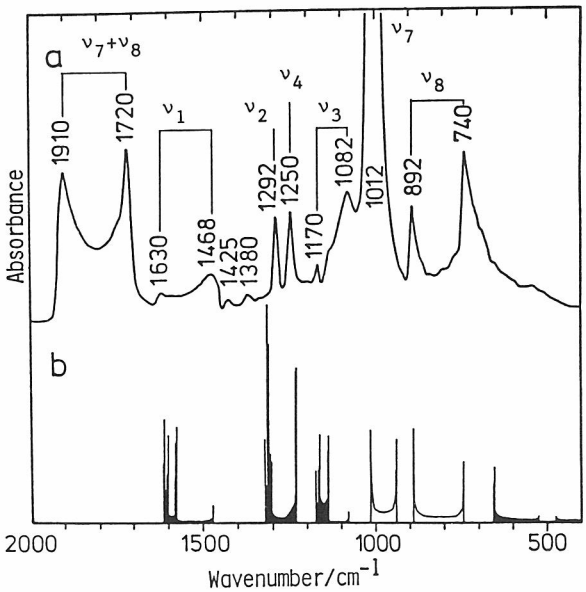

FIG. 15. Comparison of (a) the infrared spectrum of trans-$(CH)_x$ (in absorbance units) with (b) the density of states of trans-$(C_2H_2)_n$ (in arbitrary units) and the assignments. The shaded areas in the density spectrum are due to in-plane vibrations. Adapted from Ref. [142].

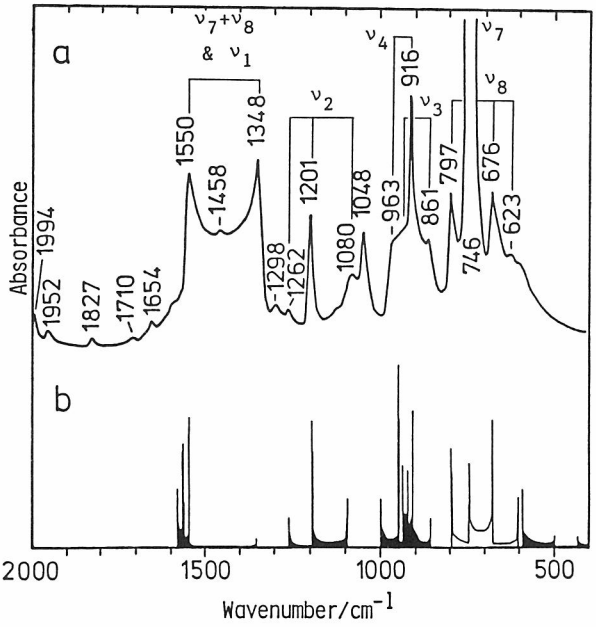

FIG. 16. Comparison of (a) the infrared spectrum of trans-$(CD)_x$ (in absorbance units) with (b) the density of states of trans-$(C_2D_2)_n$ (in arbitrary units) and the assignments. The shaded areas are due to in-plane vibrations. Adapted from Ref. [142].

TABLE 3
Assignments of Infrared Absorption Bands in trans-polyacetylene[a]

$(CH)_x$	$(^{13}CH)_x$	$(CD)_x$	Assignment
		1994	$\nu_2 + \nu_8$ (1201 + 797 = 1998)
		1952	$\nu_2 + \nu_7$ (1201 + 746 = 1947)
		1827	$2\nu_4$ (2 × 916 = 1832)
1910-1720	1883-1708	1550-1348	$\nu_7 + \nu_8$
		1710	C=O str.
	1632	1654	C=O str.
1630-1468	1573-1447	(1550-1348)	ν_1[b]
		1458	CH bend of CH_2 and CH_3 (catalyst)
1425	1412		CH_2 scissors (=CH_2?)
1380	(1380)	(1380)	CH_3 sym. deform. (catalyst)
		1298	$\nu_7 + \nu_8$ (623 + 676 = 1299)
1292	1257	1262,1201,1080	ν_2
		1048	unassigned[c]
1250	1231	963,916	ν_4
1170,1082	1166,1068	861,(916)	ν_3
1012	1010	746,623	ν_7
892,740	872,720	797,676	ν_8

[a]Peak frequencies in cm^{-1}.
[b]Overlapped by $\nu_7 + \nu_8$ bands in $(CD)_x$.
[c]See Ref. [142].

upon doping [157], it is possible to predict the potential electrical property from the infrared ν_1 band shape (see below). A similar broad absorption with peaks at 1573 and 1447 cm^{-1} in $(^{13}CH)_x$ is also reproduced in the calculated G(ν) spectrum. The ν_1 vibrations in $(CD)_x$ are expected in the 1575-1350 cm^{-1} region, where a rather strong absorption with three peaks at 1550, 1458, and 1348 cm^{-1} is observed (Fig. 16). The relative strength of the absorption in $(CD)_x$ is due to overlapping of combination bands ($\nu_7 + \nu_8$) as will be described below.

Combination and overtone bands of the CH out-of-plane bending vibrations have appreciable infrared intensities in conjugated systems [158] and polyacetylene is not an exception. The absorption contours between 1910 and 1720 cm^{-1} in $(CH)_x$ are assigned to the combinations of ν_7 and ν_8, sums of peak frequencies being 1904 (1012 + 892) and 1752 (1012 + 740) cm^{-1}. Similarly, the absorption between 1883 and 1708 cm^{-1} in the spectrum of $(^{13}CH)_x$ is attributable to $\nu_7 + \nu_8$. In the case of $(CD)_x$, the combination transitions are expected to be down-shifted to 1543 and 1299 cm^{-1} from the observed fundamental frequencies. A very weak band observed at 1298 cm^{-1} is one of these. The other transitions overlap with the broad absorption due to ν_1 described above, though the intensity in the frequency region seems to come mainly from the combination bands.

It is necessary to comment on the assignment of the 740 cm^{-1} band to ν_8 ($\delta = \pi$) because this band has been discussed in relation to remnant cis bonds [56,159-160]. The complication arose from the fact that the peak frequency coincides with that of the strongest peak in the cis film. The cis-$(CH)_x$ polymer shows three strong infrared bands due to CH in-plane bending (1329 cm^{-1}), CH out-of-plane bending (740 cm^{-1}), and CCC deformation (446 cm^{-1}) fundamentals [4]. The 1329 and 446 cm^{-1} bands disappear upon thermal isomerization, while some intensity is retained at 740 cm^{-1}. The residual 740 cm^{-1} absorption was assigned to the CH out-of-plane bend of cis CH=CH bonds isolated in trans chains [56,159-160]. However, the corresponding CD out-of-plane bending band observed at 548 cm^{-1} in cis-$(CD)_x$ [4] is absent in the spectrum of trans-$(CD)_x$ (Fig. 16). Furthermore, in the thermal isomerization process of $(^{13}CH)_x$, the cis band at 739 cm^{-1} decreases in intensity with other cis bands, while the band at 720 cm^{-1} gains intensity with the other trans bands (Fig. 17). This finding indicates that two bands due to cis and trans components have the same frequency 740 cm^{-1} in $(CH)_x$. The disappearance of the 739 cm^{-1} band in the fully isomerized $(^{13}CH)_x$ film [142] shows that the 740 cm^{-1} band in the spectrum of trans-$(CH)_x$, is not due to a vibration of remnant cis bond but due to ν_8 ($\delta = \pi$) of trans polyene chain as assigned in Table 3. The amount of remnant cis bonds must be, if any, much smaller than that proposed previously [56,159,160].

A very weak band at 1425 cm^{-1} of trans-$(CH)_x$ [1412 cm^{-1} in trans-$(^{13}CH)_x$] has been assigned to the $=CH_2$ scissoring vibration at the terminals of chains [142]. Oxidation of a trans polyacetylene film proceeds in the ambient air and gives rise to C=O stretching bands at 1670 and 1725 cm^{-1} (with ^{18}O down-shifts of 30 and 34 cm^{-1}, respectively). A weak band at 1632 cm^{-1} in the spectrum of $(^{13}CH)_x$ and those at 1654 and 1710 cm^{-1} in

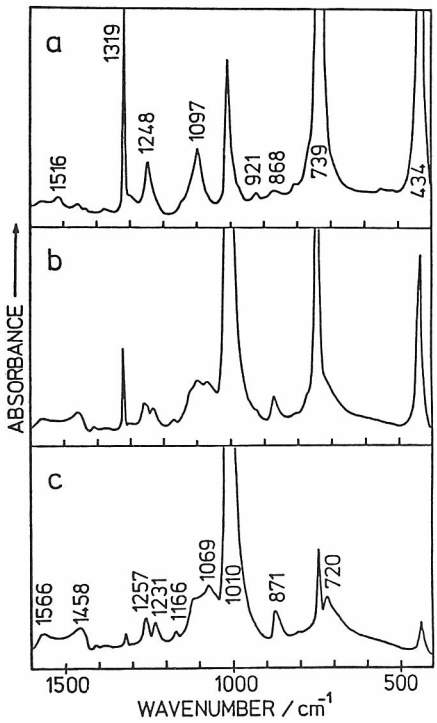

FIG. 17. Infrared spectra of $(^{13}CH)_x$ at intermediate stages of the cis→ trans isomerization: (a) cis-rich, (b) cis-trans mixture, and (c) trans-rich. Wavenumbers of cis bands are given in (a) and those of trans bands in (c). Used by permission, Ref. [142].

that of $(CD)_x$ are due to the isotopically affected C=O stretching bands.

Weak absorptions at 1380 cm^{-1} in the spectrum of $(CH)_x$ and at 1458 cm^{-1} in that of $(CD)_x$ are ascribed to the CH bending vibrations of the CH_3 and CH_2 groups. The intensities at these frequencies are different from film to film. The CH stretching bands characteristic of CH_3 and CH_2 groups are also found around 2960, 2930, and 2870 cm^{-1} in all the spectra of $(CH)_x$, $(^{13}CH)_x$, and $(CD)_x$. These observations indicate that aliphatic hydrocarbons originating from the polymerization catalyst, $Ti(OC_4H_9)_4$-$Al(C_2H_5)_3$, remain in the polymer films [4]. However, the CH stretching intensities depend also on the thermal isomerization conditions as described in the introduction (Fig. 2). Accordingly, some sp^2 carbons (=CH-) are converted to sp^3 carbons (-CH_2-) through the thermal treatment yielding breaks of conjugation. Hence, the intensity around 2900 cm^{-1} also (together with the ν_1 band shape) can be used as a monitor of the potential electrical property of a film.

As mentioned above, Raman spectra with red light excitation (Fig. 10) give selective information on the vibrations of very long trans components in the films (Table 4). Besides the ν_1, ν_2, and ν_3 modes at $\delta = 0$ (A_g), another Raman active mode ν_8 ($\delta = 0$) of B_g species appears weakly. The

TABLE 4
Assignments of Raman Bands in trans-polyacetylene[a]

$(CH)_x$	$(^{13}CH)_x$	$(CD)_x$	Assignment
		1704	$2\nu_3$
1457	1434	1347	ν_1
		1299	$\nu_7 + \nu_8$
1294	1254	1201	ν_2
1066,1174	1045,1169	852	ν_3
1013	1011	748	ν_7
884	855	816	ν_8
610	590	545	ν_5

[a]Peak frequencies in cm^{-1}.

peak frequencies of ν_1, ν_3, and ν_8 are significantly different from those observed in the infrared spectra, which arises from the fact that the resonance Raman spectra give peaks of long polyenes whereas the infrared spectra give bands consisting of overlaps of the bands of polyenes of various lengths existing in the films. The bands at 1013, 1011, and 748 cm^{-1} of $(CH)_x$, $(^{13}CH)_x$, and $(CD)_x$, respectively, are ascribed to ν_7 ($\delta = 0$) because their frequencies coincide well with the strong infrared bands due to this mode.

Polarized infrared [161-164] and Raman [134,135] spectra of highly oriented trans-$(CH)_x$ have been reported, although the spectral features depend much on the quality of the samples and the quantitative arguments must be done with care. For instance, the ν_7 infrared band is polarized completely perpendicular to the average chain axis in [161] while the parallel component with different intensities is observed in [162-164]. The ν_{12} band (3010 cm^{-1}), however, is commonly observed as a depolarized band and the large parallel component has been ascribed to the charge flux along the conjugated chain axis [163]. On the other hand, the strongly parallel character of the ν_8 bands at 892 and 740 cm^{-1} [162] cannot be explained in the same way, because the out-of-plane fundamentals are unable to induce charge fluxes along the chain by symmetry if the planarity of the chain is preserved in the polymer film. The A_g-like character of the Raman ν_4 band at 1013 cm^{-1} also cannot be explained by C_{2h} symmetry because the mode

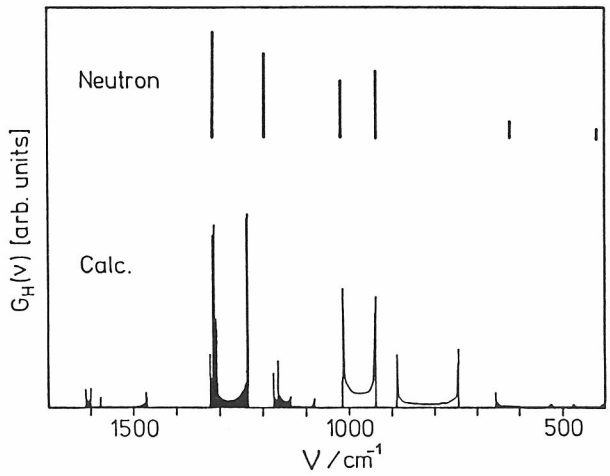

FIG. 18. Hydrogen-amplitude-weighted density of states calculated for trans-$(C_2H_2)_n$. The shaded areas are due to in-plane vibrations. Peak positions and their relative intensities in a neutron spectrum of trans-$(CH)_x$ [165] are indicated with a bar. Used by permission, Ref. [142].

would belong to A_u or B_g. A possible explanation is that the chains are slightly twisted like pleated sheet: alternating clockwise and anti-clockwise distortion around the consecutive single bonds (C_2 symmetry). The polarization characteristics of the other infrared and Raman bands are consistent with the assignments in Tables 3 and 4.

5. Comparison of Density of States and Neutron Scattering Spectrum

Incoherent inelastic neutron scattering spectra provide straightforward information on the density of states, because the scattering intensity is proportional to the product of the density of states and the squared vibrational amplitudes of hydrogen atoms. Figure 18 shows the amplitude-weighted density of states $G_H(\nu)$ calculated for $(C_2H_2)_n$. The strong peaks predicted around 1310 cm^{-1} are mainly due to the ν_2 vibration. The frequency dispersion of the ν_2 branch is very small (Fig. 12) and the contribution of the CH in-plane bend is significant at $\delta > 0.2\pi$. Thus the high density and large amplitude of the hydrogen motion result in strong peaks at 1315 and 1309 cm^{-1}. On the other hand, the ν_4 branch, whose main mode is also the CH in-plane bend, is nearly flat in the ranges $0.9\pi < \delta < \pi$ and $0 < \delta < 0.4\pi$, the vibrations in the former range giving rise to a peak at 1305 cm^{-1} and those in the latter range a strong peak at 1232 cm^{-1}. Out-of-plane motions of the hydrogen atoms are much larger in ν_7 than in ν_8 as is seen

from the frequency shifts on deuteration. The critical points of ν_7 at $\delta = 0$ and π are expected to give peaks of medium intensity at 1014 and 938 cm^{-1}, respectively. The ν_8 peaks calculated at 887 and 744 cm^{-1} are weak.

A neutron scattering spectrum of trans-$(CH)_x$ has been reported recently by Maconnachie et al. [165]. The experimental spectrum shows strong peaks around 1310 and 1190 cm^{-1} and medium intensity peaks around 1010 and 930 cm^{-1} as indicated in Fig. 18. The agreement between the experiment and calculated is satisfactory with respect to both peak position and intensity. In particular the agreement in the intensity pattern gives support to the calculated vibrational modes of ν_2, ν_4, and ν_7 branches.

6. Partly Hydrogenated trans-Polyacetylene

Now, what will happen to the spectra and electrical property if we replace some sp^2 carbons (=CH-) in the conjugated polyene segments with sp^3 carbons ($-CH_2-$ or -CHD-)? This can be done by first doping the film with sodium or potassium and then washing the doped film with alcohol [70] or alcohol-OD [166]. The mole ratio $\Delta H/Na$ or $\Delta H/K$ of increased hydrogen (or deuterium) content in the polymer (ΔH) and the dopant content in the doped precursor polymer (Na or K) is close to one at levels of heavy dope-hydrogenation [70,166], implying one to one correspondence of the dopant site and the CH_2 site. It is interesting to know whether dopant atoms exist as clusters of atoms or they are separated one (atom) by one. If they exist as isolated atoms, only the CH_2 rocking and CH_2 bending vibrations of isolated CH_2 group (=CH-CH_2-CH=) will be observed in the infrared spectra of the hydrogenated polymer films. If they exist as clusters of atoms, those vibrational bands due to consecutive methylene groups [=CH-$(CH_2)_k$-CH=] will be observed, k depending on the size of clusters. As another result of hydrogenation, the conjugation is broken and short conjugated segments are produced at the expense of long segments. The conjugation lengths of the increased segments (distances between dopant sites) will be estimated by the peak frequencies of intensity-increased Raman bands.

Infrared spectra of hydrogenated samples and an as-prepared trans film are shown in Fig. 19. The CH_2 rocking band around 730 cm^{-1} is obscured by an overlapping ν_8 band of trans polyene part in samples $(CH_{1.01})_x$ - $(CH_{1.17})_x$ (Figs. 19b-d) while the 744 cm^{-1} peak (k = 3) and the shoulders at 768 (k = 2) and 720 cm^{-1} ($k \geq 4$) on top of the much weakened ν_8 are observed in $(CH_{1.34})_x$ (Fig. 19e). The content of $(CH_2)_k$ ($k \geq 4$) is small since the 720 cm^{-1} band is relatively weak. The CH_2 bending bands at 1432 and 1464 cm^{-1} are detectable in $(CH_{1.06})_x$ (Fig. 19c) and the

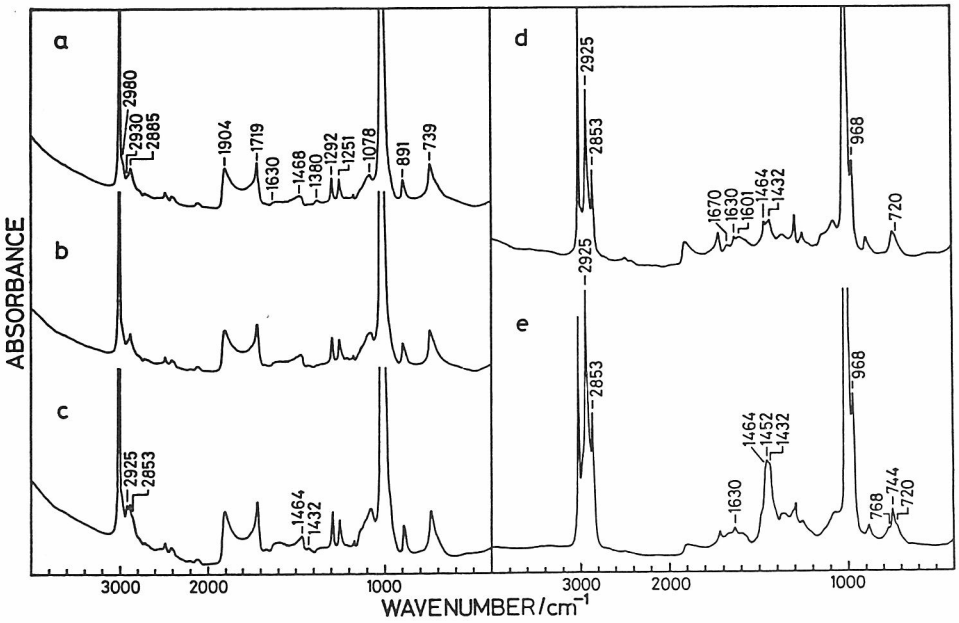

FIG. 19. Infrared spectra of trans-polyacetylene and partly hydrogenated samples. (a) trans-$(CH)_x$. (b) $(CH_{1.01})_x$, (c) $(CH_{1.06})_x$, (d) $(CH_{1.17})_x$, and (e) $(CH_{1.34})_x$. The vertical scale of (e) is 1.5 times those of (a)-(d). Used by permission, Ref. [70].

intensities of these bands together with those at 1442 and 1452 cm^{-1} are significant in Figs. 19d and e. The 1432 cm^{-1} band is assignable to isolated CH_2 and those at 1442, 1452, and 1464 cm^{-1} to longer isolated $(CH_2)_k$ groups, in that order. A band characteristic of long trans-methylene chain (at 1475 cm^{-1}) is missing in all the spectra. These observations indicate that most of the dopant sodium exist as isolated atoms or a cluster consisting of 2-5 atoms. It is generally noticed that the shape and intensity of the ν_1 band in the 1630-1460 cm^{-1} region change on hydrogenation. The change in the 1460 cm^{-1} region is due to a complex result of the appearance of the CH_2 bending bands and a decrease of long conjugated segments. The intensity increase in the region above 1500 cm^{-1} with some additional peaks reflects increased amounts of short conjugated segments yielded by the hydrogenation. A fairly strong band at 968 cm^{-1} due to the CH out-of-plane bend of isolated trans-RCH=CHR' (Figs. 19d and e) indicates that some dopant sites are closely located (like -CH*=CH-CH=CH*- which is converted to $-CH_2-CH=CH-CH_2-$) in heavily Na-doped $(CH)_x$ [70].

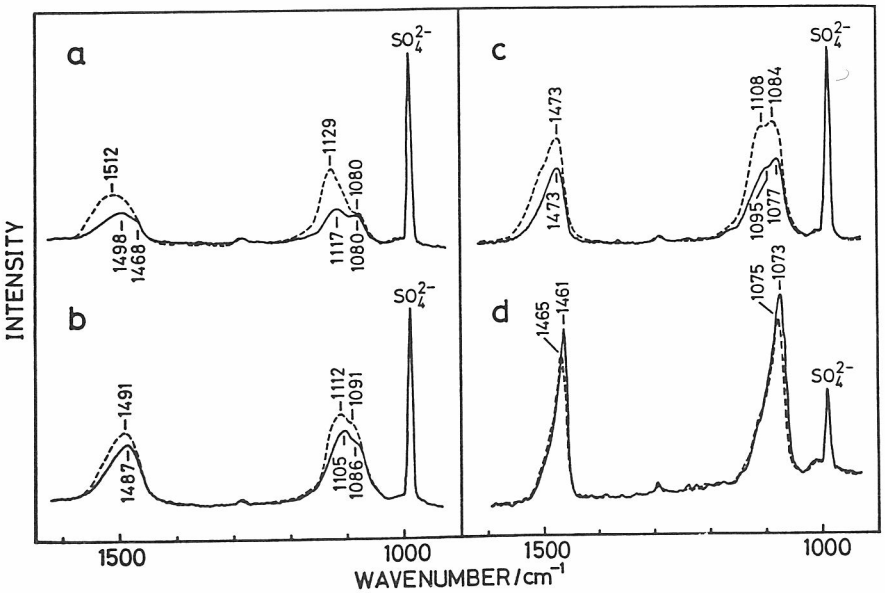

FIG. 20. Raman spectra of a partly hydrogenated trans-polyacetylene, $(CH_{1.16})_x$ (dotted line) and the precursor trans-$(CH)_x$ (solid line) excited at (a) 457.9 nm, (b) 488.0 nm, (c) 514.5 nm, and (d) 632.8 nm. Intensities are normalized to that of the 984 cm^{-1} band of SO_4^{2-} ion of a $BaSO_4$ single crystal plate (orthorhombic) pressed on the surface of the sample and corrected to the absorbance and reflectance at the respective excitation wavenumber and the absorbances at the Raman scattering wavenumbers. Used by permission, Ref. [70].

Figure 20 shows the Raman spectra of $(CH_{1.16})_x$ and the precursor trans-$(CH)_x$. The intensity decrease at 1461 cm^{-1} ($N_{C=C}$ = 103 if Eq. (1) is applied) is about 20% and the increase is 170% at 1545 cm^{-1} ($N_{C=C}$ = 7), 90% at 1512 cm^{-1} ($N_{C=C}$ = 12), 70% at 1498 cm^{-1} ($N_{C=C}$ = 16), 30% at 1491 cm^{-1} ($N_{C=C}$ = 19), and 40% at 1473 cm^{-1} ($N_{C=C}$ = 37). Thus it can be said that most of very long segments which give rise to the 1461 cm^{-1} peak have been dope-hydrogenated and the segments of 7-40 $N_{C=C}$ have been produced. The latter indicates that most dopants (atom and cluster) are randomly separated by 7-40 C=C bonds in heavily doped trans-$(CH)_x$ [70]. In lightly doped trans-$(CH)_x$, the dopants are separated by 16-35 $N_{C=C}$ and there remain very long segments of more than 100 conjugation [70].

B. cis-Polyacetylene

It is interesting that polyacetylene takes the cis-transoid structure in the as-polymerized state at low temperature, because such a configuration is very unstable in oligoene molecules and all cis-transoid isomer is scarcely isolated. The vibrational analysis is expected to provide knowledge on the force field of such an unstable configuration. Lack of data on model compounds, on the other hand, makes it difficult to make conclusive assignments of the vibrational spectra.

Analysis of vibrational spectra of cis-polyacetylene may be based on the infinite planar cis-transoid structure containing four each of carbon and hydrogen per repeating unit cell. The factor group is isomorphous to the point group D_{2h} and there are eleven Raman active ($4A_g + B_{1g} + 4B_{2g} + 2B_{3g}$), seven infrared active ($3B_{1u} + B_{2u} + 3B_{3u}$), and two optically inactive ($2A_u$) vibrations.

1. Raman Spectra

Raman spectra of cis-rich films with various excitation wavelengths have been reported [7,58,59,61,67,167,168]. Assignments of the major three bands at 1540, 1250, and 910 cm^{-1} in Fig. 21a (excited at 600 nm near the absorption maximum of the first peak in the visible spectrum) are unambiguous on the basis of the ^{13}C and D isotope effects (Figs. 21b and c, and Table 5) [67,169]. These bands are roughly the C=C stretch (ν_2), the CH in-plane bend (ν_3), and the C-C stretch (ν_4), respectively.

The peak frequencies of ν_3 and ν_4 for a wide range of excitation wavelengths are shown in Fig. 22. The frequencies are mostly constant except that small but sharp decreases are observed at about 1.97 eV (629 nm) in both cases [67]. The ν_2 band also exhibits small downshifts as the excitation wavelength becomes long [58,67]. All these shifts are very much smaller than those of ν_1 and ν_3 in trans-polyacetylene. Since the relations between cis conjugation length and the Raman frequencies are not established because of the lack of the data of oligomers except the frequency (1622 cm^{-1}) of cis-hexatriene (liquid) [170], a conclusive interpretation has not been made yet. It is suggested that these shifts arise from selective excitation of different cis polyene chains with slightly different vibrational and electronic energies [67]. The well-resolved vibrational structure in the optical absorption spectrum of a cis-rich film indicates a high mean value of the cis conjugation lengths [58]. Interestingly, the Raman cis bands change little in frequency and width during the thermal isomerization from cis-film to trans

TABLE 5
Observed Frequencies (in cm^{-1}) of cis-polyacetylenes and Assignments

		$\nu_{obs.}$			r^a		
		$(CH)_x$	$(CD)_x$	$(^{13}CH)_x$	obs.	calc.[b]	Assignment
A_g	ν_1	--	--	--	--	1.35	ν_{CH}
	ν_2	1540[c]	1470[c]	1500[d]	1.05	1.03	$\nu_{C=C}$
	ν_3	1250[c]	976[c]	1231[d]	1.28	1.34	δ_{CH}
	ν_4	910[c]	835[c]	881[d]	1.09	1.08	ν_{C-C}
B_{1g}	ν_5	826[c]	685[c]	816[d]	1.21	1.21	π_{CH}
B_{2g}	ν_6	--	--	--	--	1.35	ν_{CH}
	ν_7	1390[c]	--	--	--	1.11	$\nu_{C-C}+\delta_{CH}$
	ν_8	1170[c]	917[c]	--	1.28	1.18	$\nu_{C-C}+\delta_{CH}$
	ν_9	755[c]	--	750[d]	--	1.13	δ_{CCC}
B_{3g}	ν_{10}	--	--	--	--	1.20	π_{CH}
	ν_{11}	600[c]	558[c]	583[d]	1.08	1.18	$\tau_{C=C}$
A_u	ν_{12}	983[c]	765[c]	--	1.28	1.30	π_{CH}
	ν_{13}	295[c]	270[c]	283[d]	1.09	1.09	τ_{C-C}
B_{1u}	ν_{14}	3047[d,e,f,g]	2248[d,e]	3026[d]	1.36	1.36	ν_{CH}
	ν_{15}	1330[d,e,f,g]	1048[d,e]	1319[d]	1.27	1.27	δ_{CH}
	ν_{16}	447[d,e,f,g]	402[d,e]	435[d]	1.11	1.11	δ_{CCC}
B_{2u}	ν_{17}	740[d,e,f,g]	546[d,e]	738[d]	1.36	1.36	π_{CH}
B_{3u}	ν_{18}	3058[d,e,f,g]	2266[d,e]	3045[d]	1.35	1.35	ν_{CH}
	ν_{19}	1483[g]	--	--	--	1.02	$\nu_{C=C}$
	ν_{20}	1246[d,e,f,g]	890[d,e]	1249[d]	1.40	1.40	δ_{CH}

[a] $r = \nu(CH)/\nu(CD)$.
[b] Ref. [182].
[c] Ref. [67].
[d] Ref. [169].
[e] Ref. [180].
[f] Ref. [162].
[g] Ref. [183].

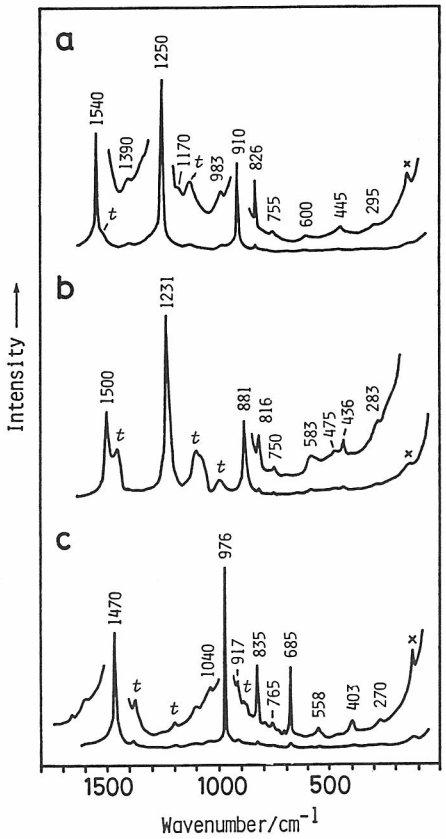

FIG. 21. Raman spectra of cis-polyacetylenes. (a) cis-$(CH)_x$ (600 nm, 77K) [67], (b) cis-$(^{13}CH)_x$ (^{13}C > 91%, 632.8 nm, 77K), and (c) cis-$(CD)_x$ (600 nm, 77K) [67]. Peaks with t are due to trans segments and those with x are ghost lines. Adapted from [67] and [169].

film [67,168]. This is in contrast to the marked changes in the profiles of the trans bands during the isomerization [67,168, 171,172].

A long progression of overtone and combination bands are observed in addition to broad luminescence bands at about 1.9 eV (653 nm) and 1.5 eV (827 nm) as shown in Fig. 23 [173-177]. A Franck-Condon analysis can give a satisfactory fit to the Raman excitation profiles for not only the fundamentals but also the first overtones and combinations [178]. The emission at 1.9 eV turns on sharply for excitation energies greater than 2.05 eV, indicating a Stokes shift of 0.15 eV [173]. It arises from the cis segments because it is quenched by thermal isomerization [173-175]. On the other hand, during the thermal treatment the 1.5 eV band shifts to lower energy with decreasing intensity and even in a fully converted trans film the band is observed at 1.2 eV (1033 nm) [174,176]. Thus, the 1.2 - 1.5 eV band is associated with trans segments existing in a cis-rich film [174,176]. Imhoff et al. [174] proposed that the band is assigned to trans 2^1A_g luminescence. In this connection Kajzar et al. [179] have indicated the presence of the

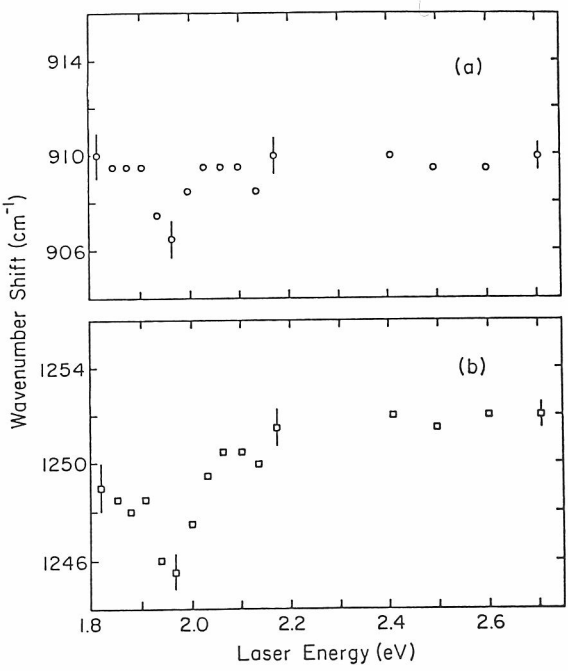

FIG. 22. Raman peak frequencies (in cm^{-1}) of cis-$(CH)_x$ vs. excitation photon energy (in eV). (a) ν_4 and (b) ν_3. Sample was 96% cis, held at 77K. Used by permission, Ref. [67].

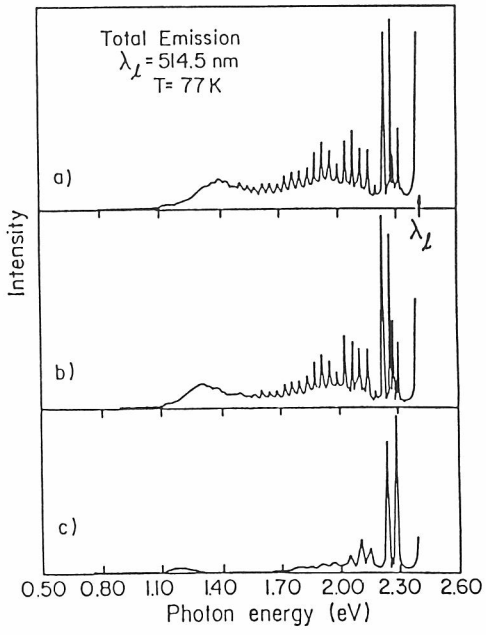

FIG. 23. Polyacetylene Raman scattering and photoluminescence excited by 514.5 nm (2.41 eV) light (77K). The cis fractions are about (a) 90, (b) 80, and (c) 0%. Used by permission, Ref. [174].

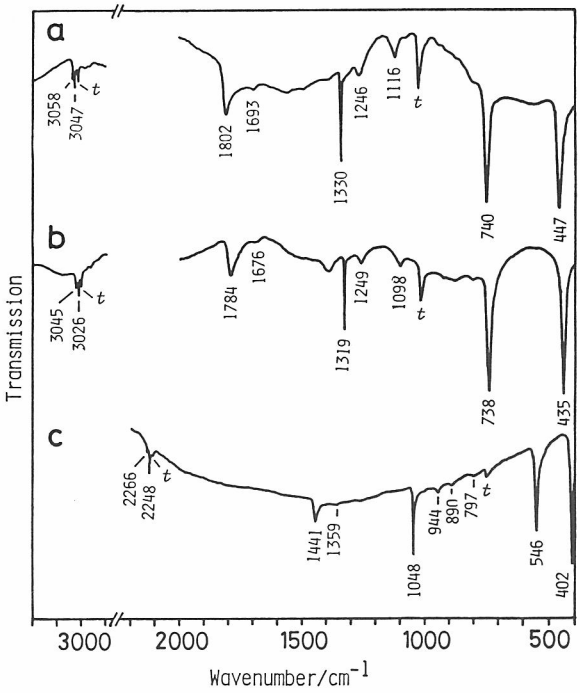

FIG. 24. Infrared spectra of cis-polyacetylenes. (a) cis-$(CH)_x$, (b) cis-$(^{13}CH)_x$, and (c) cis-$(CD)_x$. Peaks with t are due to trans segments.

trans 2^1A_g state at 1.9 eV by measurements of the third order optical susceptibility (χ^3) through a technique of the third harmonic generation.

2. Infrared Spectra

In the infrared spectrum of a thin cis-rich film the strongest band at 740 cm^{-1} is assigned to the CH out-of-plane bending vibration (ν_{17}) of cis -CH=CH- [5] based on the 2 and 194 cm^{-1} downshifts on ^{13}C and D substitutions, respectively (Fig. 24). The intensities of this and trans ν_7 (1012 cm^{-1}) bands have been useful in estimating the contents of the trans and cis parts in polyacetylene [4,56,57]. The relation between the compositions and the intensities of these bands was obtained under the assumption that each band arose solely from trans or cis part,

$$[C](\%) = 100 \times [fA_{740}/(fA_{740} + A_{1012})] \quad (3)$$

$$[T](\%) = 100 - [C] \quad (4)$$

where [C], cis content; [T], trans content; A_{740}, absorbance of the 740 cm^{-1} band; and A_{1012}, absorbance of the 1012 cm^{-1} band [4,56,57]. The f value was estimated to be 1.30 ± 0.01 [4], 1.66 ± 0.11 [56], or 1.57 ± 0.20 [57]. This equation is applicable to the estimation of cis and trans contents, because the compositions obtained with f = 1.57 agreed well with those determined by cross polarization (CP) MAS-NMR [57]. Although this equation is not exact because the 740 cm^{-1} band has a small contribution from a trans band as described in Sec. II.A.4, it seems to be practically usable except at the final stages of isomerization.

3. Assignments of Infrared and Raman Bands

The assignments of the infrared bands of cis-polyacetylene were first proposed by Shirakawa and Ikeda [5] and modified on the basis of the data of polarized infrared spectra of highly oriented films [162,180]. Raman spectra were first assigned by Kuzmany [61], and Lichtmann et al. proposed different assignments of A_g species based on the data of a film with less trans contents (96% cis) [67]. A normal coordinate calculation of in-plane vibrations of infinite cis-transoid structure [181] and an ab initio calculation including the out-of-plane vibrations [182] were performed. However, the complete assignments have not been established yet due to lack in vibrational data of smaller cis-transoid molecules. In Table 5 are given possible assignments based on the ab initio calculation [182], frequency shifts on deuteration [67] and ^{13}C substitution [169], and infrared dichroism [162,180,183]. Some comments are made in the followings.

Since only one vibration belongs to each of the B_{1g} and B_{2u} species, the ratio (r) of the frequencies of isotopomers is equal to the ratio of the G-matrix elements and independent of the force constants. The good agreements between the observed and calculated ratios seem to support the assignments of B_{1g} and B_{2u} species.

In the Raman spectra some additional bands that are not assignable to gerade fundamentals are observed. The Raman bands at (445, 436, 403 cm^{-1}) for [$(CH)_x$, $(^{13}CH)_x$, $(CD)_x$] are assigned to ν_{16} (B_{1u}) because the frequencies agree well with those of strong infrared bands at (447, 435, 402 cm^{-1}). The Raman bands at 983 and 295 cm^{-1} in $(CH)_x$ and those at 765 and 270 cm^{-1} in $(CD)_x$ are assigned to ν_{12} and ν_{13} in A_u species, because the frequencies and r's correspond well with the results of the ab initio calculation [182]. The band at 299 cm^{-1} observed in the far-infrared [184] also is considered to arise from ν_{13}. Accordingly, D_{2h} symmetry [29] does not hold strictly for cis-polyacetylene. A possible explanation for the

observations is that the polymer chain is not planar but twisted slightly around the double and/or single bonds. It is interesting to note that the distortion of 10° around the C-C bonds is reported for cis-hexatriene by an electron diffraction study [185].

C. Doped Polyacetylene

One of the properties of conjugated polymers is the small band gap between LUMO and HOMO as is evident from the visible absorption spectra. This leads to a small ionization potential and large electron affinity. Upon doping with an electron acceptor like iodine and AsF_5, part of the π-electrons in the conjugated polymer are donated to the acceptor and the electrical conductivity of the material increases drastically (insulator → semiconductor → metallic conductor). The conjugated polymer can also be doped by a donor like Na and K and accepts electrons from the dopant becoming a conductor. Doping is expressed in the following charge transfer reactions,

$$P_x + xyA \rightarrow (P^{+y}A_y^-)_x \tag{5}$$

and

$$P_x + xyD \rightarrow (P^{-y}D_y^+)_x \tag{6}$$

where P is the minimum structural unit like CH in polyacetylene, A is acceptor, and D is donor. P_x is a conjugated polymer. Acceptor and donor become A^- anion and D^+ cation, respectively, through one electron transfer. On the other hand, in polymer P_x only y ($y < 0.3$) electrons per one structural unit P are transferred. According to theories, the charge on the polymer is not localized at one particular unit P that is closest to a dopant but is delocalized among P_z where z (in polyacetylene) is predicted to be about 15 [81] (or 7-8 C=C double bonds). Then, at a dopant concentration of $y = 0.01$, i.e., one dopant per 100 P or 50 CH=CH, each P_z is isolated by surrounding undoped (insulating) parts of $N_{C=C} = 43$. If $y = 0.1$, i.e., one dopant per 10 P, each doped P_z is overlapped by the neighboring doped P_z and electrons tend to be delocalized throughout the polymer chain. In practice, some dopants exist as clusters and undoped (but possible perturbed) parts still exist in heavily doped material as has been seen in the hydrogenated polyacetylene (Sec. II.A.6). The difference in structure between P_z^+ and P_z^- is apparent in the vibrational spectra although the infrared spectra of donor doped polyacetylenes have not yet been extensively studied because of experimental difficulties.

As mentioned previously, cis → trans isomerization takes place upon doping a cis film. Detailed studies on structural changes in the repeated doping-undoping processes have been reported [129].

1. Doping Induced Infrared Spectra of Lightly Doped Polyacetylene

Figure 25 shows infrared difference spectra of lightly iodine doped ($y < 0.01$) trans $(CH)_x$, $(^{13}CH)_x$, and $(CD)_x$ [62]. Doping with other acceptors gives practically the same spectral pattern [129]. Polarization measurements of stretch-oriented $(CH)_x$ films have shown that these doping-induced infrared absorptions are polarized primarily along the polymer chain [115,162], which is indicative of predominant contributions of in-plane vibrations to the infrared activity compared with out-of-plane ones. Major infrared bands of doped $(CH)_x$ are at 1397 (to be termed ν_{d1}), 1288 (ν_{d2}), and 888 cm^{-1} (ν_{d3}). The frequencies are reported differently depending on the samples: ν_{d1}, 1398 - 1390 cm^{-1}; ν_{d2}, 1290 - 1288 cm^{-1}; ν_{d3}, 880 - 830 cm^{-1}. All the bands show ^{13}C- and D-shifts like the Raman ν_1 - ν_3 bands. In fact, the frequency of ν_{d2} is practically the same as that of Raman ν_2 and its $\Delta\nu(^{13}C)$ (-38 cm^{-1}) and $\Delta\nu(D)$ (-78 cm^{-1}) are similar to those of ν_2, -35 and -92 cm^{-1}, respectively. On the other hand, $\Delta\nu(^{13}C)$ of ν_{d1} (-15 cm^{-1}) is smaller than that of ν_{d3} (-25 cm^{-1}) contrary to the Raman $\Delta\nu(^{13}C)$, -27 cm^{-1} of ν_1 vs. -25 cm^{-1} of ν_3. The deuteration shift of ν_{d1} (-257 cm^{-1}) is largest as is that of Raman ν_3 (-224 cm^{-1}) and the value of ν_{d3} (-98 cm^{-1}) is similar to that of Raman ν_1 (-105 cm^{-1}). Namely, the vibrational modes of ν_{d1} and ν_{d3} correspond to those of ν_3 and ν_1, respectively, while the ν_{d2} mode is similar to the ν_2 mode. Then, what kind of structural change is induced by the doping?

Infrared spectra of doped copolymers provide information on doped domain and the vibrational mode behaviors (Fig. 26) [148,149]. The spectra are hardly accounted for by concentration-weighted superpositions of those of doped $(C_2H_2)_x$ and $(C_2D_2)_x$, indicating that the absorptions are not concerned with only one (doped) monomer unit but induced by generation of a doped domain consisting of more than one monomer unit. The spectra of doped copolymers reflect statistical distribution of C_2H_2 and C_2D_2 units within such domain. As indicated in the figure the ν_{d1} band shows two-mode behavior, while the ν_{d2} and ν_{d3} bands show one-mode behavior. So for these behaviors to be observed, the doped domain must be composed of several or more successive monomer units. The abovementioned expectation of ν_{d1} - ν_3 and ν_{d3} - ν_1 correspondences is supported by the mode behaviors. The mode behavior of ν_{d2} turned out to be different from that of ν_2. Since

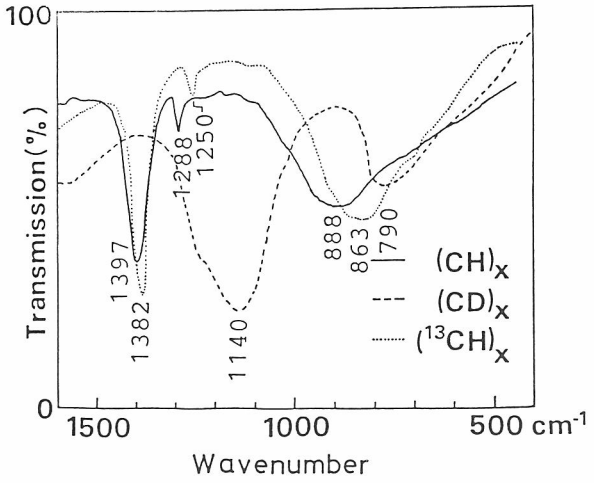

FIG. 25. Infrared difference spectra of iodine-doped trans-polyacetylenes. The dopant concentrations are less than 0.01. Adapted from Ref. [62].

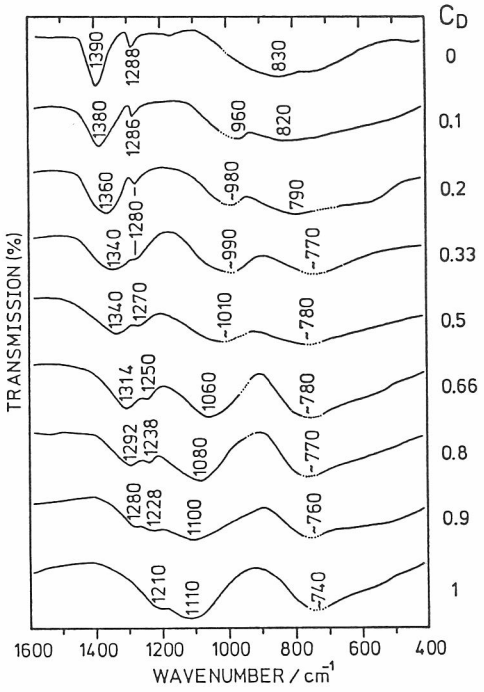

FIG. 26. Infrared spectra of iodine-doped trans-polyacetylenes with various C_D values. Used by permission, Ref. [148].

the spectral behavior of a band on isotopic mixing is a direct consequence of the force field, the force field for the doped part of polyacetylene must differ significantly from that for pristine polymer. Presumably, the electron delocalization as a result of the charge transfer induces a decrease in the 'C=C' stretching force constant and causes the ν_1 frequency to decrease to 888 cm^{-1} and the ν_3 frequency to increase to 1397 cm^{-1}. Since both ν_1 and ν_3 are one and the other of two coupled modes of s_1 and s_2 basis modes, frequency alternation between the two is possible depending on the relative values of 'C=C' stretching and CH bending force constants.

Concomitant with the appearance of the three infrared bands, the absorption in the visible region decreases in intensity and a new band appears in the near infrared (Fig. 4). On further doping the latter band shows a great enhancement of intensity and a shift of absorption maximum toward lower frequencies. Consequently, the whole infrared region becomes nontransparent. However, Rabolt et al. were able to find that the ν_{d3} band in AsF_5-doped $(CH)_x$ shifts significantly to a lower frequency as the dopant concentration is increased [118]. Similar but much smaller shifts are also found for the other bands. This observation may imply that the ν_{d3} mode is especially sensitive to interaction among neighboring charged domains.

Very recently [186], Castiglioni et al. have shown that the three Raman A_g frequencies (ν_1, ν_2, and ν_3) and the three infrared doping-induced or photogenerated bands (ν_{1d}, ν_{2d}, and ν_{3d}) are explained by simply changing the value of long range interaction force constants (ΔK in the paper). It was shown that the modes of ν_1 and ν_3 are actually interchanged as the diagonal C=C stretching force constant is decreased as a result of a large negative contribution from the long range forces in the latter cases.

Although the infrared spectrum of a doped sample reflects the structure and properties of doped domains in the polymer chains, it can not be simply correlated with electrical conductivity, a macroscopic property. In Fig. 27 are compared the infrared spectra of lightly iodine doped hydrogenated polyacetylene (Sec. II.A.6) with that of doped polyacetylene. The spectra are quite similar to one another while the conductivities at the maximally doped state are significantly low for the hydrogenated samples. In the case of a heavily hydrogenated sample $(CH_{1.34})_x$, changes in peak frequencies and band shapes of ν_{d1} and ν_{d3} are observed as the doping proceeds (Fig. 27e), indicating that very short as well as long conjugated segments are doped and the structures are slightly different among the doped domains formed within long segments and short ones [70,187].

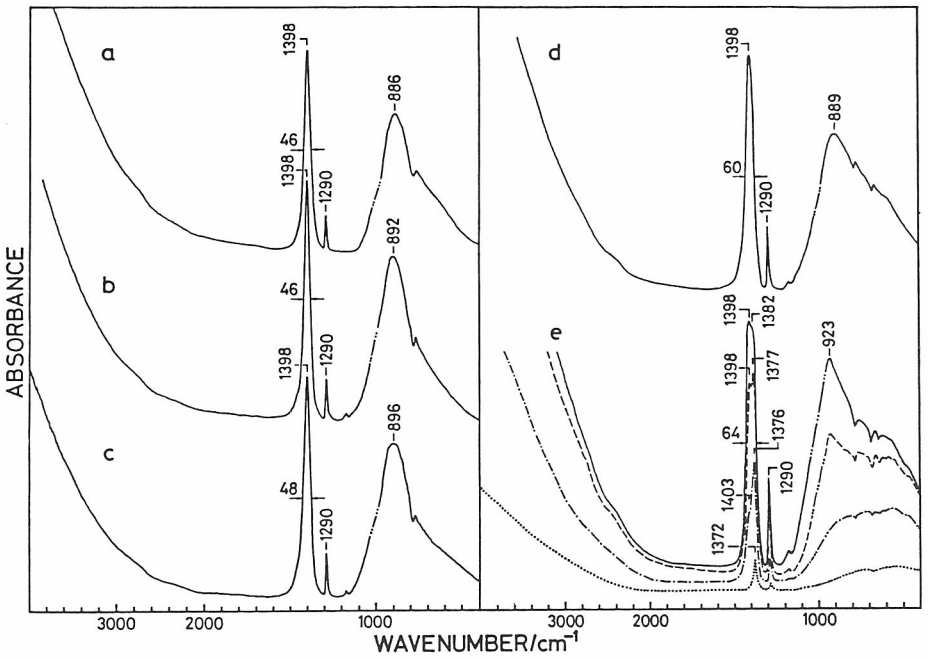

FIG. 27. Infrared difference spectra of iodine-doped trans-polyacetylenes and partly hydrogenated samples. (a) Doped trans-$(CH)_x$ (iodine content < 0.1%; conductivity at the maximum doping, 1.6×10^2 Scm^{-1}), (b) doped $(CH_{1.01})_x$ (< 0.1%; 1.1×10^2), (c) doped $(CH_{1.06})_x$ (0.2%; 7.4×10), (d) doped $(CH_{1.17})_x$ (1%; 8.1×10^{-1}), and (e) doped $(CH_{1.34})_x$ (1% for the solid-line spectrum; $<10^{-4}$). Spectra at different iodine contents are shown in (e). Used by permission, Ref. [70].

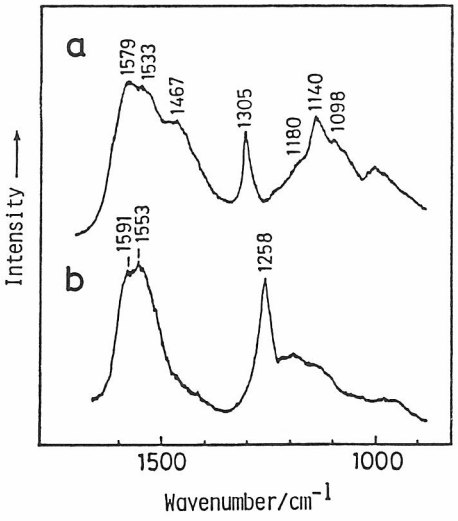

FIG. 28. Raman spectra of (a) AsF_5-doped trans-$(CH)_x$ and (b) Na-doped trans-$(CH)_x$ with 488.0 nm excitation (room temperature). Adapted from Ref. [121].

2. Raman Spectra of Heavily Doped Polyacetylene

Raman spectra of trans-polyacetylene heavily doped with AsF_5 (Fig. 28a) and Na (Fig. 28b) are quite different from that of pristine films (Fig. 6), indicating large structural changes upon doping [62,121]. The Raman spectra reported by other authors [61,122-126,128,188] are similar to these spectra. As described in Sec. II.C.1, charged domains are formed at a lightly doped state. Raman spectra of lightly doped trans-polyacetylene are essentially the same as that of pristine film with decreased band intensities, because the Raman bands of the doped part are negligibly weaker than those of the undoped part due to the off-resonant condition for the former (Sec. II.D). The Raman spectra of heavily doped films can be interpreted by a mixture of the bands attributed to charged domains and remaining polyene parts, as described below. In the AsF_5-doped spectrum of Fig. 28a, two bands at 1579 and 1533 cm^{-1} are observed in the C=C stretching region. These frequencies correspond to those of segments of conjugation lengths, 5 and 8, respectively, if we simply apply Eq. (1). As the excitation wavelength becomes short, the frequencies of the bands become high and the relative intensities strong. Thus, these bands are assigned to the ν_1 vibrations arising from the remaining polyene parts. Based on similar reasons the band at 1140 cm^{-1} is assigned to ν_3 of the polyene parts. The 1467 cm^{-1} band becomes strong as the excitation wavelength is lowered, which is explained as a result of post-resonance with the near-infrared absorption induced by doping. Accordingly, this band arises from the gerade modes corresponding to the infrared ν_{d1} in the doped domains. The origin of the 1305 cm^{-1} band is complicated. Its intensity depends little on excitation wavelength. Since the ν_2 frequency is independent of the excitation wavelength and the infrared ν_{d2} frequency also coincides with the Raman ν_2, the band is assigned to an overlap of the ν_2 bands in the polyene parts and the gerade ν_{d2} bands in the doped domains. The weak and broad band extending from 1005 cm^{-1} to lower frequency is assigned to the gerade ν_{d3} in the doped domains.

The Raman spectrum of donor-doped trans-polyacetylene (Fig. 28b) is slightly different from that of the acceptor-doped one (Fig. 28a). As described above, the bands at 1591 and 1553 cm^{-1} and the broad one in the 1200 - 1100 cm^{-1} region arise from ν_1 and ν_3 vibrations in the remaining polyene parts, respectively. The 1258 cm^{-1} band is assigned to the gerade ν_{d2} of charged domains. (The infrared ν_{d2} is observed at 1268 cm^{-1} [189].) The frequency is 47 cm^{-1} lower than the gerade ν_{d2} of the acceptor-doped sample (1305 cm^{-1}), indicating the structural difference between the positively charged and negatively charged domains. The weak ν_2 peak of the polyene

part is overlapped by the contour at the high frequency side of ν_{d2}. The reason of missing (or very weak) ν_{d1} is yet to be studied.

Tanaka et al. [126] have studied the dependence of Raman spectra on dopant (Na) concentration. Spectral changes have been attributed to the changes from isolated charged soliton structure to repeating structure of a charged soliton, a single -C=C- bond, and a uniform chain unit. According to them, the observed band at 1570 cm^{-1} (assigned to the -(C=C)- stretch) indicates the absence of a long uniform structure consisting of bonds of an equal bond order [126]. However, these observations also can be interpreted by the coexistence of a series of doped structures and remaining short undoped polyene parts in the heavily doped films.

Raman and infrared spectroscopy affords also the information of dopant species [190,191]: for example, $(I_3^-)_x$, 105 and 210 cm^{-1} (Raman).

D. Correlation Between Structure of Pristine trans-Polyacetylene and Conductivity Upon Doping

As explained in Sec. II.A.4, it is possible to tell from the infrared ν_1 band shape the relative contents of segments with different conjugation lengths. Raman spectra of Film A and Film B mentioned earlier (with infrared spectra in Fig. 2) are shown in Figs. 29a and c. The spectra were taken at 80K with 457.9 nm excitation. The low frequency components in the ν_1 and ν_3 regions arise from the long segments with the off-resonance condition and the high frequency peaks are the resonance enhanced scattering from the short segments which absorbs the 457.9 nm light. The difference in compositions is clearer in these figures than it is in Fig. 2. The content of long segments in Film B has been estimated 0.6 times that in Film A [157,187]. Upon light doping with iodine, all the peaks lose intensities (Figs. 29b and d). They arise from the remaining undoped segments. Practically, the Raman bands of doped segments are not observed in the spectra because of the off-resonance condition mentioned in Sec. II.C.2. Accordingly, the decreased intensities are directly related to the amounts of doped short and long segments. If one measures the Raman spectrum and electrical conductivity of each doped film, one can study the relation between the conductivity and the amounts of doped segments. In Fig. 30 are plotted the conductivity versus the decrease in intensity (ΔI). The important finding is that good correlation exists between electrical conductivity and the amount of doped long segment. In other words, the doped long segments play the major role in the electrical conduction, at least, at the low doping levels. At heavy doping levels, Raman bands of doped parts overlap the much weakened bands

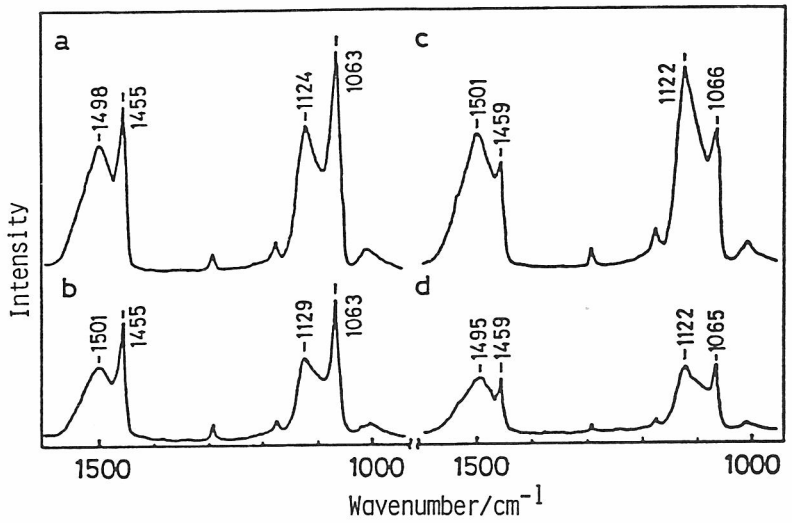

FIG. 29. Raman spectra of trans-$(CH)_x$ and iodine-doped trans-$(CH)_x$ (457.9 nm, 80K). (a) trans-$(CH)_x$ (Film A, see the caption of Fig. 2), (b) iodine-doped Film A [σ = 0.5 Scm^{-1}, $(CHI_{0.011})_x$], (c) trans-$(CH)_x$ (Film B, see the caption of Fig. 2), and (d) iodine-doped Film B [σ = 1 Scm^{-1}, $(CHI_{0.042})_x$]. The spectra are normalized to the intensity of the 984 cm^{-1} band of $BaSO_4$ single crystal. Used by permission, Ref. [157].

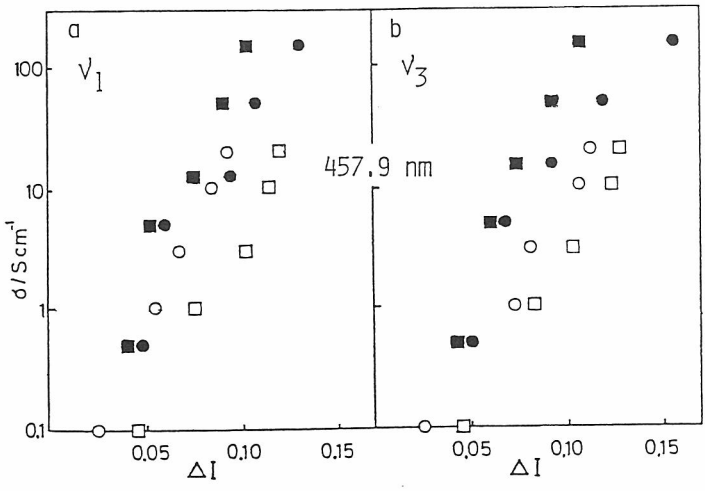

FIG. 30. Relation between electrical conductivity (σ) and decreased intensities (ΔI's) of (a) ν_1 and (b) ν_3 (457.9 nm, 80K). •; ν_1 (1455 cm^{-1}) and ν_3 (1063 cm^{-1}) due to long segments in Film A. o; ν_1 and ν_3 due to long segments in Film B. ■; ν_1 (1498 cm^{-1}) and ν_3 (1124 cm^{-1}) due to short segments in Film A. □; ν_1 and ν_3 due to short segments in Film B. See Fig. 29. Adapted from Ref. [157].

of undoped parts and the method is impractical. At the maximum doping, the conductivity of Film A (190 Scm^{-1}, at I/C=C = 0.45) is much larger than that of Film B (10 Scm^{-1}, at I/C=C = 0.49) although the content of long segments in Film B is not significantly low compared to that in Film A as mentioned above. This has been explained as a result of inadequate contacts between long polyenes in Film B due to the distortion of polymer chains caused by the intervening short segments. In order that a high electrical conductivity is attained, a film must be rich in long conjugated segments (intra-chain conductivity) with few sp^3 carbons and kinks, and adequate contacts among the long doped polyene segments (inter-chain conductivity) must be held as well as those among the fibrils (inter-fibril conductivity).

III. POLYTHIOPHENE

The films prepared by electrochemical polymerization of thiophene are conducting (10^{-2}-10^{2} Scm^{-1}), the conductivity being dependent on the synthetic conditions [192-204]. They are doped with electrolyte anions (BF_4^-, ClO_4^-, etc.) during the polymerization and the dopant concentrations are 6.8-30 mol% per thiophene unit for BF_4^--doped films [194,196,199,201] and 14-26 mol% for ClO_4^--doped ones [193,203,204]. The maximum conductivity obtained so far for the as-polymerized film at room temperature is 190 Scm^{-1} (PF_6^--doped film with 17 mol% doping [200,202]). A high anisotropy in conductivity was reported: the ratio of the conductivity parallel to the surface to that perpendicular to the surface was ca. 10^5 [193,204]. The dopant can be removed (undoped) by electrochemical reduction and/or the treatment with ammonia water or gaseous ammonia. The undoped film, called neutral polythiophene, is insulating and stable in air. As the starting material, 2,2'-bithiophene [197,198,205,206], 2,2':5',2"-terthiophene [206,207], and substituted thiophenes [197,198,200,202,208-212] also have been used. Conductivity of PF_6^--doped poly(3-methylthiophene) was reported to be 510 Scm^{-1} [200,202]. Undoped films become conducting again on redoping with acceptors [201,213-216] and donors [213]. Neutral polythiophene and poly(3-methylthiophene) are synthesized also by condensation polymerization of 2,5-dihalothiophenes and its 3-substituted derivatives, respectively [217-222]. These polymers can be doped with electron acceptors and become conducting [217-227]. Although most of the polythiophenes are insoluble in organic solvents, neutral and doped polymers of 3-alkylthiophenes with large alkyl groups ($\geq$ butyl group) are soluble completely or partly in

common organic solvents such as THF, chloroform, benzene, etc. [210,211,220]. Because of their solubility, the degree of polymerization (N_{dp}) can be determined by vapor-phase osmometry [210,211,222] and gel permeation chromatography [212,221]. It is 2.3×10^2 for neutral poly(3-hexylthiophene) [210]. The density of neutral polythiophene was estimated to be 0.5-0.8 gcm^{-3} from the weight and volume measurement and 1.4 gcm^{-3} by the floating method [195].

Electrochemically prepared films can be smooth-surfaced, granular, or fibrillar, depending on the synthetic conditions [193,197,199,201,208,228,229]. Infrared and CP-MAS-NMR studies of neutral polythiophene [199,215,230-233] and poly(3-methylthiophene) [233-235] show that the electrochemical polymerization proceeds predominantly through α,α'-coupling. According to an X-ray diffraction study, the crystal data of chemically coupled neutral polythiophene are: either orthorhombic, a = 7.80, b = 5.55, and c = 8.03 Å; or monoclinic, a = 7.83, b = 5.55, c = 8.20 Å, and $\beta = 96°$ [236]. Polythiophene prepared by an electrochemical method is amorphous [192,229]. There is a report that electron and X-ray diffraction data for a $SO_3CF_3^-$-doped poly(3-methylthiophene) film prepared electrochemically imply a hexagonal lattice (a = 9.7 and b = 12.2 Å) consistent with a coil structure [229].

Neutral polythiophene films give rise to a π-π^* absorption at ca. 480 nm [195,199,202,203,205,206,213,220] and are transparent in the red region. Upon electrochemical doping, peaks at 0.6-0.7 eV (2070-1770 nm) and 1.5-1.8 eV (830-690 nm) appear and the 480 nm band decreases in intensity and shifts towards a short wavelength [205,213]. At the maximum doping a structureless absorption developing from the visible and increasing towards the infrared region is observed [205,237]. The interpretation of the spectral behavior is controversial. According to Heeger and coworkers on films prepared from 2,2'-bithiophene, dications exist at low doping levels (<20 mol%) and metal-like free carriers exist at the highest doping level [205,237]. An ESR study on such films indicated the presence of dication for concentrations up to at least 14 mol% [238]. On the other hand, absorption and ESR studies on films prepared from thiophene indicated the presence of two kinds of radical cations at low doping levels (<3 mol%), the formation of dications from the radical cations at intermediate doping levels, and metallic properties at high doping levels (>15 mol%) [239-242]. For poly(3-methylthiophene), analysis of g factor in ESR spectra of the doped films suggested that the electron transport occurs along the carbon skeleton of the polymeric chain [243]. An absorption study suggested the presence of radical cations at dilute doping levels [244]. A metal type reflectance with nearly zero transition energy was found for a heavily doped sample [245]. According to

ESR and spectroscopic studies on doped poly(3-hexylthiophene) in solution, the spinless dications is the lowest energy charge-storage configuration on a single polymer chain in dilute solution and radical cations are formed as a result either of storage of an odd number of charges on a single polymer chain or of interchain interactions [246,247]. A restricted Hartree-Fock SCF ab initio study on quaterthiophene at neutral and Na-doped states indicated the formation of charged defects such as dications associated with structural deformations [248]. The formation of one dication is thermodynamically more stable by 0.26 eV than that of two radical cations according to valence-effective Hamiltonian band-structure calculations [249].

Infrared and Raman spectra of neutral polythiophene, 2,5-^{13}C-substituted and deuterated analogs, and oligomers were studied [215,250-252]. N_{dp} was estimated from the intensity ratio of the infrared CH out-of-plane bends arising from 2-monosubstituted and 2,5-disubstituted thiophene rings [251]. Several key bands, sensitive to the structure of neutral polymer, were compared with the conductivity upon redoping with iodine and it was concluded that the conductivity of the doped film correlates better with the average conjugation length (N_c) in the polymers than with N_{dp} [215,251]. Infrared (absorption and ATR) and Raman spectra of doped polythiophene were reported [192,196,199,201,227,250,253,254]. Photoinduced absorption and ESR studies of chemically coupled neutral polythiophene showed that the dominant photoexcited charged species are dications [255,256]. On the other hand, in the case of neutral film prepared electrochemically from thiophene, the change of absorption spectrum induced by the photoexcitation suggested the formation of 'shallow' radical cations [239,240]. Infrared absorption of lightly doped film under DC electric field was studied [257]. Infrared and Raman spectra of neutral and doped poly(3-methylthiophene) were reported [253,258-260] and overtone and combination bands were observed in the resonance Raman spectra of the doped sample [260].

A. Key-Bands Sensitive to the Structure of Neutral Polythiophene

Infrared and Raman spectra of α,α'-coupled oligomers (2T, 3T, 4T, 6T, and 8T), and neutral films of polythiophene (PT), 2,5-^{13}C-polythiophene (PTC), and deuteropolythiophene (PTD) are shown in Figs. 31 and 32, respectively. The strong infrared band around 786-798 cm^{-1} in Figs. 31b-g and the band around 676-702 cm^{-1} in Figs. 31a-g arise from the CH out-of-plane bends of α,α'-disubstituted and α-monosubstituted thiophene rings, respectively [261]. The assignments of the weak band at 695 cm^{-1} in the

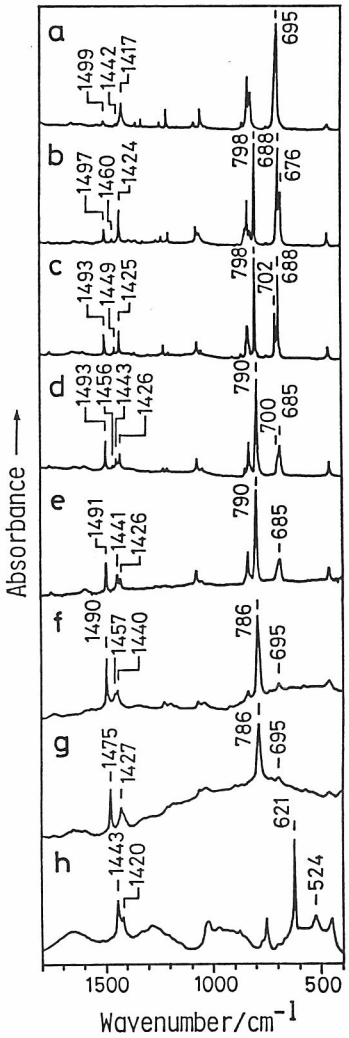

FIG. 31. Infrared spectra of (a) α-bithiophene (2T), (b) α-terthiophene (3T), (c) α-quaterthiophene (4T), (d) α-sexithiophene (6T), (e) α-octithiophene (8T), (f) polythiophene (PT), (g) 2,5-^{13}C-polythiophene (PTC), and (h) deuterated polythiophene (PTD). (a)-(e) in KBr disks and (f)-(h) in films.

polymers (Figs. 31f and g) as well as the strong band at 786 cm^{-1} to the CH bends are verified by the large downshifts on deuteration (Fig. 31h). The degree of polymerization can be estimated from the intensity ratio of the two bands, $R = I_2/I_{2,5}$ (I_2 = the area intensity of the 695 cm^{-1} band and $I_{2,5}$ = the area intensity of the 786 cm^{-1} band), by the following relation,

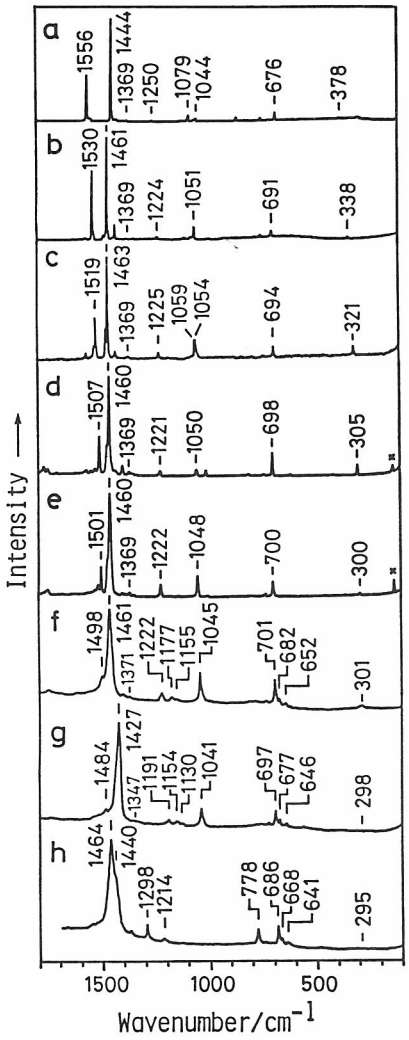

FIG. 32. Raman spectra of oligothiophenes and polythiophenes. (a)-(h) are of the same compounds as those in Fig. 31 except that the spectra of oligomers were taken for pure solid. (c)-(e) with 632.8 nm excitation and others with 514.5 nm excitation.

$$N_{dp} = 2R_0/R + 2, \tag{7}$$

where R_0 = 1.07 [251]. For example, R = 0.12 in Fig. 31f and hence N_{dp} is estimated to be 20 for the polymer.

Oligomers, 3T through 8T, are considered to take a trans-planar structure in the solid because the spectral patterns are similar to those of

2,2'-bithiophene (2T) which takes a trans-planar structure in the crystal [262]. In the infrared absorption a single band for each oligomer due to the C=C antisymmetric stretch [263] (ν_{as}^{ir}) lies in a narrow region of 1499-1491 cm^{-1} with increasing intensity from 2T to 8T, whereas, two or three C=C symmetric stretching bands (ν_{s}^{ir}) assignable to the modes with different phases are observed in the wide 1460-1417 cm^{-1} region with decreasing intensity from 2T to 8T. The intensity ratio of these bands (I_{sym}/I_{anti}) decreases monotonically (but not linearly) as the number of rings increases, implying that it serves as an approximate measure of average number of trans conjugated successive rings (N_c).

In the Raman spectra (Fig. 32), both frequency and intensity of the C=C antisymmetric stretch (ν_{as}^{R}) decreases as the number of thiophene rings increase (1556 cm^{-1} in 2T to 1501 cm^{-1} in 8T). In PT it is observed as a shoulder of the strong C=C symmetric stretch (ν_{s}^{R}) at 1461 cm^{-1}. Contrary to the large dispersion of ν_{as}^{R}, the ν_{s}^{R} frequencies are practically the same for 3T-8T and PT.

The Raman 1222 cm^{-1} band is assigned to the inter-ring CC stretch in the trans-planar part of the polymer on the basis of a large ^{13}C-shift (-31 cm^{-1}) and a small D-shift (-8 cm^{-1}), and a corresponding single band in this region in the spectra of solid oligomers. The 1045 cm^{-1} band is a pure CH in-plane bend, since it shifts down to 778 cm^{-1} on D-substitution. The bands at 1177 and 1155 cm^{-1} with large ^{13}C-shifts arise from the inter-ring CC stretches in the parts where the CC torsion angle is different from trans, because relatively strong ones at similar frequencies are observed for 3T in CS_2 and polar solvents with different intensity patterns indicating the co-existence or rotational isomers in addition to the trans-trans form (Fig. 33). Based on the reasoning similar to that described above, the 701 cm^{-1} band is assigned to the ring deformation in the trans coplanar part and the 682 and 652 cm^{-1} bands to those in the distorted parts (kinks). Hence, the intensity ratios, I_{1177}/I_{1222}, I_{1155}/I_{1222}, I_{682}/I_{700}, and I_{652}/I_{700} can be used as the indicators of the relative amounts of kinks of the same or different origin (A_k).

Vibrational assignments of neutral polythiophene are summarized in Table 6.

B. Structure-Conductivity Relation

Akimoto et al. studied the relation between the structure of neutral polymers in undoped films and the conductivity upon redoping them with a common dopant to the maximum [215,251]. They prepared ten doped films

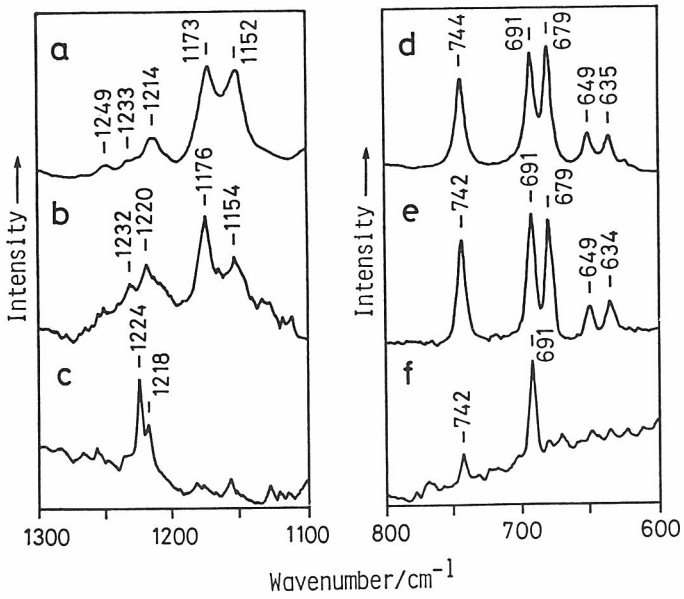

FIG. 33. Raman spectra of 3T in solutions and solid (514.5 nm). (a) and (d) acetonitrile solution, (b) CS_2 solution, (c) and (f) solid, and (e) 1,4-dioxane solution. Used by permission, Ref. [251].

with different synthetic conditions and undoped them. A part of each neutral film was used for spectroscopic measurements and the other part was doped maximally with iodine and the conductivity was measured. The infrared and Raman spectra of three of them are shown in Figs. 34 and 35, respectively. It is easily understood from the figures that N_{dp} and N_c decrease and A_k increases from PT-2 through PT-1 to PT-10. In Fig. 36 are plotted the conductivity vs. relative intensities of infrared and Raman bands. First we compare two films, one with the largest N_{dp} (PT-6, N_{dp} = 35, N_c = 3.5) and another with the largest N_c (PT-2, N_{dp} = 20, N_c > 8). The film with the highest N_{dp} does not necessarily contain long conjugated segments. The conductivity of PT-2 (2.0×10^2 Scm^{-1}) is four times higher than that of PT-6 (5.0×10 Scm^{-1}). Next we compare the three films which showed electrical conductivity higher than 100 Scm^{-1}. Conductivity, N_{dp}, I_{sym}/I_{anti} (N_c), and I_{682}/I_{700} of these films are: PT-2, 2.0×10^2, 20, 0.89 (>8), 0.16; PT-4, 1.7×10^2, 30, 1.10 (>8), 0.18; and PT-3, 1.2×10^2, 18, 1.60 (4), 0.23, respectively. Clearly, the conductivity correlates much better with N_c than with N_{dp}. It was concluded that a small amount of kinks and concomitant enrichment of long trans conjugated segments (a high N_c or a low I_{sym}/I_{anti}) are indispensable for a film to gain high electrical conductivity at the doped state.

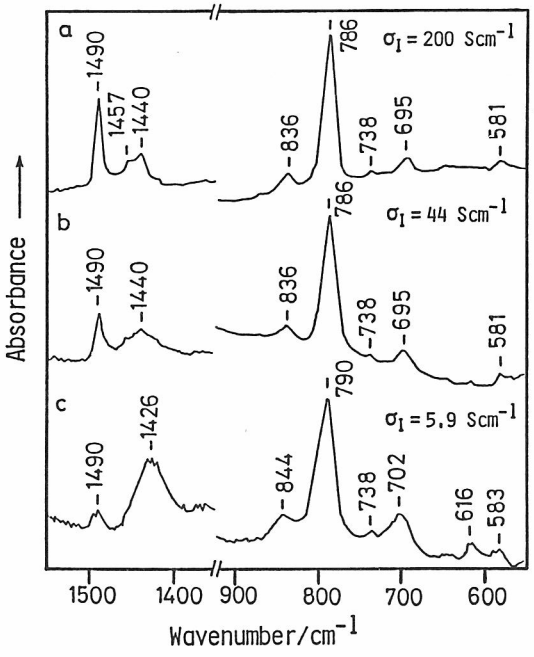

FIG. 34. Infrared spectra of undoped polythiophene films. (a) PT-2, (b) PT-1, and (c) PT-10. The σ_I values are electrical conductivities of the films upon maximum redoping with iodine. For details of synthetic conditions of the films, see [251]. Used by permission, Ref. [215].

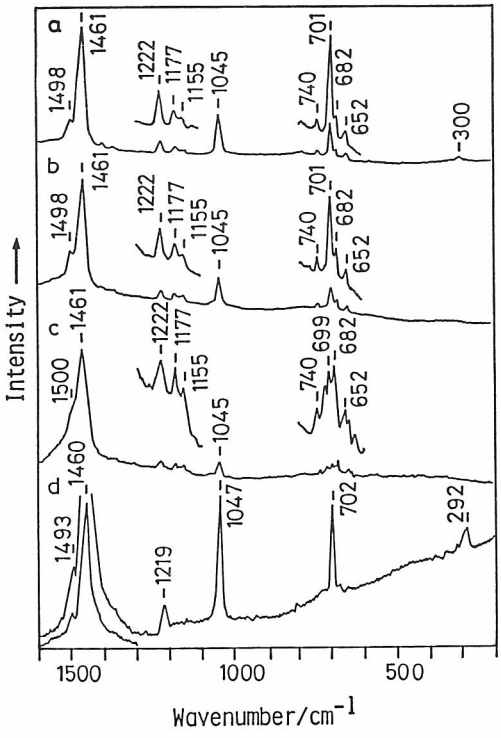

FIG. 35. Resonance Raman spectra of undoped polythiophene films (514.5 nm). (a) PT-2, (b) PT-1, (c) PT-10, and (d) PT-MT (polythiophene synthesized in the interlayer of transition-metal-ion exchanged montmorillonite). Used by permission, Ref. [215].

TABLE 6
Vibrational Assignments of Neutral Polythiophene

ν_{obs} ($\Delta\nu(^{13}C)$, $\Delta\nu(D)$)[a]		Assignment
Raman	Infrared	
1498 (-14, -54)		C=C antisym. str.
1461 (-34, +3)		C=C sym. str.
1405 (- , -31)		2 x 701
1371 (-24, -73)		CS sym. str. + C-C str.
1222 (-31, -8)		inter-ring CC str. (trans)
1177 (-23, -)		inter-ring CC str. (distorted)
1155 (-25, -)		inter-ring CC str. (distorted)
1045 (-4, -267)		CH in-plane bend
701 (-4, -15)		sym. ring deform (trans)
682 (-5, -14)		sym. ring deform (distorted)
652 (-6, -11)		sym. ring deform (distorted)
301 (-3, -6)		skeletal deform
	1490 (-15, -47)	C=C antisym. str.
	1440 (-13, -20)	C=C sym. str.
	1068 (-5, -186)	CH in-plane bend
	786 (0, -165)	CH o.p.-bend (2,5-disubstituted)[b]
	695 (0, -171)	CH o.p.-bend (2-monosubstituted)[b]

[a]Peak frequency (frequency shift on 2,5-^{13}C-substitution, frequency shift on deuteration) in cm^{-1}.
[b]o.p., out-of-plane

Finally, it is interesting to point out that neutral polythiophene (PT-MT) polymerized in the interlayer of transition metal-ion exchanged montmorillonite (a clay mineral) has much less kinks as judged from the Raman spectral pattern (Fig. 35d).

C. Doped Polythiophene

Hotta et al. studied FTIR spectra of electrochemically prepared polythiophene films doped with various dopant species at varying doping levels [230]. They observed four conspicuous absorption bands at 1330-1310, 1200, 1120-1080, and 1030-1020 cm^{-1} independent of the difference in dopant species and contents [230]. In Fig. 37 are compared the infrared spectra of neutral

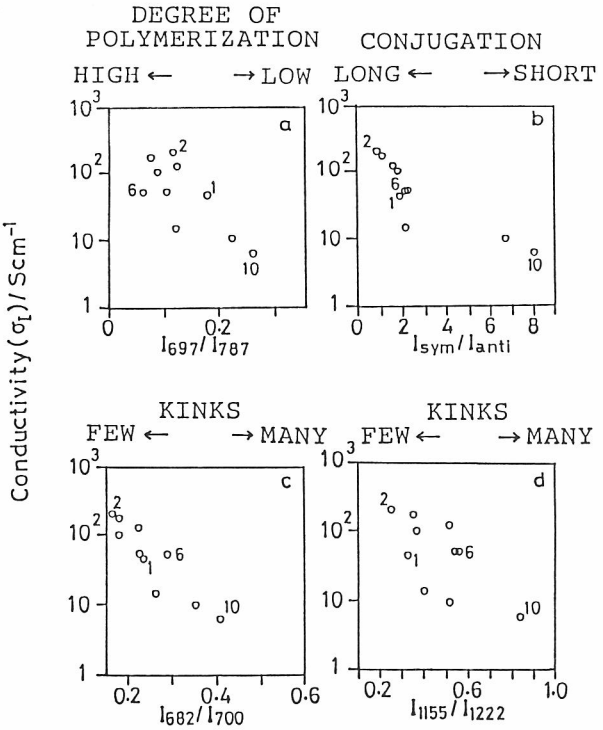

FIG. 36. Plots of electrical conductivity versus relative area-intensities of infrared and Raman bands of polythiophenes. Numbers 1, 2, 6, and 10 in the figures denote the data of PT-1, PT-2, PT-6, and PT-10, respectively. Adapted from Ref. [215].

and redoped polythiophenes. Neutral thiophene rings remain even at a high doping level (Fig. 37d) but diminish at the maximal doping (Fig. 37e) as judged from the disappearance of the 1490 and 1440 cm^{-1} bands. All the bands in Fig. 37e arising from the doped parts are of molecular vibrational origin because of their frequency shifts on ^{13}C- and D-substitution. Whether they arise from either of radical cation and dication or from the both is not clear. However, small spectral changes have been noticed at the beginning and the final stages of redoping. If we assume that radical cation is less stable than dication, each radical cation isolated at very low doping levels will tend to combine to form dication whenever another nearby radical cation is generated by additional doping. This could be related to the spectral change at the beginning of the redoping. At the intermediate doping levels, the content of dication will be much larger than that of radical cation. At doping levels higher than a certain dopant concentration each dication will

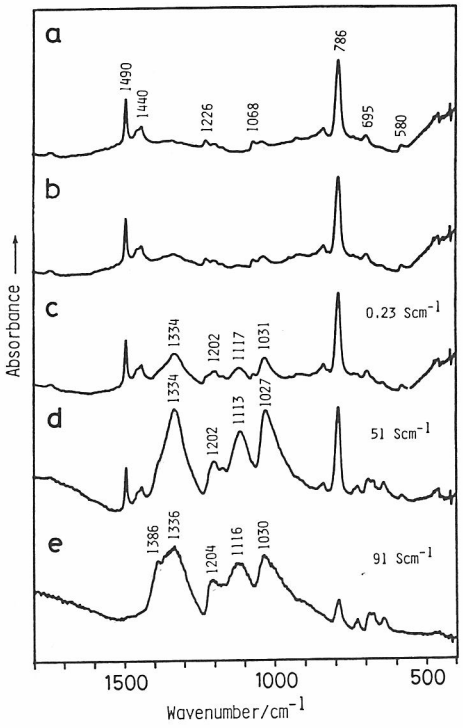

FIG. 37. Infrared spectra of undoped and redoped polythiophenes. (a) Undoped polythiophene and (b)-(e) iodine-doped polythiophenes. Conductivity of (b) was 1.8×10^{-2} Scm^{-1}. The values of the other doped films are given in the figure. The vertical scale of (e) is 2.5 times those of the others.

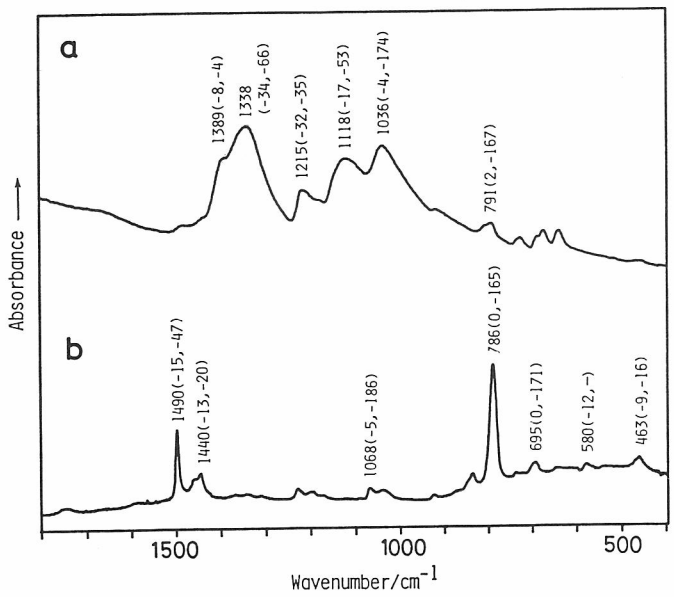

FIG. 38. Infrared spectra of (a) as-polymerized (doped) polythiophene and (b) undoped polythiophene. The values in parentheses are the frequency shifts (in cm^{-1}) on 2,5-^{13}C-substitution and deuteration in that order.

interact strongly with the neighboring ones to cause a further change in structure corresponding to the change in the spectra. However, such structural changes are much less significant than that from neutral to doped (radical cation or dication) structures as is evident from the spectra. The formation of radical cation or dication breaks the homogeneity in structure, and the force field of neutral polymer and the vibrational selection rule for a homogeneously long polymer do not hold any more, but the vibrational activities depend on the symmetry and structure of the restricted domains. This is one of the reasons of the broad widths of some of the bands.

Among the four strong bands in the 1340-1030 cm^{-1} region the one at 1036 cm^{-1} is assigned to the in-plane CH bend because it shifts down to 862 cm^{-1} on deuteration (Fig. 38). The frequency and the D-shift are comparable to those of the neutral polymer (1068 cm^{-1} and -186 cm^{-1}, respectively). On the other hand, the intensity is the second strongest in the spectrum in contrast to the weak intensity of the 1068 cm^{-1} band in the neutral polymer. In relation to this, the out-of-plane CH (CD) bend is slightly upshifted to 791 (624) cm^{-1} with very much decreased relative intensity. Such drastic intensity changes indicate formation of a large polarization in the ring plane. The remaining three bands arise from the ring stretching modes involving large displacements of α-carbons judged from the large ^{13}C-shifts. They also involve motions of β-hydrogen. Presumably, a π electron is taken out by a dopant in radical cation or two π electrons by two dopants in dication and the remaining π electrons are delocalized within the finite domains. As a result, the modes corresponding to the antisymmetric and symmetric C=C stretches in neutral polymer would mix with the CHCH stretch, the CS stretch, and the inter-ring CC stretch to yield the frequency lowered bands.

The Raman spectra of as-prepared films with 457.9-514.5 nm excitation are similar to one another and to those of the neutral films except the followings. The intensities of the bands arising from the distorted parts (at 1177, 1157, 682, and 649 cm^{-1}) relative to those from the trans parts (at 1224 and 696 cm^{-1}) are stronger in the doped film than in the neutral one. The frequency of the antisymmetric C=C stretch in the former is higher than that in the latter. The symmetric C=C stretching frequency, on the other hand, is lower in the former. These observations are interpreted as the rings near the kinks remaining undoped in the film and giving the resonance Raman spectra with these excitation wavelengths. Hence, the weak absorption in the visible region arises mostly from these parts. The trans conjugated part is mostly doped and absorbs the red-infrared light. Accordingly, the Raman scattering from the doped part is hardly observed with the violet-green

excitation. The 632.8 nm excited spectrum retains the spectral pattern of neutral polymer although the strongest peak is shifted down to 1431 cm^{-1} with a shoulder at 1362 cm^{-1}. The typical spectrum of doped polythiophene would be that of the sample polymerized in the interlayer of Cu^{2+} -montmorillonite in a dry atmosphere where the strongest peak lies at 1411 cm^{-1} with other peaks at 1520, 1360, 1219, 1144, 1069, and 955 cm^{-1} [264].

IV. POLYPYRROLE

Conducting polypyrrole films are obtained by electrochemical oxidative polymerization of pyrrole in organic electrolyte solution [192,193,198, 266-277] and aqueous electrolyte solution [278-288]. They are doped with the electrolyte anions (BF_4^-, ClO_4^-, p-toluenesulphonate anion, etc.) and the dopant concentrations are 25-32 mol% per pyrrole unit for BF_4^--doped films [265-267,271] and 23-38 mol% for ClO_4^--doped ones [192,193,270,271,276,277]. As-polymerized doped films become insulating upon electrochemical reduction [270,289] and the undoped films are unstable in air. The films prepared in propylene carbonate containing 1% water and Et_4NClO_4 at -20°C can be stretched 2.2 times the original length and the conductivity in the direction of stretch is raised from 300 to 1005 Scm^{-1} [276,277]. The highest conductivity among the films prepared in aqueous solution is 500 Scm^{-1} [281,282]. The conductivity of doped film decreases over four orders of magnitude on treatment with strong alkalis and it is recovered upon treatment with proton acids [290]. Neutral polypyrrole films can be redoped electrochemically or chemically [270]. Substituted pyrroles [198,268,271,272,275, 279,291,292] and 2,2'-bipyrrole [293] are also used as the starting material of electrochemical polymerization. Poly(1-methyl-2,5-pyrrolylene) was synthesized by coupling of the Grignard reagent of 1-methyl-2,5-dibromopyrrole and the conductivity of the doped polymers was low [294]. Composites of polypyrrole and other polymers (poly(vinyl chloride), poly(vinyl alcohol), latexes, etc.) have been obtained [295-300].

For the as-polymerized films prepared in organic solvents, the floating and apparent densities are 1.37-1.58 [266,267,271,280,282] and 0.26-0.37 [280] gcm^{-3}, respectively. On the other hand, for some films prepared in aqueous electrolytes, floating densities (1.364-1.558 gcm^{-1}) are close to the apparent densities and thus these films are dense [280,283]. The morphology of as-polymerized films is granular with small differences [192,193,267,271, 280,283] and no fibrillar structure has been observed. The degree of poly-

merization of poly(3,4-dimethylpyrrole) was 100-1000 by the ^{3}H labeling method [301,302].

A monoclinic structure (a = 8.2, b = 7.35, c = 6.82 Å, and β = 117°) has been proposed for neutral polypyrrole from the analysis of electron diffraction [272]. According to ^{13}C NMR studies, the polymerization proceeds predominantly through α,α'-coupling [232,270]. An infrared study on neutral polypyrrole and oligomers (2,2'-bipyrrole and 2,2':5',2"-terpyrrole) has suggested that neutral polypyrrole has a planar all-trans structure [302,303]. Raman results of neutral polypyrrole and its 2,5-^{13}C-substituted and C-deuterated derivatives are consistent with this structure [304]. Neutral polypyrrole and poly(3,4-dimethylpyrrole) give a π-π* transition at 387-412 nm [270,305,306] and 387 nm [307], respectively.

X-ray and electron diffraction studies have shown that as-polymerized doped polypyrrole is amorphous [266,267,276-278]. The chain structure of doped polypyrrole has been studied by optical absorption [267-270,306, 308-312], ESR [270,277,308,311,313-316], NMR [232,270], infrared [192, 268,270,277,279,289,317,318], and Raman [268,277,304,317,319,320] spectroscopy and quantumchemical calculations [248,321,322]. ESR and optical absorption observations on doped polypyrrole have indicated the formation of radical cation and dication [306,309-316]. However, the assignments of the optical spectra were controversial [306,309,311,312]. Their assignments have been possible on the basis of the resonance Raman spectral dependences on undoping processes and excitation wavelengths [304]. Raman spectra of doped polypyrrole and its 2,5-^{13}C-substituted and C-deuterated analogs [304] and theoretical calculations [248,321,322] indicated that the molecular structure changes from an aromatic structure to quinoid-like structures upon doping.

A. Optical Absorption Spectra

Figure 39 shows absorption spectra of a ClO_4^--doped film on an ITO electrode at as-polymerized state [DPP(ClO_4^-)] (Fig. 39a) and at different stages of electrochemical reduction (Figs. 39b-f; 39f is the spectrum of almost completely reduced 'neutral' polypyrrole, NPP). As reduction proceeds, the peak of the visible band (B-band) shifts from 462 nm to longer wavelengths. The intensity first increases a little and then decreases substantially. The intensity of the near-infrared band (C-band) decreases monotonically. A band is observed around 350 nm (A-band) in Fig. 39c and it exhibits bathochromic shifts towards 412 nm on further reduction with concomitant increases in intensity. A-band arises from the π-π* transitions in the neutral

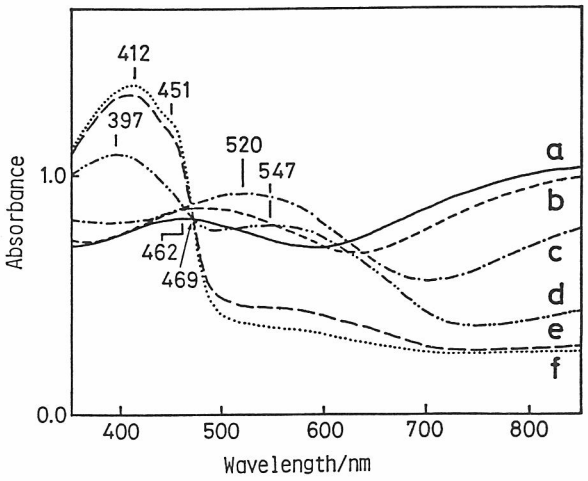

FIG. 39. Dependence of absorption spectrum of ClO_4^--doped polypyrrole [DPP(ClO_4^-)] on the reduction potential. (a) DPP (ClO_4^-) prepared at a voltage of 3.5 V versus counter electrode, (b) the same film with a lowered potential of 2.8 V, (c) 2.5 V, (d) 2.2 V, (e) 2.0 V, and (f) 1.6 V (neutral polypyrrole, NPP). The doping level decreases in alphabetical order. Used by permission, Ref. [304].

parts of the polymer since 2,2'-bipyrrole and 2,2':5',2"-terpyrrole give such peaks at 285 and 345 nm, respectively [305]. The bathochromic shift of A-band has been explained as a result of elongation of the successive neutral part in the polymer in the course of reduction [304,306]. Thus, the band shape and λ_{max} of A-band give information on the contents of various conjugated segments in the neutral part of the polymers.

The origin of B- and C-bands are of particular interest in relation to the structure of the doped part. Scott et al. [311] and Brédas et al. [309] have attributed the both bands to dication (at high doping levels) and radical cation (at low doping levels). Genies and Pernaut [312] have observed two bands at 540 and 440 nm and assigned the former to radical cation and the latter to radical cation and dication.

A simple-minded interpretation of the monotonical decrease of the C-band intensity upon reduction is that the band arises mostly from one species and the content decreases monotonically. On the other hand, the complex behavior of the B-band during the reduction strongly indicates the presence of species other than those that give rise to C-band. Between the two possible species reported to exist in the doped polymer, the content of dication would be relatively high at high doping levels [309,311]. According to Furukawa et al. C-band is mainly contributed by dications and B-band is an

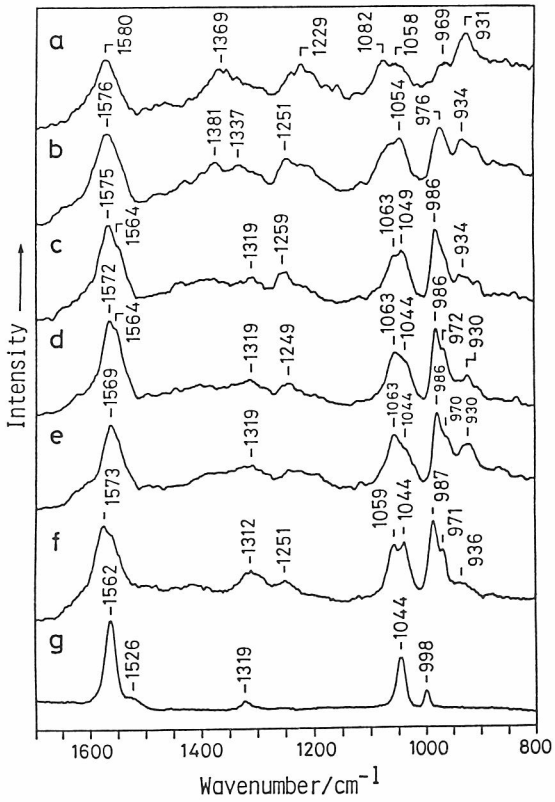

FIG. 40. Raman spectra of as-polymerized ClO_4^--doped polypyrrole [DPP(ClO_4^-)] and films at various stages of electrochemical reduction. (a)-(f) 632.8 nm, 80K; and (g) 457.9 nm, 80K. (a) DPP(ClO_4^-), (b) 2.8 V, (c) 2.5 V, (d) 2.2 V, (e) 2.0 V, (f) 1.6 V (NPP), and (g) 1.6 V (NPP). Each spectrum was measured for a different sample. Used by permission, Ref. [304].

overlap of the bands of radical cations plus the short-wavelength contour of C-band. The spectral behavior during the reduction has been explained as a result of dications → neutral form processes [304].

B. Raman Spectral Dependence on Reduction Potential

Raman spectra with 632.8-457.9 nm excitation have been studied at conditions similar to those at which the optical spectra were recorded [304]. The 632.8 nm spectra are in resonance with both B- and C-bands and disappearance of some bands at the early stages of reduction concomitant with the decrease of the C-band intensity is noticed: those at 1580, 1369, 1337, 1229, 1082, and 931 cm^{-1} (Fig. 40). The frequencies and intensity are slightly different for different samples indicating that the compositions of the species giving rise to C-band vary from sample to sample. The spectral pattern of the remaining bands which changes depending on the stage of reduction is different from that of neutral polymer with 457.9 nm excitation in resonance with A-band (Fig. 40g). The bands of the former group have

been assigned to dications and those of the latter to radical cations with different segment lengths [304]. In this way the optical and Raman spectra are consistently understood.

C. Structure of Radical Cation and Dication

The mode assignments have been made on the basis of 2,5-^{13}C- and C-deuteration shifts (Table 7). The data of 3,4-^{13}C- and ^{15}N-analogs would make the assignments more specified. By tracing back the spectral pattern from the neutral state to the as-polymerized one, it is possible to assign the bands belonging to the A_g species which are dominant in the resonance Raman spectra of neutral polymers. Some bands characteristic of the doped species do not arise from the ungerade modes which might have become active due to possible symmetry lowering by doping, because the mutual exclusion rule holds generally for the Raman and infrared spectra of doped polymers. They are assigned to the B_{1g} modes which become enhanced through vibronic coupling between the excited electronic states in each of the cationic species.

Some comments can be made on the structures of radical cation and dication. The deuteration downshift of ν_3 is only 3 cm^{-1} in the neutral form indicating almost null contribution from $\nu(C_3C_4)$ to this mode. The shift increases to 9 cm^{-1} in radical cation and 18 cm^{-1} in dication showing increased contribution from $\nu(C_3C_4)$. The frequency also increases in the same order, which seems to arise from the increased force constant of C_3C_4 bond by the doping. The ν_5 frequency also is upshifted in cations. On the other hand, the other ring vibrations, ν_4 and ν_7 are downshifted, implying that the force constants of the other bonds in the ring are decreased by the doping. Even the pure CH bending, ν_6, is affected by the doping. The structure in dication is more distorted than that in radical cation, judging from the changes in frequencies and the modes. However, the changes are much less significant than those in polyacetylene (Sec. II.C).

V. POLYANILINE

Among various conducting polymers, polyaniline is the first material that has been commercialized (September, 1987); it is used as the cathode of a secondary lithium battery. It can be prepared by electrochemical or chemical polymerization of aniline in aqueous acid solution. There are many forms of

TABLE 7

Raman Bands of Neutral Polypyrrole (NPP) and Radical Cation and Dication in Doped Polypyrrole (DPP), and the Assignments

		$\nu_{obs}(\Delta\nu(^{13}C), \Delta\nu(CD))$[a]	Assignment[b]
NPP[c]			
A_g	ν_3	1562 (-34, -3)	$\nu(C_2C_3$ sym) + ν(inter-ring CC)
	ν_4	1526 (-34, -36)	ν(NC sym) + $\nu(C_3C_4)$
	ν_5	1319 (-16, -42)	ν(inter-ring CC) + $\nu(C_3C_4)$
	ν_6	1044 (-4, -276)	β(CH sym)
	ν_7	998 (-8, -7)	δ(ring)
	ν_8	385 (- , -)	δ(skeletal)
B_{1g}	ν_{11}	634 (- , -)	δ(ring)
DPP			
Radical cation[d]			
A_g	ν_3	1587 (-20, -9)	$\nu(C_2C_3$ sym) + $\nu(C_3C_4)$ + ν(inter-ring CC)
	ν_4	1464 (- , -13)	ν(NC sym) + $\nu(C_3C_4)$
	ν_5	1346 (-39, -34)	ν(inter-ring CC) + $\nu(C_3C_4)$
	ν_6	1063 (-12, -287)	β(CH sym)
	ν_7	973 (0, -3)	δ(ring)
B_{1g}	ν_9	1374 (-11, -9)	ν(NC anti)
	ν_{10}	1235 (-5, -57)	β(CH anti) + βNH
	ν_{11}	622 (0, -59)	δ(ring)
Dication[e]			
A_g	ν_3	1593 (-25, -18)	$\nu(C_3C_4)$ + $\nu(C_2C_3$ sym) + ν(inter-ring CC)
	ν_5	1327 (-36, -)	ν(inter-ring CC)
	ν_6	1086 (-3, -205)	β(CH sym)
	ν_7	933 (0, +14)	δ(ring)
B_{1g}	ν_9	1376 (-23, -)	ν(NC anti)
	ν_{10}	1236 (-5, -60)	β(CH anti) + βNH
	ν_{11}	680 (- , -)	δ(ring)

[a] Peak frequency (frequency shift on 2,5-^{13}C-substitution, frequency shift on ^{2}C-deuteration) in cm^{-1}.
[b] ν, stretch; β, in-plane bend; δ, in-plane deform; sym, symmetric; anti, antisymmetric
[c] 457.9 nm excitation
[d] 514.5 nm excitation
[e] 632.8 nm excitation

polyaniline with different electrical properties which are converted to each other by acid/base treatments and/or oxidation/reduction in aqueous solution [323-350]. The conductivity depends on pH and applied potential and a window for high conductivity opens at (0.35 V, pH 1.0) [351].

As-polymerized bluish green sample (to be termed 2S, see Fig. 41) conducts electricity (5 Scm^{-1}) [323-331,333-335,339-349] but it becomes insulating by treatment with aqueous alkaline solution (2A, purple) [325-330, 333,334,337,339,341,343,347] or by electrochemical oxidation (purple) as well as by reduction in aqueous acid solution (1S, greenish yellow) [331]. Reduced-alkali-treated polyaniline (1A, white) is insulating [327,332,350] and unstable in air; its color changes to blue upon exposure to oxygen or air [1A(O_2)] [350]. 2A becomes conducting upon iodine doping [336]. 1A doped with electrolyte anions (doped 1A, bluish green) is obtained by electrochemical oxidation of 1A in non-aqueous electrolytes [352] and it is conductive (5.8 Scm^{-1}) [350]. It has been shown that batteries using polyaniline (especially 1A) have attractive characteristics [352-358].

Polyaniline 2S is smooth-surfaced, netlike, granular, or fibrillar (fibril diameter, 600-4000 Å), depending on the polymerization conditions [359-363]. Molecular structure and reaction mechanism during acid/base treatments and oxidation/reduction were studied by vibrational spectroscopy [327,328,330, 334-336,340,346,350,364-371], UV-VIS absorption [332,334,335,346,355,366-368,370-377], CP-MAS-NMR [378-380], ESR [328,329,337,338,340,342,346,366, 377,381,382], XPS [340,383-386], and electrochemical method [326,327,331, 346,347,352,354,355,358-362,364,372-374,376,377,381,387-391].

Resonance Raman spectroscopy is suited to the structural studies of this multi-chromophore material. The infrared spectra give clear information concerning the nitrogen moiety. Under acid conditions the polymerization proceeds predominantly through head-to-tail coupling at N and C_4 [334,364]. White 1A has been revealed to be poly(imino-1,4-phenylene) [(-NH-C_6H_4-)$_n$, see Fig. 42] which has UV absorption (<330 nm) but no visible one [350,366]. The spectroscopic basis of the structures of 1A and other forms is given in Fig. 43. (This figure is to be referred to in the following subsections.) 1S consists of imino-1,4-phenylene (IP) unit and its salt (IP^+) unit (-$NH_2^+A^-$-C_6H_4-, A^-: anion) [350] absorbing at 305 nm [372,373]. 2A is composed of IP unit and nitrilo-2,5-cyclohexadiene-1,4-diylidenenitrilo-1,4-phenylene (NP) unit (-N=C_6H_4=N-C_6H_4-) [332,334,378,379]. The quinone diimine structure (-N=C_6H_4=N-) in NP has a broad absorption in the visible region and the reported wavelengths are between 580 and 632 nm [332,334, 346,367,375]. Treatment of 1A with oxygen converts part of consecutive IP units to NP unit [350]. IP, IP^+ and the radical cation of IP ($IP^{+\cdot}$,

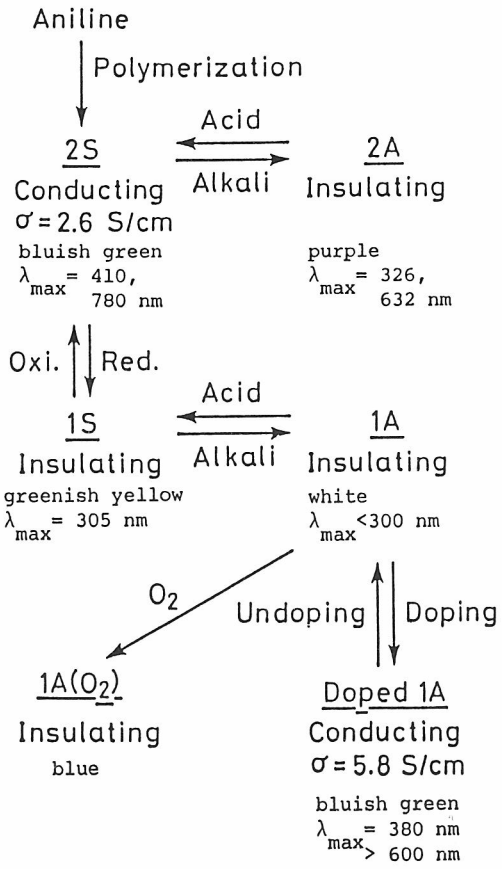

FIG. 41. Various forms of polyaniline. Adapted from Ref. [350].

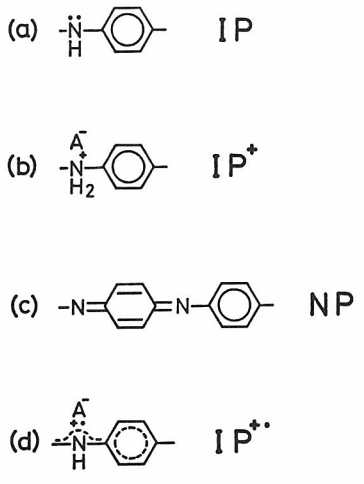

FIG. 42. Constitution units of polyanilines. (a) Imino-1,4-phenylene (IP), (b) imino-1,4-phenylene salt (IP^+), (c) nitrilo-2,5-cyclohexadiene-1,4-diylidene-nitrilo-1,4-phenylene (NP), and (d) radical cation of imino-1,4-phenylene ($IP^{+\cdot}$). A^-: anion. Adapted from Ref. [350].

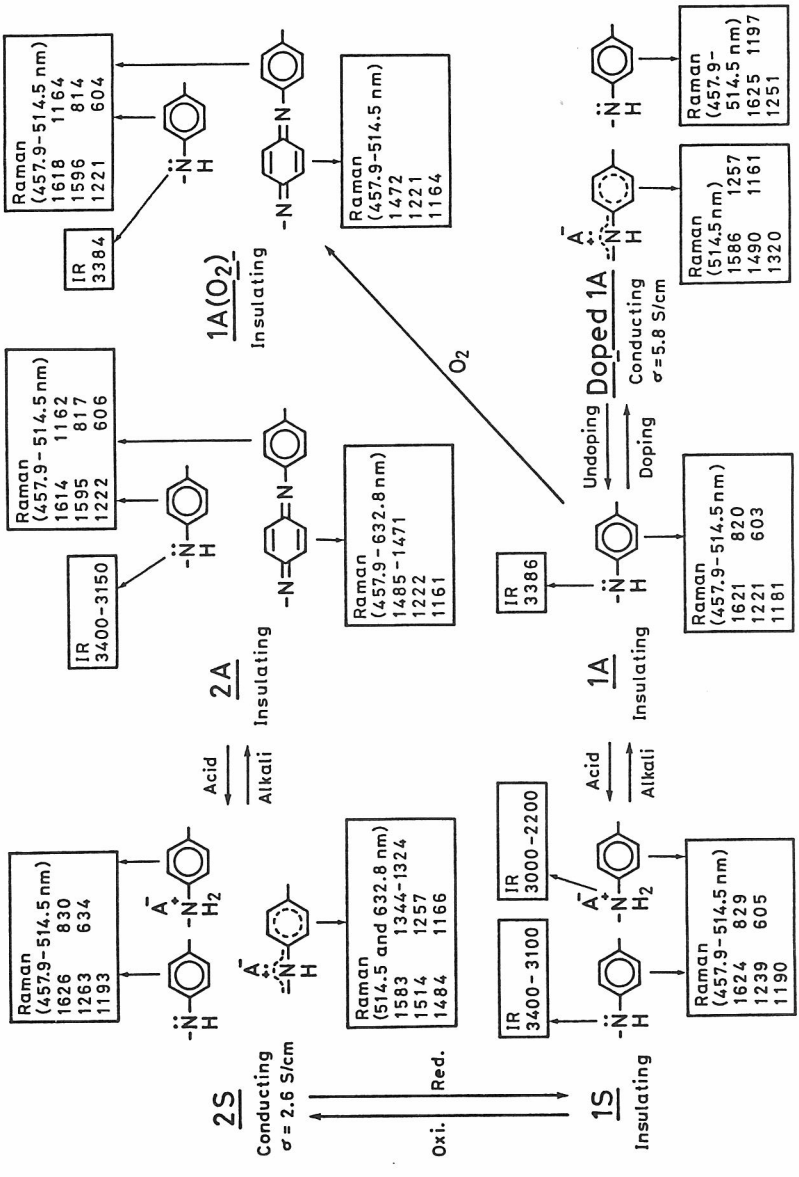

FIG. 43. Constitutional units and vibrational key bands of various forms of polyaniline. The content of NP in 1A(O_2) is less than that in 2A. Used by permission, Ref. [350].

semiquinone radical cation) exist in conducting 2S [334,350,386]. The broad absorption of 2S at 780 nm is due to $IP^{+\cdot}$ [334,350] to which the high conductivity is attributed [335,337,338,340,342,347,348,350,392,393]. Conducting doped 1A consists of IP and $IP^{+\cdot}$ [350].

The decrease of conductivity on electrochemical oxidation of 2S has been attributed to the formation of quinone diimine [347,361] and degradation [347,361,374]. An absorption which appears at 800 nm during electrochemical reduction of 2A in phthalate buffer (pH 5.9) has been assigned to radical cations in relation to the concomitant increase of conductivity [332]. Cyclic voltamograms may be analyzed on models including the structures mentioned above [361,373,376,377,387,388].

Abbreviations of the names of model compounds which appear in the following are: BBB, N,N'-diphenyl-1,4-benzenediamine, C_6H_5-NH-C_6H_4-NH-C_6H_5; BBB-2HCl, N,N'-diphenyl-1,4-benzene-diamine dihydrochloride; $BBB^{+\cdot}$, semiquinone radical cation of BBB; BQB, N,N'-2,5-cyclohexadiene-1,4-diylidenebisbenzenamine, C_6H_5-N=C_6H_4=N-C_6H_5.

A. Reduced-Alkali-Treated Polyaniline (1A), $(-NH-C_6H_4-)_n$

The Raman and infrared spectra of polyaniline and ^{15}N-substituted and C-deuterated analogs in various forms have been studied [334,350]. The Raman spectral pattern of white 1A does not vary with the excitation wavelength and is interpreted as that of p-disubstituted benzene (Fig. 44a). The infrared spectra are consistently explained: e.g., the band at 811 cm^{-1} (711 cm^{-1} in the deuterated analog) is characteristic of p-substitution (Fig. 45a). The CH out-of-plane bend of the monosubstituted benzene ring is not observed indicating absence of oligomers (phenyl capped octamer gives the band of an appreciable intensity). The rings are mostly coupled at C_4 and N position (head-to-tail coupling) because the C=N stretching Raman band is very strong for 2A (see below) and the corresponding C-N stretching band in 1A is observed at 1221 cm^{-1}. The infrared bands at 3386 and 3025 cm^{-1} are definitely assigned to the NH and CH stretches on the basis of -10 cm^{-1} ^{15}N-shift of the former and -776 cm^{-1} D-shift of the latter. Accordingly, 1A is para-$(-NH-C_6H_4-)_n$. It is interesting to note that all the NH groups are involved in H-bondings most of which are similar in strength. An important implication of this is that each nitrogen atom in a polymer chain is located at a certain short distance from a nitrogen or a benzene ring in a neighboring polymer to form an H-bond chain. Such close contacts of chains are considered to be important for charge transport in the conducting forms.

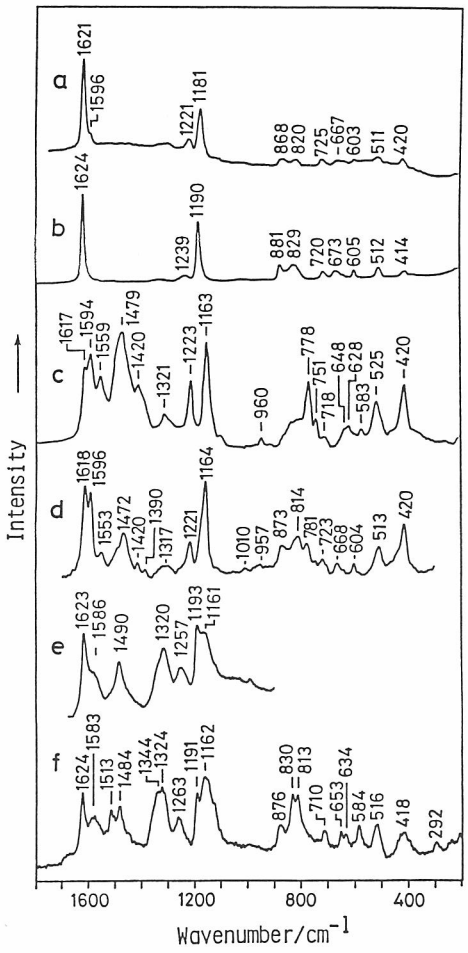

FIG. 44. Raman spectra of various forms of polyaniline (80K). (a) 1A (488.0 nm), (b) 1S (488.0 nm), (c) 2A (488.0 nm), (d) 1A(O_2) (488.0 nm), (e) doped 1A (514.5 nm), and (f) 2S (514.5 nm).

B. Acid-Treated 1A (1S)

Raman and infrared spectral patterns of 1S in the range below 1800 cm^{-1} are similar to those of 1A, although the peak frequencies are more or less different (Figs. 44b and 45b). A remarkable difference is observed in the high frequency infrared region. The broad band with two or three peaks in the 3400-3100 cm^{-1} region due to H-bonded NH stretches of C_6H_4-NH-C_6H_4- groups indicates a difference in H-bonding between 1A and 1S. A large number of -NH- groups become strongly H-bonded by the acid treatment, because the absorbance at 3386 cm^{-1} is smaller than those of lower frequency NH stretching bands. Moreover, the bands ranging from 3000 to 2200 cm^{-1} are assigned to the vibrations associated with the NH_2^+ part in -C_6H_4-NH_2^+-C_6H_4- groups [350,394]. Thus, 1S consists of IP unit and its salt unit (IP^+).

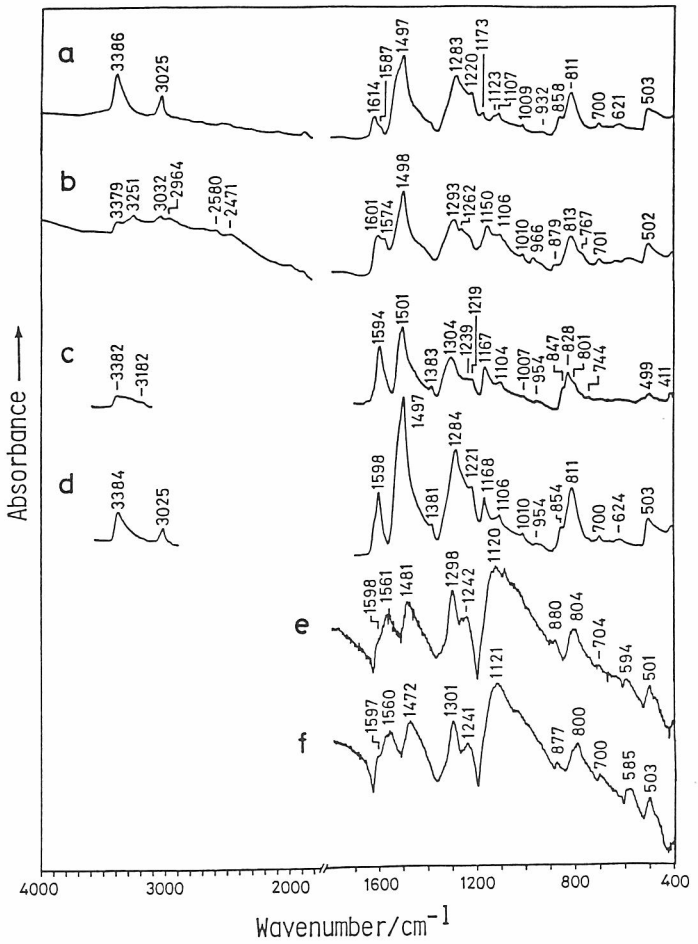

FIG. 45. Infrared spectra of various forms of polyaniline (room temperature). (a) 1A, (b) 1S, (c) 2A, (d) 1A(O_2), (e) doped 1A, and (f) 2S.

The degree of protonation depends on acids, because shapes of the bands due to -NH- and -NH_2^+- groups are different for the acids used [350].

C. Alkali-Treated Polyaniline (2A)

1. Presence of Quinone Diimine and p-Disubstituted Benzene Structures

Of the two absorptions at 326 and 632 nm the latter arises from the quinone diimine part and the former from 'perturbed' p-disubstituted benzene [350] (see below). This became clear through analysis of the resonance Raman spectra [334]. The strongest peak at 1471 cm^{-1} in the 632.8 nm

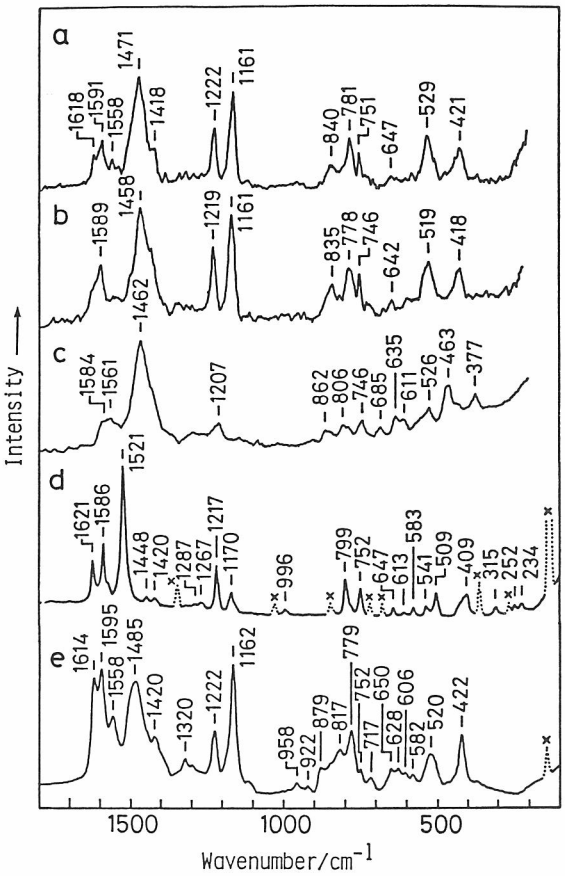

FIG. 46. Raman spectra of (a) alkali-treated polyaniline film prepared electrochemically on a Pt electrode [2A(Pt), 632.8 nm], (b) ^{15}N-substituted analog [2AN(Pt), 632.8 nm], (c) C-deuterated analog [2AD(Pt), 632.8 nm], (d) BQB (solid, 457.9 nm), and (e) 2A(Pt) (457.9 nm). Adapted from Ref. [334].

excited spectrum (Fig. 46a) is assigned to a mixed mode of the C=N stretch and the C=C stretch (to be termed ν_Q) in the quinone diimine (-N=C_6H_4=N-) part on the basis of the isotopic shifts and the data of model compounds (Fig. 46 and Table 8). Hence, the polymerization proceeds predominantly through head-to-tail coupling. The peaks at 1614, 1595, 1558, 1162, 879, 817, 628, and 606 cm^{-1} which gain intensities with 457.9 nm excitation (Fig. 46e) owing to pre-resonance with the 326 nm absorption are assigned to perturbed benzene in the vicinity of quinone diimine.

The ν_Q frequency has been found to be sensitive to the sequence consisting of NP and IP units. It is 1521 cm^{-1} in BQB (Fig. 46d, λ_{max} at

TABLE 8

Raman CN Stretching Frequencies (in cm^{-1}) of Polyanilines and Model Compounds

	Compounds	ν_{CN}
(a)	Aromatic amines and their hydrochlorides	
	N-phenylbenzenamine HCl	1200[a]
	N,N'-Diphenyl-1,4-benzenediamine (BBB)	1212[a]
	N-Phenylbenzenamine	1219[b]
	N,N'-Diphenyl-1,4-benzenediamine 2HCl (BBB-2HCl)	1220[a]
	1A	1221[a]
	1A(O_2)	1221[a]
	2A	1222[c]
	1S(HCl)	1239[a]
	Doped 1A	1251[a]
	2S	1263[a]
(b)	Radical cations	
	Doped 1A	1312-1320[a]
	2S	1324-1344[c]
	Radical cation of BBB ($BBB^{+\cdot}$)	1383 and/or 1401[a]
(c)	Quinone diimines	
	1A(O_2)	1472[a]
	2A	1471-1485[c]
	N,N'-2,5-Cyclohexadiene-1,4-diylidenebisbenzenamine (BQB)	1521[c]

[a]Ref. [350].
[b]Ref. [395].
[c]Ref. [334].

447 nm). In 2A it is 1471 cm^{-1} with 632.8 nm excitation and increases as the excitation wavelength decreases: 1475 cm^{-1} (514.5 nm), 1479 cm^{-1} (488.0 nm), and 1485 cm^{-1} (457.9 nm). The broad band width is explained by an overlap of bands with different peak frequencies and excitation profiles. The isotopic shifts also increase as the excitation wavelength decreases: the ^{15}N- and D-shifts are; -13 and -9 cm^{-1} (632.8 nm); -13 and -16 cm^{-1} (514.5 nm); -17 and -24 cm^{-1} (488.0 nm); and -23 and -19 cm^{-1} (457.9 nm). A study on phenyl capped octamer [396] indicates that the absorption maximum shifts to a shorter wavelength as the content of quinone diimine increases, which implies that the ν_Q frequency is high for a segment with a small number of p-disub-

stituted benzene rings between quinone diimine rings! The relation must be studied further.

Among the Raman bands of simple p-disubstituted benzenes the 1595 cm^{-1} band (mode 8b) is usually very weak in non-resonant Raman spectra. It is strong in the Raman spectra in resonance with the L_a transition (~220 nm) [397-399]. Accordingly, if we assume that the 326 nm peak of 2A corresponds to the allowed transition ($B_{a,b'}$ ~ 190 nm) and its long-wavelength shoulder to the forbidden transitions ($L_{a'}$ ~ 200 nm; L_b ~ 270 nm), the enhancement of the 1595 cm^{-1} band is reasonably understood. Such a bathochromic shift is possible in the p-disubstituted benzene part in NP and in the IP part adjacent to NP. We may call these rings 'perturbed benzene' rings. The vibration arising from an inner part of $(IP)_y$ would be weak like that in 1A and 1S.

2. Relation Between Structure and Synthetic Conditions

Figure 47 shows the Raman spectra of polyaniline 2A prepared under different conditions and emeraldine (supposed to be octamer). The spectrum of 2A via 2S prepared on Pt electrode (2A(Pt), Fig. 47a) is similar to that polymerized chemically (2A(chem), Fig. 47b). It is interesting to note that the ν_Q frequency of 2A(chem) is higher than that of 2A(Pt) by 10 cm^{-1}. This implies that the relative amounts and distributions of NP and IP are slightly different between the two. The infrared spectra are less sensitive to such small differences and are identical to each other.

The peak frequencies in the emeraldine spectrum (Fig. 47d) are also similar to those of 2A(Pt) and 2A(chem). However, the 1599 cm^{-1} band is relatively strong. Since the Raman bands arising from quinone diimine and perturbed benzene are both observed with 457.9-514.5 nm excitation, even a slight difference in compositions among the samples can be detected by the intensity ratio of the bands at 1480 and 1590 cm^{-1}. The ratio, I_{1490}/I_{1590}, in the 488.0 nm spectra is between 1.25 and 0.76. The value is largest for 2A(Pt) and 2A(chem) and becomes smaller for emeraldine and 2A(HOPG) (2A prepared electrochemically on highly oriented pyrolytic graphite) in that order. Such small differences are not detectable in the infrared spectra.

In the spectrum of 2A(HOPG), additional bands are observed at 1404, 1197, and 1141 cm^{-1} (Fig. 47c). The 1404 cm^{-1} band which shifts to 1366 cm^{-1} on ^{15}N-substitution is certainly due to the N=N stretching vibration, since the corresponding bands are observed at 1420 and 1356 cm^{-1} for methyl orange and the ^{15}N-substituted analogs, respectively [400]. The presence of the N=N stretching band signifies that aniline is partly polymerized through

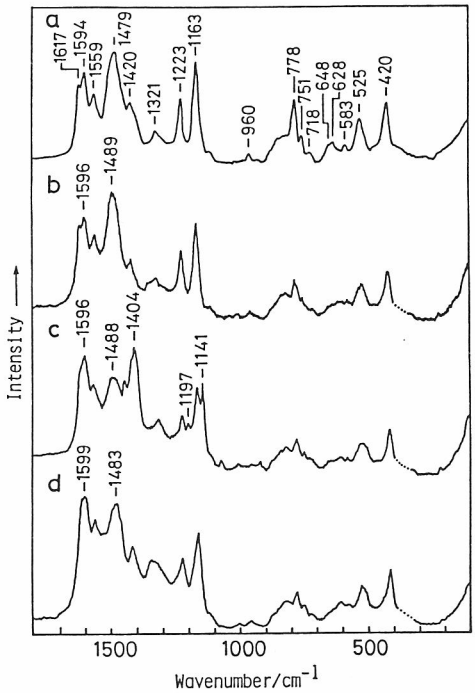

FIG. 47. Raman spectra of 2A by different synthetic procedures (488.0 nm, 80K). (a) 2A(Pt), (b) 2A prepared chemically [2A(chem)], (c) 2A prepared electrochemically on an HOPG electrode [2A(HOPG)], and (d) emeraldine (solid). Used by permission, Ref. [334].

head-to-head coupling on the HOPG electrode. Since the infrared spectrum is essentially the same as those of other samples, the amount of the N=N part is estimated to be small. The strong Raman band is a result of the resonance enhancement. On this basis, the amounts of head-to-head coupled part in other samples are negligibly small, if any.

Three NH stretching bands are observed in the infrared spectra (Fig. 45c). The one at 3382 cm^{-1} is related to the NH groups which form H-bond similar to those in 1A. The bands at 3254 and 3182 cm^{-1} indicate the presence of stronger H-bonds presumably between the -NH- and -N= groups.

The results of elemental analysis show the absence of sulfur in 2A(Pt) indicating that doping of SO_4^{2-} does not take place in the sample.

On the basis of the above mentioned observations the structure of 2A(Pt) and 2A(chem) has been concluded to be:

$$\cdots\text{-}(NP)_x\text{-}(IP)_y\text{-}\cdots.$$

D. 1A Treated with Oxygen [1A(O_2)]

The color turns to blue when white 1A is exposed to air or oxygen. This is because some -NHC_6H_4NH- parts are converted to -$N{=}C_6H_4{=}N$-. In

fact, the Raman bands in Fig. 44d at 1596, 1553, 1472, 1164, 814, and 781 cm^{-1} are characteristic of 2A (Fig. 44c). The relative intensity, I_{1480}/I_{1590} (I_{1472}/I_{1596} in this case), however, is smaller than that in 2A, indicating that the content of quinone diimine in 1A(O_2) is less than that in 2A.

In the infrared spectrum the area intensity of the NH stretching band around 3380 cm^{-1} is 25% of that of 1A. The decrease of the NH stretching intensity is reasonably understood because the formation of quinone diimine from benzenoid is accompanied by loss of NH bonds. Furthermore, an increase of the intensity of the 1598 cm^{-1} band relative to that of the 1497 cm^{-1} one as compared to that in 1A (Fig. 45a) is noticed. Since the former band arises mainly from NP and the latter mainly from IP, the relative intensity reflects the content of NP [335,350]. Thus the increase of I_{1598}/I_{1497} is also explained by the formation of quinone diimine structure by exposure of 1A to oxygen.

E. 1A Oxidized in Non-Aqueous Solution (Doped 1A)

The Raman spectrum of doped 1A excited with the 457.9 nm light is that of p-disubstituted benzene rings (Fig. 48a). In the polyanilines mentioned above, p-disubstituted benzene exists as IP unit and/or IP^+ unit. Since protonation does not occur and IP^+ unit cannot exist in non-aqueous electrolytes, p-disubstituted benzene in doped 1A must take the form of IP. An XPS study has shown the presence of IP and the absence of IP^+ [386].

When excited with the 514.5 nm light (Fig. 48c), new bands are observed at 1586, 1490, 1320, 1257, and 1161 cm^{-1}. The spectrum is different from those of 2A, 1A, 1S, and 1A(O_2). The Raman spectrum of semiquinone radical cation of BBB ($BBB^{+\cdot}$) with 632.8 nm excitation in resonance with a broad absorption around 710 nm [350] (Fig. 48d) is similar to Fig. 48c except for a significant difference between the bands in the range 1300-1400 cm^{-1}: doped 1A, 1320 cm^{-1}; and $BBB^{+\cdot}$, 1401 and 1383 cm^{-1}. (The frequencies of these bands probably depend on the size of doped domain where electrons are delocalized.) Thus, semiquinone radical cations of IP ($IP^{+\cdot}$) are formed in doped 1A, which is consistent with the results of ESR [366], electronic absorption [366], and XPS [386] studies.

When doped 1A is washed with sodium hydroxide solution, the band at 1320 cm^{-1} disappears and a band at 1480 cm^{-1} (ν_Q) appears with 514.5 nm excitation. Hence, the semiquinone radical is converted to quinone diimine by treatment with sodium hydroxide.

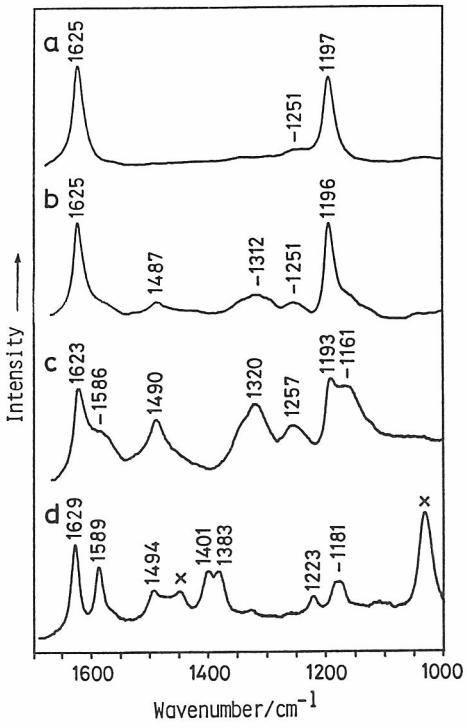

FIG. 48. Raman spectra of doped 1A and BBB+·. (a)-(c) Doped 1A. (1A film was oxidized electrochemically at 3.8 V in propylene carbonate containing $LiBF_4$.) (d) BBB+· in methanol. Excitation wavelengths are (a) 457.9 nm, (b) 488.0 nm, (c) 514.5 nm, and (d) 632.8 nm. The bands with x are due to methanol. Used by permission, Ref. [350].

F. As-Polymerized Polyaniline (2S)

The infrared spectrum of 2S is essentially the same as that of doped 1A (Figs. 45e and f) except that the infrared NH stretching regions can not be compared because of strong background absorption. However, the XPS spectra indicate the presence of IP and IP^+ in 2S and the absence of IP^+ in doped 1A [386]. The Raman spectra are also substantially similar to each other with some minor differences in peak frequencies (Figs. 44e and f) and the intensity dependence on excitation wavelengths. The doublet at 1344 and 1324 cm^{-1} show the largest and the second largest ^{15}N-shifts of -6 and -4 cm^{-1}, respectively, which are much smaller than the corresponding shift

of ν_Q in 2A, -13 cm^{-1}. This is interpreted as a result of electron delocalization around the nitrogen atom. The elimination of an electron from the lone pair of nitrogen makes the remaining electron delocalized. Probably, the CNC part in 2S corresponding to the 'C=N-C' part of 2A is nearly symmetric in bond order and the 1344-1324 cm^{-1} bands are almost the symmetric CNC stretching vibrations. The presence of two peaks indicates that there exists at least two slightly different structures in 2S. In doped 1A the 1320 cm^{-1} peak is much stronger than the higher frequency one.

The Raman peaks around 1513-1484 cm^{-1} in 2S (Fig. 44f) are not related to ν_Q but originate from the ring vibrations because of the small ^{15}N-shifts (1 cm^{-1}) and large D-shifts (37-61 cm^{-1}).

G. Relation Between Structure and Electrical Conductivity

Polyaniline shows three types of conductor/insulator transitions: 2S/2A, 2S/1S, and doped 1A/1A. Structural changes accompanying such transitions are the following.

Conducting 2S is converted to insulating 2A by alkali treatment and 2A is reversibly converted to 2S by acid treatment. As mentioned above, 2S consists of IP, IP^+, and $IP^{+\cdot}$ and 2A consists of IP and NP. Two IP-$IP^{+\cdot}$ units of 2S are considered to be converted to one NP and one IP-IP by disproportionation reaction similar to the case of BBB [401,402]. An example of such a reaction is shown in Fig. 49a. Disproportionation may take place between IP-$IP^{+\cdot}$'s on the same chain [337,338]. Those on the adjacent polymer chains also are possibly involved in the reaction because the chains are associated through H-bonding. IP^+ is simply converted to IP (Fig. 49a).

2S is also converted to insulating 1S upon electrochemical reduction and 1S is reversed to 2S by oxidation. 1S consists of IP and IP^+. Thus, $IP^{+\cdot}$ units are reduced to IP and IP^+ as shown in Fig. 49b [361, 373]. The structural change during reduction of 2S has been studied by Raman spectroscopy [334]. Concomitant decreases and increases in intensity of the $IP^{+\cdot}$ bands and IP and IP^+ bands, respectively, are observed as the reduction proceeds (Fig. 50) [350]. The electrical conductivity also decreases during the process.

Insulating 1A is converted to doped 1A by electrochemical oxidation in non-aqueous solution and the process also is reversible. In the oxidation process IP is transformed to $IP^{+\cdot}$ (Fig. 49c).

The presence of $IP^{+\cdot}$ is characteristic of conducting doped 1A and 2S. Accordingly, the semiquinone radical cations play the decisive role in

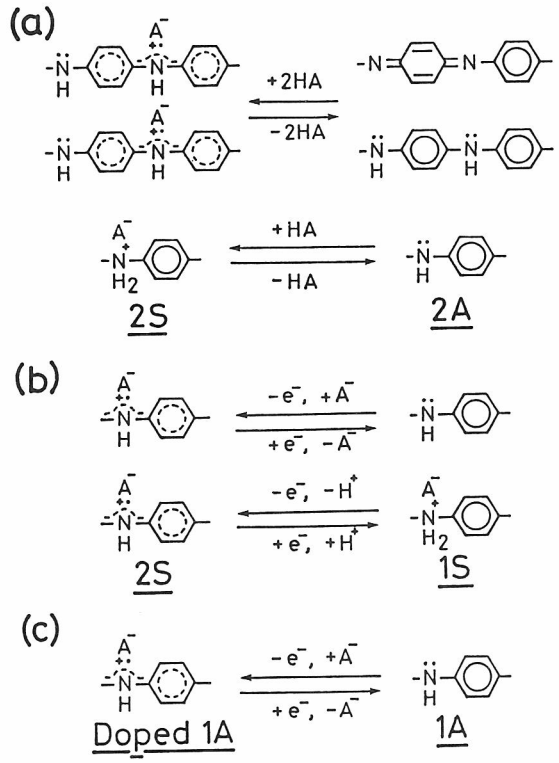

FIG. 49. Reaction schemes of conductor/insulator transitions. (a) 2S ⇄ 2A, (b) 2S ⇄ 1S, and (c) doped 1A ⇄ 1A. A^-, anion; e^-, electron; and H^+, proton. Used by permission, Ref. [350].

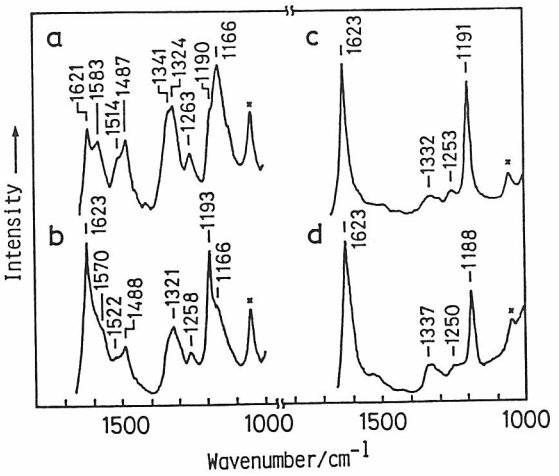

FIG. 50. In situ Raman spectra (514.5 nm) at various stages of reduction (pH 1). (a) As-polymerized 2S(Pt), 0.4 versus the reference electrode; (b) 0.2 V; (c) 0.0 V; and (d) -0.3 V [1S(Pt)]. The band with x is due to HSO_4^- ion in solution. Used by permission, Ref. [334].

electrical conduction in polyaniline. The charge delocalization extends to the neighboring benzene rings, because vibrations of distorted benzene rings are observed in the 514.5 nm spectra. This delocalization of an electron makes the charge transport within a chain possible. On the other hand, much less disturbed benzene rings which give the 457.9 nm spectra similar to those of 1A and 1S, would tend to terminate the intra-chain charge transport. It is tempting to consider that the inter-chain charge transport is facilitated by the closely connected nitrogen-nitrogen or nitrogen-benzene ring networks whose presence is evident (at least in insulating 1A, 1S, and 2A) by the H-bonded NH stretching infrared bands.

VI. OTHER POLYMERS

A. Polypara-phenylene

Neutral polypara-phenylene (PPP) is prepared by oxidative cationic polymerization of benzene in the presence of aluminum chloride-cupric chloride catalyst (Kovacic method) [403-405], by polycondensation of p-dihalobenzenes via dehalogenation with magnesium in the presence of nickel compounds catalyst [406,407] (Yamamoto method), by electrochemical polymerization of benzene [408,409], etc. Neutral PPP is insulating [410,411] and becomes conducting (σ = 500 Scm^{-1}) upon doping with AsF_5 [411]. However, it can not be doped with iodine because of its rather high ionization potential. It can be doped with alkali metals to give 7 Scm^{-1} [411]. Prolonged exposure of p-phenylene oligomers (biphenyl, p-terphenyl, p-quaterphenyl, p-quinoquephenyl, p-sexiphenyl) to AsF_5 causes polymerization of the oligomers to give highly conducting doped PPP [412].

An X-ray diffraction study showed an increase in crystallinity of Kovacic's neutral PPP by an increase in molding or annealing temperature [413]. Although the crystal structure was studied by X-ray [413] and electron diffraction [414], unequivocal unit cell constants were not obtained because of the low crystallinity. Neutral polymers show an absorption at about 380 nm (Kovacic PPP) [415,416]. In the infrared spectrum the bands in the 802-807 cm^{-1} range are assigned to the CH out-of-plane bend in p-disubstituted benzene and the bands around 758-765 and 690-697 cm^{-1} to those in monosubstituted benzene [404]. The intensity ratio of these bands has been used as a measure of molecular weight [404]. The chain length of Yamamoto PPP is shorter than that of Kovacic PPP on the basis of the

ultraviolet and infrared observations [417]. Three Raman bands of PPP around 1600, 1280, and 1220 cm^{-1} [418-424] have been assigned to a ring stretch, the inter-ring stretch, and a CH in-plane bend, respectively [420,421]. The ratio of the intensity at 1270 cm^{-1} to that at 1220 cm^{-1} decreases as the number of phenyl rings increases [418]. Calculations of the vibrational frequencies were performed [423-428].

Magnetic susceptibility measurements [429,430] of AsF_5-doped PPP suggested the presence of dication. In the Raman spectrum of AsF_5-doped PPP new bands are observed at 1355 and 1244 cm^{-1} with 514.5 and 647.1 nm excitation, indicating modification of polymer chain structure [423,424]. These bands correspond to the bands at 1280 and 1220 cm^{-1} in neutral PPP and the upshift of inter-ring CC stretching frequency upon doping suggests an increase in bond order of the inter-ring CC bonds. AsF_5-doped PPP gives broad infrared bands at 1530, 1280, 1180, and 980 cm^{-1} [412].

B. Polypara-phenylenesulfide

Polypara-phenylenesulfide (PPS) becomes conducting (1-10 Scm^{-1}) when doped with AsF_5 [431-435]. Raman and infrared spectra of neutral PPS have been reported [435]. The g values obtained from ESR spectra indicated the presence of sulfur radical cations in electron acceptor doped PPS [436]. Heavy doping with AsF_5 induces the formation of C-C bonds bridging the sulfur linkages to result in thiophene rings as demonstrated by elemental analysis and infrared spectra [433]. The infrared [433,435] and Raman [435] spectra of AsF_5-doped PPS have been reported.

C. Polypara-phenylenevinylene

Polypara-phenylenevinylene (PPV) was prepared in film via pyrolysis of a precursor polymer (in the form of water soluble sulfonium salt) [437,438]. By stretching the precursor polymer under heat, highly oriented films can be obtained. The film stretched up to ten fold showed a high conductivity (2.8×10^3 Scm^{-1}) upon AsF_5 doping [437]. Infrared spectroscopy was used to investigate the conditions for the transformation reaction from the precursor to PPV [439]. The dichroic ratio ($A_{\parallel}/A_{\perp}$) of the phenyl group vibration at 1520 cm^{-1} was used as an index of the orientation ratio [440]. Photoexcitation in PPV was studied [441].

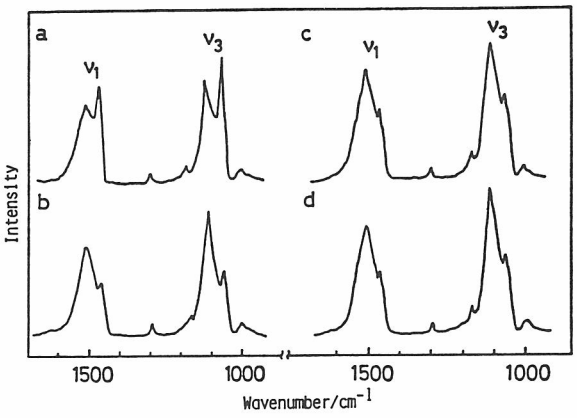

FIG. 51. Raman spectra of trans-polyacetylene films (457.9 nm, 80K). (a) Shiny side of Film A', (b) dull side of Film A', (c) shiny side of Film B', and (d) dull side of Film B'. Adapted from Ref. [157].

VII. CONCLUDING REMARKS

A decade has past since the first discovery of high electrical conduction of doped polyacetylene. A number of conjugated or π-electron rich polymers have been prepared and the physico-chemical properties including electrical conductivity were studied. Many contradicting conclusions have been obtained and discussed vigorously. It has become a common understanding that the physico-chemical properties of these polymers depend very much on the synthetic condition and the treatment after the synthesis. The difference in the vibrational spectra of Film A and Film B (Fig. 2) is one of the examples. The last figure in this chapter is again concerned with Film A' and Film B' (Fig. 51). In the figure are shown the Raman spectra of both sides of the films, i.e., shiny side which has been in contact with the inside wall of a polymerization flask and the other dull side. Apparently, the spectra of the shiny side are consistent with the infrared observation that the content of long segments in Film A is higher than that in Film B. The spectra of the dull side are not much different between the two. It has turned out that the electrical property is closely related to the spectral pattern of the shiny side but not to that of the dull side. If a group of scientists study the correlation on the data of the shiny side, another group on the data of the dull side, and the third group on random data of both sides, three contradicting conclusions will be derived. Actually, this had been done by our group before we noticed the situation. If one is going to compare different physico-chemical properties, it is strongly recommended to study the properties on the same sample or on the different parts of one sample with care. Some of the contradictory results mentioned in the texts may have originated from the difference in the samples.

On the other hand, the above description indicates that vibrational spectroscopy is a powerful tool in discriminating subtle differences among the samples. Conducting polymers and their mother polymers are often mixtures of components absorbing UV-VIS-IR region. Resonance Raman spectroscopy is suited for problems of this kind because it affords selective information on the components with a proper choice of the light source. It is easy to measure resonance Raman spectra in situ during the electrochemical treatment. In the case of polyaniline this method has been routinely used to check the sample degradation after repeated charge-discharge cycles.

In order to raise the value of electrical conductivity, it seems necessary to increase the area of contact among the segments (fibrils). Abundance in long conjugated segments is essentially important to raise intra-segment conductivity and eventually the overall conductivity. However, high electrical conduction is not the only goal of utilization of these polymers. Polyaniline whose conductivity is at most 30 Scm^{-1}, is practically used because of its long lasting stability and a small self-discharge rate. There are various prospects for conducting polymers, and vibrational spectroscopy is expected to play an important role in basic research and applications.

Since the completion of this review, several later review articles have appeared and are added as Refs. [442-445].

ACKNOWLEDGMENT

We thank Professor H. Shirakawa for providing SEM micrographs of polyacetylene and Professor G. Zerbi for sending a preprint [186]. The works from I. Harada's laboratory cited here were supported by Grant-in-Aid for Special Project Research (58218001 and 59212001) from the Ministry of Education, Science and Culture and by a grant from Bridgestone Corporation.

REFERENCES

1. H. Shirakawa, E. J. Louis, A. G. MacDiarmid, C. K. Chiang, and A. J. Heeger, J. Chem. Soc., Chem. Commun., 578 (1977).

2. C. K. Chiang, C. R. Fincher, Jr., Y. W. Park, A. J. Heeger, H. Shirakawa, E. J. Louis, S. C. Gau, and A. G. MacDiarmid, Phys. Rev. Lett., 39, 1098 (1977).

3. Handbook of Conducting Polymers, Vols. 1 and 2 (T. A. Skotheim, ed.), Marcel Dekker, New York, 1986.

4. T. Ito, H. Shirakawa, and S. Ikeda, J. Polym. Sci., Pol. Chem., 12, 11 (1974).

5. H. Shirakawa and S. Ikeda, Polym. J., 2, 231 (1971).

6. T. Ito, H. Shirakawa, and S. Ikeda, J. Polym. Sci., Pol. Chem., 13, 1943 (1975).

7. H. Shirakawa, T. Ito, and S. Ikeda, Polym. J., 4, 460 (1973).

8. H. Shirakawa, M. Sato, A. Hamano, S. Kawakami, K. Soga, and S. Ikeda, Macromolecules, 13, 457 (1980).

9. K. Soga, S. Kawakami, H. Shirakawa, and S. Ikeda, Makromol. Chem., Rapid Commun., 1, 523 (1980).

10. G. Wegner, Angew. Chem., Int. Ed. Engl., 20, 361 (1981).

11. G. Lieser, G. Wegner, W. Müller, and V. Enkelmann, Makromol. Chem. Rapid Commun., 1, 621 (1980).

12. V. Enkelmann, G. Lieser, M. Monkenbusch, W. Müller, and G. Wegner, Mol. Cryst. Liq. Cryst., 77, 111 (1981).

13. M. A. Schen, J. C. W. Chien, and F. E. Karasz, J. Phys. Colloq., 44, C3-163 (1983).

14. J. C. W. Chien, F. E. Karasz, M. A. Schen, and J. A. Hirsch, Macromolecules, 16, 1694 (1983).

15. M. A. Schen, F. E. Karaz, and J. C. W. Chien, J. Polym. Sci., 21, 2787 (1983).

16. J. C. W. Chien, J. D. Capistran, F. E. Karasz, L. C. Dickinson, and M. A. Schen, J. Polym. Sci., Pol. Lett., 21, 93 (1983).

17. F. E. Karasz, J. C. W. Chien, R. Galkiewicz, G. E. Wnek, A. J. Heeger, and A. G. MacDiarmid, Nature, 282, 286 (1979).

18. H. Shirakawa and S. Ikeda, Synthetic Met., 1, 175 (1979/1980).

19. Y. W. Park, M. A. Druy, C. K. Chiang, A. G. MacDiarmid, A. J. Heeger, H. Shirakawa, and S. Ikeda, J. Polym. Sci., Pol. Lett., 17, 195 (1979).

20. C. R. Fincher, Jr., D. Moses, A. J. Heeger, and A. G. MacDiarmid, Synthetic Met., 6, 243 (1983).

21. K. Akagi, S. Katayama, H. Shirakawa, K. Araya, A. Mukoh, and T. Narahara, Synthetic Met., 17, 241 (1987).

22. T. Ito, H. Shirakawa, and S. Ikeda, Kobunshi Ronbunshu, 33, 339 (1976).

23. T. Akaishi, K. Miyasaka, K. Ishikawa, H. Shirakawa, and S. Ikeda, J. Polym. Sci., Pol. Phys., 18, 745 (1980).

24. C. R. Fincher, Jr., D. L. Peebles, A. J. Heeger, M. A. Druy, Y. Matsumura, A. G. MacDiarmid, H. Shirakawa, and S. Ikeda, Solid State Commun., 27, 489 (1978).

25. S. Kuroda, M. Tokumoto, N. Kinoshita, and H. Shirakawa, J. Phys., Soc. Jpn., 51, 693 (1982).

26. S. Kuroda and H. Shirakawa, Solid State Commun., 43, 591 (1982).

27. W. H. Meyer, Synthetic Met., 4, 81 (1981).

28. G. Leising, E. Faulques, and S. Lefrant, Synthetic Met., 11, 123 (1985).

29. H. Kahlert and G. Leising, Mol. Cryst. Liq. Cryst., 117, 1 (1985).

30. G. Leising, R. Uitz, B. Ankele, W. Ottinger, and F. Stelzer, Mol. Cryst. Liq. Cryst., 117, 327 (1985).

31. M. Ozaki, Y. Ikeda, and T. Arakawa, J. Polym. Sci., Pol. Lett., 21, 989 (1983).

32. T. Woerner, A. G. MacDiarmid, A. Feldblum, A. J. Heeger, J. Polym. Sci., Pol. Lett., 22, 119 (1984).

33. Y. Yamashita, S. Nishimura, K. Shimamura, and K. Monobe, Makromol. Chem., 187, 1757 (1986).

34. K. Araya, A. Mukoh, T. Narahara, and H. Shirakawa, Proceedings of Symposium on Molecular Structure, Nagoya, 326 (1984).

35. K. Araya, A. Mukoh, T. Narahara, and H. Shirakawa, Chem. Lett., 1141 (1984).

36. K. Araya, A. Mukoh, T. Narahara, and H. Shirakawa, Synthetic Met., 14, 199 (1986).

37. K. Araya, A. Mukoh, T. Narahara, K. Akagi, and H. Shirakawa, Synthetic Met., 17, 247 (1987).

38. R. H. Baughman, S. L. Hsu, G. P. Pez, and A. J. Signorelli, J. Chem. Phys., 68, 5405 (1978).

39. T. Akaishi, K. Miyasaka, K. Ishikawa, H. Shirakawa, and S. Ikeda, Rep. Prog. Polym. Phys. Jpn., 22, 125 (1979).

40. C. R. Fincher, Jr., C.-E. Chen., A. J. Heeger, A. G. MacDiarmid, and J. B. Hastings, Phys. Rev. Lett., 48, 100 (1982).

41. R. H. Baughman, B. E. Kohler, I. J. Levy, and C. Spangler, Synthetic Met., 11, 37 (1985).

42. H. Kahlert, O. Leitner, and G. Leising, Synthetic Met., 17, 467 (1987).

43. G. Liesser, G. Wegner, W. Müller, V. Enkelmann, and W. H. Meyer, Makromol. Chem.-Rapid, 1, 627 (1980).

44. K. Shimamura, F. E. Karasz, J. A. Hirsch, and J. C. W. Chien, Makromol. Chem.-Rapid, 2, 473 (1981).

45. K. Shimamura, F. E. Karasz, J. C. W. Chien, and J. A. Hirsh, Makromol. Chem.-Rapid, 3, 369 (1982).

46. J. C. W. Chien, F. E. Karasz, and K. Shimamura, Macromolecules, 15, 1012 (1982).

47. F. S. Bates and G. L. Baker, Macromolecules, 16, 1013 (1983).

48. D. White and D. C. Bott, Polym. Commun., 25, 98 (1984).

49. G. Leising, Polym. Commun., 25, 201 (1984).

50. M. Stamm, J. Hocker, and A. Axmann, Mol. Cryst. Liq. Cryst., 77, 125 (1981).

51. C. Riekel, H. W. Hässlin, K. Menke, and S. Roth, J. Chem. Phys., 77, 4254 (1982).

52. C. S. Yannoni and T. C. Clarke, Phys. Rev. Lett., 51, 1191 (1983).

53. F. Sondheimer, D. A. Ben-Efraim, and R. Wolovsky, J. Am. Chem. Soc., 83, 1675 (1961).

54. H. Eckhardt, J. Chem. Phys., 79, 2085 (1983).

55. J. Norris and J. W. White, Chem. Phys. Lett., 102, 534 (1983).

56. H. W. Gibson, R. J. Weagley, W. M. Prest, Jr., R. Mosher, and S. Kaplan, J. Phys. Colloq., 44, C3-123 (1983).

57. H. W. Gibson, S. Kaplan, R. A. Mosher, W. M. Prest, Jr., and R. J. Weagley, J. Am. Chem. Soc., 22, 6843 (1986).

58. I. Harada, M. Tasumi, H. Shirakawa, and S. Ikeda, Chem. Lett., 1411 (1978).

59. S. Lefrant, L. S. Lichtmann, H. Temkin, D. B. Fitchen, D. C. Miller, G. E. Whitwell II, and J. M. Burlitch, Solid State Commun., 29, 191 (1979).

60. L. S. Lichtmann, D. B. Fitchen, and H. Temkin, Synthetic Met., 1, 139 (1979/1980).

61. H. Kuzmany, Phys. Status Solidi, B, 97, 521 (1980).

62. I. Harada, Y. Furukawa, M. Tasumi, H. Shirakawa, and S. Ikeda, J. Chem. Phys., 73, 4746 (1980).

63. D. B. Fichen, Mol. Cryst. Liq. Cryst., 83, 95 (1982).

64. S. Lefrant, E. Faulques, L. Lauchlan, M. J. Kletter, and S. Etemad, Mol. Cryst. Liq. Cryst., 83, 117 (1982).

65. P. Knoll, H. Kuzmany, P. Surjan, and M. Kertesz, J. Phys. Colloq., 4, C3-155 (1983).

66. S. Lefrant, J. Phys. Colloq., 44, C3-247 (1983).

67. L. S. Lichtmann, E. A. Imhoff, A. Sarhangi, and D. B. Fitchen, J. Chem. Phys., 81, 168 (1984).

68. D. Gill, R. G. Kilponen, and L. Rimai, Chem. Phys. Lett., 8, 634 (1971).

69. L. Rimai, M. E. Heyde, and D. Gill, J. Am. Chem. Soc., 95, 4493 (1973).

70. Y. Furakawa, T. Arakawa, H. Takeuchi, I. Harada, and H. Shirakawa, J. Chem. Phys., 81, 2907 (1984).

71. A. Baruya, D. L. Gerrard, and W. F. Maddams, Macromolecules, 16, 578 (1983).

72. M. Hatano, S. Kambara, and S. Okamoto, J. Polym. Sci., 51, S26 (1961).

73. D. J. Berets and D. S. Smith, Trans. Faraday Soc., 64, 823 (1968).

74. H. Shirakawa, T. Ito, and S. Ikeda, Makromol. Chem., 179, 1565 (1978).

75. A. Snow, P. Brant, D. Weber, and N.-L. Yang, J. Polym. Sci., Pol. Lett., 17, 263 (1979).

76. J. C. W. Chien, F. E. Karasz, G. E. Wnek, A. G. MacDiarmid, and A. J. Heeger, J. Polym. Sci., Pol. Lett., 18, 45 (1980).

77. P. Bernier, M. Rolland, C. Linaya, and M. Disi, Polymer, 21, 7 (1980).

78. I. B. Goldberg, H. R. Crowe, P. R. Newman, A. J. Heeger, and A. G. MacDiarmid, J. Chem. Phys., 70, 1132 (1979).

79. B. R. Weinberger, E. Ehrenfreund, A. Pron, A. J. Heeger, and A. G. MacDiarmid, J. Chem. Phys., 72, 4849 (1980).

80. M. Nechtschein, F. Devreaux, R. L. Greene, T. C. Clarke, G. B. Street, Phys. Rev. Lett., 44, 356 (1980).

81. W. P. Su, J. R. Schrieffer, and A. J. Heeger, Phys. Rev. Lett., 42, 1698 (1979).

82. M. J. Rice, Phys. Lett., 71A, 152 (1979).

83. H. Takayama, Y. R. Lin-liu, and K. Maki, Phys. Rev. B, 21, 2388 (1980).

84. W. P. Su, J. R. Schrieffer, and A. J. Heeger, Phys. Rev. B, 22, 2099 (1980).

85. J. Orenstein and G. L. Baker, Phys. Rev. Lett., 49, 1043 (1982).

86. Z. Vardeny, J. Strait, D. Moses, T.-C. Chung, and A. J. Heeger, Phys. Rev. Lett., 49, 1657 (1982).

87. C. V. Shank, R. Yen, R. L. Fork, J. Orenstein, and G. L. Baker, Phys. Rev. Lett., 49, 1661 (1982).

88. Z. Vardeny, J. Orenstein, and G. L. Baker, J. Phys. Colloq., 44, C3-325 (1983).

89. J. Orenstein, G. L. Baker, and Z. Vardeny, J. Phys. Colloq., 44, C3-407 (1983).

90. Z. Vardeny, J. Orenstein, and G. L. Baker, Phys. Rev. Lett., 50, 2032 (1983).

91. G. B. Blanchet, C. R. Fincher, T. C. Chung, and A. J. Heeger, Phys. Rev. Lett., 50, 1938 (1983).

92. G. B. Blanchet, C. R. Fincher, and A. J. Heeger, Phys. Rev. Lett., 51, 2132 (1983).

93. Z. Vardeny, J. Tanaka, H. Fujimoto, and M. Tanaka, Solid State Commun., 50, 937 (1984).

94. R. Dorsinville, S. Krimchansky, R. R. Alfano, J. L. Birman, R. Tubino, and G. Dellepiane, Solid State Commun., 56, 857 (1985).

95. Z. Vardeny, E. Ehrenfreund, O. Brafman, B. Horovitz, H. Fujimoto, J. Tanaka, and M. Tanaka, Phys. Rev. Lett., 57, 2995 (1986).

96. J. D. Flood, E. Ehrenfreund, A. J. Heeger, and A. G. MacDiarmid, Solid State Commun., 44, 1055 (1982).

97. J. D. Flood and A. J. Heeger, Phys. Rev. B, 28, 2356 (1983).

98. F. Moraes, Y. W. Park, and A. J. Heeger, Synthetic Met., 13, 113 (1986).

99. H. Naarmann and N. Theophilou, Synthetic Met., 22, 1 (1987).

100. C. K. Chiang, Y. W. Park, A. J. Heeger, H. Shirakawa, E. J. Louis, and A. G. MacDiarmid, J. Chem. Phys., 69, 5098 (1978).

101. Y. W. Park, A. Denenstein, C. K. Chiang, A. J. Heeger, and A. G. MacDiarmid, Solid State Commun., 29, 747 (1979).

102. J. F. Kwak, T. C. Clarke, R. L. Greene, and G. B. Street, Solid State Commun., 31, 355 (1979).

103. Y. W. Park, A. J. Heeger, M. A. Druy, and A. G. MacDiarmid, J. Chem. Phys., 73, 946 (1980).

104. B. R. Weinberger, J. Kaufer, A. J. Heeger, A. Pron, and A. G. MacDiarmid, Phys. Rev. B, 20, 223 (1979).

105. S. Ikehata, J. Kaufer, T. Woerner, A. Pron, M. A. Druy, A. Sivak, A. J. Heeger, and A. G. MacDiarmid, Phys. Rev. Lett., 45, 1123 (1980).

106. F. Moraes, J. Chen, T.-C. Chung, and A. J. Heeger, Synthetic Met., 11, 271 (1985).

107. C. R. Fincher, Jr., D. L. Peebles, A. J. Heeger, M. A. Druy, Y. Matsumura, A. G. MacDiarmid, H. Shirakawa, and S. Ikeda, Solid State Commun., 27, 489 (1978).

108. C. R. Fincher, Jr., M. Ozaki, M. Tanaka, D. Peebles, L. Lauchlan, A. J. Heeger, and A. G. MacDiarmid, Phys. Rev. B, 20, 1589 (1979).

109. M. Tanaka, A. Watanabe, and J. Tanaka, Bull. Chem. Soc. Jpn., 53, 645 (1980).

110. M. Tanaka, A. Watanabe, and J. Tanaka, Bull. Chem. Soc. Jpn., 53, 3430 (1980).

111. H. Kiess, D. Baeriswyl, and G. Harbeke, Mol. Cryst. Liq. Cryst., 77, 147 (1981).

112. S. L. Hsu, A. J. Signorelli, G. P. Pez, and R. H. Baughman, J. Chem. Phys., 69, 106 (1978).

113. R. H. Baughman, N. S. Murthy, G. G. Miller, and L. W. Shacklette, J. Chem. Phys., 79, 1065 (1983).

114. R. H. Baughman, N. S. Murthy, and G. G. Miller, J. Chem. Phys., 79, 515 (1983).

115. C. R. Fincher, Jr., M. Ozaki, A. J. Heeger, and A. G. MacDiarmid, Phys. Rev. B, 19, 4140 (1979).

116. J. F. Rabolt, T. C. Clarke, and G. B. Street, J. Chem. Phys., 71, 4614 (1979).

117. S. I. Yaniger, S. M. Riseman, T. Frigo, and E. M. Eyring, J. Chem. Phys., 76, 4298 (1982).

118. J. F. Rabolt, T. C. Clarke, and G. B. Street, J. Chem. Phys., 76, 5781 (1982).

119. B. Francois, M. Bernard, and J. J. Andre, J. Chem. Phys., 75, 4142 (1981).

120. S. M. Riseman, S. I. Yaniger, E. M. Eyring, D. Macinnes, A. G. MacDiarmid, and A. J. Heeger, Appl. Spectrosc., 35, 557 (1981).

121. Y. Furukawa, I. Harada, M. Tasumi, H. Shirakawa, and S. Ikeda, Chem. Lett., 1489 (1981).

122. E. Faulques, S. Lefrant, F. Rachdi, and P. Bernier, Synthetic Met., 9, 53 (1984).

123. S. Lefrant, E. Faulques, F. Rachdi, and P. Bernier, Mol. Cryst. Liq. Cryst., 117, 377 (1985).

124. H. Eckhardt, L. W. Shacklette, J. S. Szobota, and R. H. Baughman, Mol. Cryst. Liq. Cryst., 117, 401 (1985).

125. S. Lefrant, P. Bernier, R. B. Kaner, and A. G. MacDiarmid, Mol. Cryst. Liq. Cryst., 121, 233 (1985).

126. J. Tanaka, Y. Saito, M. Chimizu, C. Tanaka, and M. Tanaka, Bull. Chem. Soc. Jpn., 60, 1595 (1987).

127. I. Harada, Y. Furukawa, M. Tasumi, H. Shirakawa, and S. Ikeda, Proc. VIIth Int. Conf. Raman Spectrosc., 144 (1980).

128. B. Schügerl and H. Kuzmany, Phys. Status Solidi B, 111, 607 (1982).

129. A. Feldblum, A. J. Heeger, T.-C. Chung, and A. G. MacDiarmid, J. Chem. Phys., 77, 5114 (1982).

130. K. Tanaka, K. Yoshizawa, K. Ohzeki, and T. Yamabe, Solid State Commun., 45, 391 (1983).

131. D. M. Hoffman, H. W. Gibson, A. J. Epstein, and D. B. Tanner, Phys. Rev. B, 27, 1454 (1983).

132. P. Meisterle, H. Kuzmany, and G. Nauer, Phys. Rev. B, 29, 6008 (1984).

133. Y. Tomkiewicz, T. D. Schultz, H. B. Broom, T. C. Clarke, and G. B. Street, Phys. Rev. Lett., 43, 1532 (1979).

134. G. Masetti, E. Campani, G. Gorini, L. Piseri, R. Tubino, P. Piaggio, and G. Dellepiane, Solid State Commun., 55, 737 (1985).

135. E. Faulques, E. Rzepka, S. Lefrant, E. Mulazzi, G. P. Brivio, and G. Leising, Phys. Rev. B, 33, 8622 (1986).

136. M. R. Bunow and I. W. Levin, Biochim. Biophys. Acta, 464, 202 (1977).

137. H. Okamoto, S. Saito, H. Hamaguchi, M. Tasumi, and C. H. Engsten, J. Raman Spectrosc., 15, 331 (1984).

138. E. J. Mele, Solid State Commun., 44, 827 (1982).

139. H. Eckhardt, S. W. Steinhauser, R. R. Chance, M. Schott, and R. Silbey, Solid State Commun., 55, 1075 (1985).

140. R. G. Snyder, J. Mol. Spectrosc., 4, 3605 (1960).

141. R. F. Schaufele and T. Shimanouchi, J. Chem. Phys., 47, 3605 (1967).

142. H. Takeuchi, T. Arakawa, Y. Furukawa, I. Harada, and H. Shirakawa, J. Mol. Struct., 158, 179 (1987).

143. F. Inagaki, M. Tasumi, and T. Miyazawa, J. Raman Spectrosc., 3, 335 (1975).

144. M. Tasumi, J. Raman Spectrosc., 13, 202 (1982).

145. G. Zannoni and G. Zerbi, J. Mol. Struct., 100, 485 (1983).

146. E. J. Mele, Mol. Cryst. Liq. Cryst., 77, 25 (1981).

147. L. Piseri, R. Tubino, L. Paltrinieri, and G. Dellepiane, Solid State Commun., 46, 183 (1983).

148. H. Takeuchi, Y. Furukawa, I. Harada, and H. Shirakawa, J. Chem. Phys., 80, 2925 (1984).

149. H. Takeuchi, Y. Furukawa, I. Harada, and H. Shirakawa, J. Chem. Phys., 84, 2882 (1986).

150. H. Takeuchi and I. Harada, J. Chem. Phys., 85, 1707 (1986).

151. J. R. Scherer and J. Overend, Spectrochim. Acta, 17, 719 (1961).

152. J. R. Scherer, J. C. Evans, W. W. Muelder, and J. Overend, Spectrochim. Acta, 18, 57 (1962).

153. T. Shimanouchi, H. Matsuura, Y. Ogawa, and I. Harada, J. Phys. Chem. Ref. Data, 7, 1323 (1978).

154. C. La Lau and R. G. Synder, Spectrochim. Acta, 27A, 2073 (1971).

155. C. A. Coulson and H. C. Longuet-Higgins, Proc. R. Soc. London, Ser. A, 193, 456 (1948).

156. R. J. Elliot, J. A. Krumhansl, and P. L. Leath, Rev. Mod. Phys., 46, 465 (1974).

157. T. Arakawa, Y. Furukawa, H. Takeuchi, I. Harada, and H. Shirakawa, Chem. Lett., 1637 (1984).

158. L. J. Bellamy, The Infrared Spectra of Complex Molecules, Wiley, New York, 1954.

159. H. W. Gibson, R. J. Weagley, R. A. Mosher, S. Kaplan, W. M. Prest, Jr., and A. J. Epstein, Mol. Cryst. Liq. Cryst., 117, 315 (1985).

160. H. W. Gibson, R. J. Weagley, R. A. Mosher, S. Kaplan, W. M. Prest, Jr., and A. J. Epstein, Phys. Rev. B, 31, 2338 (1985).

161. G. Leising, Polym. Bull., 11, 401 (1984).

162. P. Piaggio, G. Dellepiane, L. Piseri, R. Tubino, and C. Taliani, Solid State Commun., 50, 947 (1984).

163. C. Castiglioni, G. Zerbi and M. Gussoni, Solid State Commun., 56, 863 (1985).

164. G. Leising, H. Kahlert, and O. Leitner, in Electronic Properties of Polymers and Related Compounds, (H. Kuzmany, M. Mehring, and S. Roth, eds.), Springer-Verlag, Berlin, 1985, p. 56.

165. A. Maconnachie, A. J. Dianoux, H. Shirakawa, and M. Tasumi, Synthetic Met., 14, 323 (1986).

166. K. Soga, S. Kawakami, H. Shirakawa, and S. Ikeda, Makromol. Chem.-Rapid, 1, 643 (1980).

167. L. S. Lichtmann, A. Sarhangi, and D. B. Fitchen, Solid State Commun., 36, 869 (1980).

168. S. Lefrant and M. Aldissi, J. Phys., 44, 235 (1983).

169. Y. Furukawa, I. Harada, and H. Shirakawa, unpublished data.

170. E. R. Lippincott and T. E. Kenny, J. Am. Chem. Soc., 84, 3641 (1962).

171. H. Kuzmany, E. A. Imhoff, D. B. Fitchen, and A. Sarhangi, Mol. Cryst., Liq. Cryst., 77, 197 (1981).

172. S. Lefrant, E. Faulques, L. Lauchlan, M. J. Kletter, and S. Etemad, Mol. Cryst. Liq. Cryst., 83, 117 (1982).

173. L. Lauchlan, S. Etemad, T.-C. Chung, A. J. Heeger, and A. G. MacDiarmid, Phys. Rev. B, 24, 3701 (1981).

174. E. A. Imhoff, D. B. Fitchen, and R. E. Stahlbush, Solid State Commun., 44, 329 (1982).

175. K. Yoshino, S. Hayashi, T. Sakai, Y. Inuishi, H. Kato, and Y. Watanabe, Jpn. J. Appl. Phys., 21, L653 (1982).

176. K. Yoshino, S. Hayashi, Y. Inuishi, K. Hattori, and Y. Watanabe, Solid State Commun., 46, 583 (1983).

177. D. B. Fitchen, Synthetic Met., 9, 341 (1984).

178. W. Siebrand and M. Z. Zgierski, J. Chem. Phys., 81, 185 (1984).

179. F. Kajzar, S. Etemad, G. L. Baker, and J. Messier, Synthetic Met., 17, 563 (1987).

180. M. Galtier, M. Charbonnel, A. Montaner, and J. L. Ribet, Polymer, 25, 1253 (1984).

181. M. Galtier, C. Benoit, and A. Montaner, Mol. Cryst. Liq. Cryst., 83, 109 (1982).

182. H. Teramae, T. Yamabe, and A. Imamura, J. Chem. Phys., 81, 3564 (1984).

183. P. Piaggio, G. Dellepiane, R. Tubino, L. Piseri, G. Zannoni, G. Zerbi, and G. Lugli, J. Mol. Struct., 115, 193 (1984).

184. G. Bechtold, L. Genzel, and S. Roth, Solid State Commun., 53, 1 (1985).

185. M. Traetteberg, Acta Chem. Scand., 22, 2294 (1968).

186. C. Castiglioni, J. T. Lopez Navarrete, G. Zerbi, and M. Gussoni, Solid State Commun., 65, 625 (1988).

187. I. Harada, Y. Furukawa, T. Arakawa, H. Takeuchi, and H. Shirakawa, Mol. Cryst. Liq. Cryst., 117, 335 (1985).

188. E. Faulques and S. Lefrant, J. Phys. Colloq., 44, C3-337 (1983).

189. H. Shirakawa, private communication.

190. R. C. Teitelbaum, S. L. Ruby, and T. J. Marks, J. Am. Chem. Soc., 100, 3215 (1978).

191. K. Nakamoto, Infrared and Raman Spectra of Inorganic and Coordination Compounds, Wiley-Interscience, CITY, 1986.

192. G. Tourillon and F. Garnier, J. Electroanal. Inf., 135, 173 (1982).

193. K. Kaneto, K. Yoshino, and Y. Inuishi, Jpn. J. Appl. Phys., 21, L567 (1982).

194. K. Kaneto, Y. Kohno, K. Yoshino, and Y. Inuishi, J. Chem. Soc., Chem. Commun., 382 (1983).

195. K. Kaneto, K. Yoshino, and Y. Inuishi, Solid State Commun., 46, 389 (1983).

196. S. Hotta, T. Hosaka, and W. Shimotsuma, Synthetic Met., 6, 69 (1983).

197. R. J. Waltman, J. Bargon, and A. F. Diaz, J. Phys. Chem., 87, 1459 (1983).

198. M. Gazard, J. C. Dubois, M. Champagne, F. Garnier, and G. Tourillon, J. Phys., 44, C3-537 (1983).

199. S. Tanaka, M. Sato, and K. Kaeriyama, Makromol. Chem., 185, 1295 (1984).

200. M. Sato, S. Tanaka, and K. Kaeriyama, J. Chem. Soc., Chem. Commun., 713 (1985).

201. Y. Cao, P. Wang, and R. Qian, Makromol. Chem., 186, 1093 (1985).

202. M. Sato, S. Tanaka, and K. Kaeriyama, Synthetic Met., 14, 279 (1986).

203. K. Tanaka, T. Shichiri, and T. Yamabe, Synthetic Met., 16, 207 (1986).

204. M. Ito, H. Shioda, and K. Tanaka, J. Polym. Sci., Pol. Lett., 24, 147 (1986).

205. T.-C. Chung, J. H. Kaufman, A. J. Heeger, and F. Wudl, Phys. Rev. B, 30, 702 (1984).

206. J. Roncali, F. Garnier, M. Lemaire, and R. Garreau, Synthetic Met., 15, 323 (1986).

207. Y. Yumoto and S. Yoshimura, Synthetic Met., 13, 185 (1986).

208. S. Hotta, T. Hosaka, and W. Shimotsuma, Synthetic Met., 6, 317 (1983).

209. G. Dian, G. Barbey, and B. Decroix, Synthetic Met., 13, 281 (1986).

210. M. Sato, S. Tanaka, and K. Kaeriyama, J. Chem. Soc., Chem. Commun., 873 (1986).

211. M. Sato, S. Tanaka, and K. Kaeriyama, Synthetic Met., 18, 229 (1987).

212. S. Hotta, S. D. D. V. Rughooputh, A. J. Heeger, and F. Wudl, Macromolecules, 20, 212 (1987).

213. K. Kaneto, S. Ura, K. Yoshino, and Y. Inuishi, Jpn. J. Appl. Phys., 23, L189 (1984).

214. S. Hotta, T. Hosaka, M. Soga, and W. Shimotsuma, Synthetic Met., 9, 381 (1984).

215. M. Akimoto, Y. Furukawa, H. Takeuchi, I. Harada, Y. Soma, and M. Soma, Synthetic Met., 15, 353 (1986).

216. J.-E. Österholm and P. Passiniemi, Synthetic Met., 18, 213 (1987).

217. T. Yamamoto, K. Sanechika, and A. Yamamoto, J. Polym. Sci. Pol. Lett., 18, 9 (1980).

218. J. W-P. Lin and L. P. Dudek, J. Polym. Sci., Pol. Chem., 18, 2869 (1980).

219. T. Yamamoto, K. Sanechika, and A. Yamamoto, Bull. Chem. Soc. Jpn., 56, 1497 (1983).

220. M. Kobayashi, J. Chen, T.-C. Chung, F. Moraes, A. J. Heeger, and F. Wudl, Synthetic Met., 9, 77 (1984).

221. J. P. Montheard, T. Pascal, G. Seytre, G. Steffan-boiteux, and A. Douillard, Synthetic Met., 9, 389 (1984).

222. K.-Y. Jen, G. G. Miller, and R. L. Elsenbaumer, J. Chem. Soc., Chem. Commun., 1346 (1986).

223. G. Kossmehl and G. Chatzitheodorou, Makromol. Chem.-Rapid, 2, 551 (1981).

224. G. Kossmehl and G. Chatzitheodorou, Mol. Cryst. Liq. Cryst., 83, 291 (1982).

225. G. Kossmehl and G. Chatzitheodorou, Makromol. Chem.-Rapid, 4, 639 (1983).

226. T. Yamamoto, K. Sanechika, and A. Yamamoto, Bull. Chem. Soc. Jpn., 56, 1503 (1983).

227. Y. Cao, Q. Wu, K. Guo, and R. Qian, Makromol. Chem., 185, 389 (1984).

228. G. Tourillon and F. Garnier, J. Polym. Sci., Pol. Phys., 22, 33 (1984).

229. G. Tourillon and F. Garnier, Mol. Cryst. Liq. Cryst., 121, 349 (1985).

230. S. Hotta, T. Hosaka, M. Soga, and W. Shimotsuma, Synthetic Met., 10, 95 (1984/85).

231. S. Hotta, T. Hosaka, and W. Shimotsuma, J. Chem. Phys., 80, 954 (1984).

232. F. Devreux, G. Bidan, A. A. Syed, and C. Tsintavis, J. Phys., 46, 1595 (1985).

233. J.-E. Østerholm, P. Sunila, and T. Hjertberg, Synthetic Met., 18, 169 (1987).

234. H. Neugebauer, G. Nauer, A. Neckel, G. Tourillon, F. Garnier, and P. Lang, J. Phys. Chem., 88, 652 (1984).

235. S. Hotta, T. Hosaka, M. Soga, and W. Shimotsuma, Synthetic Met., 9, 87 (1984).

236. Z. Mo, K.-B. Lee, Y. B. Moon, M. Kobayashi, A. J. Heeger, and F. Wudl, Macromolecules, 18, 1972 (1985).

237. T.-C. Chung, J. H. Kaufman, A. J. Heeger, and F. Wudl, Mol. Cryst., Liq. Cryst., 118, 205 (1985).

238. J. Chen, A. J. Heeger, and F. Wudl, Solid State Commun., 58, 251 (1986).

239. K. Kaneto, Y. Kohno, and Y. Yoshino, Solid State Commun., 51, 267 (1984).

240. K. Kaneto, Y. Kohno, and K. Yoshino, Mol. Cryst. Liq. Cryst., 118, 217 (1985).

241. K. Kaneto, S. Hayashi, S. Ura, and K. Yoshino, J. Phys. Soc. Jpn., 54, 1146 (1985).

242. K. Kaneto and K. Yoshino, Synthetic Met., 18, 133 (1987).

243. G. Tourillon, D. Gourier, P. Garnier, and D. Vivien, J. Phys. Chem., 88, 1049 (1984).

244. G. Harbeke, E. Meier, W. Kobel, M. Egli, H. Kiess, and E. Tosatti, Solid State Commun., 55, 419 (1985).

245. S. Hasegawa, K. Kamiya, J. Tanaka, and M. Tanaka, Synthetic Met., 18, 225 (1987).

246. M. J. Nowak, S. D. D. V. Rughooputh, S. Hotta, and A. J. Heeger, Macromolecules, 20, 965 (1987).

247. S. D. D. V. Rughooputh, M. Nowak, S. Hotta, A. J. Heeger, and F. Wudl, Synthetic Met., 21, 41 (1987).

248. J. L. Brédas, B. Thémans, J. G. Fripiat, J. M. André, and R. R. Chance, Phys. Rev. B, 29, 6761 (1984).

249. J. L. Brédas, F. Wudl, and A. J. Heeger, Solid State Commun., 63, 577 (1987).

250. C. Yong and W. Renyuan, Solid State Commun., 54, 211 (1985).

251. Y. Furukawa, M. Akimoto, and I. Harada, Synthetic Met., 18, 151 (1987).

252. C. Taliani, R. Danieli, R. Zamboni, P. Ostoja, and W. Porzio, Synthetic Met., 18, 177 (1987).

253. H. Neugebauer, A. Neckel, G. Nauer, N. Brinda-Konopik, F. Garnier, and G. Tourillon, J. Phys., 44, C10-517 (1983).

254. S. Hotta, W. Shimotsuma, and M. Taketani, Synthetic Met., 10, 85 (1984/85).

255. F. Moraes, H. Schaffer, M. Kobayashi, A. J. Heeger, and F. Wudl, Phys. Rev., B, 30, 2948 (1984).

256. Z. Vardeny, E. Ehrenfreund, O. Brafman, M. Nowak, H. Schaffer, A. J. Heeger, and F. Wudl, Phys. Rev. Lett., 56, 671 (1986).

257. A. Ivaska, J.-E. Osterholm, P. Passiniemi, P. Kuivalainen, H. Isotalo, and H. Stubb, Synthetic Met., 21, 215 (1987).

258. G. Tourillon and F. Garnier, J. Phys. Chem., 87, 2289 (1983).

259. S. Hotta, W. Shimotsuma, M. Taketani, and S. Kohiki, Synthetic Met., 11, 139 (1985).

260. E. F. Steigmeier, H. Auderset, W. Kobel, and D. Baeriswyl, Synthetic Met., 18, 219 (1987).

261. F. P. Hochgesang, Molecular Structure and Spectroscopy of Thiophene and its Derivatives, in H. D. Hartough (ed.), Thiophene and Its Derivatives, Interscience, New York, 1952, Ch. IV, pp. 81-141.

262. G. J. Visser, G. J. Heeres, J. Wolters, and A. Vos, Acta Crystallogr. B, 24, 467 (1968).

263. D. W. Scott, J. Mol. Spectrosc., 31, 451 (1969).

264. Y. Soma, M. Soma, Y. Furukawa, and I. Harada, Clay Miner., 35, 53 (1987).

265. A. F. Diaz, K. K. Kanazawa, and G. P. Gardini, J. Chem. Soc., Chem. Commun., 635 (1979).

266. K. K. Kanazawa, A. F. Diaz, R. H. Geiss, W. D. Gill, J. F. Kwak, J. A. Logan, J. F. Rabolt, and G. B. Street, J. Chem. Soc., Chem. Commun., 854 (1979).

267. K. K. Kanazawa, A. F. Diaz, W. D. Gill, P. M. Grant, G. B. Street, G. P. Gardini, and J. F. Kwak, Synthetic Met., 1, 329 (1979/1980).

268. K. K. Kanazawa, A. F. Diaz, M. T. Krounbi, and G. B. Street, Synthetic Met., 4, 119 (1981).

269. A. Watanabe, M. Tanaka, and J. Tanaka, Bull. Chem. Soc. Jpn., 54, 2278 (1981).

270. G. B. Street, T. C. Clarke, M. Krounbi, K. K. Kanazawa, V. Lee, P. Pfluger, J. C. Scott, and G. Weiser, Mol. Cryst. Liq., Cryst., 83, 253 (1982).

271. M. Salmon, A. F. Diaz, A. J. Logan, M. Krounbi, and J. Bargon, Mol. Cryst. Liq. Cryst., 83, 265 (1982).

272. G. B. Street, T. C. Clarke, R. H. Geiss, V. Y. Lee, A. Nazzal, P. Pfluger, and J. C. Scott, J. Phys. Colloq., 44, C3-599 (1983).

273. F. Devreux, F. Genoud, M. Nechtschein, J. P. Travers, and G. Bidan, J. Phys. Colloq., 44, C3-621 (1983).

274. S. Hotta, T. Hosaka, and W. Shimotsuma, Synthetic Met., 6, 319 (1983).

275. J. P. Travers, P. Audebert, and G. Bidan, Mol. Cryst. Liq. Cryst., 118, 149 (1985).

276. M. Ogasawara, K. Funahashi, and K. Iwata, Mol. Cryst. Liq. Cryst., 118, 159 (1985).

277. M. Ogasawara, K. Funahashi, T. Demura, T. Hagiwara, and K. Iwata, Synthetic Met., 14, 61 (1986).

278. W. Wernet, M. Monkenbusch, and G. Wegner, Makromol. Chem.-Rapid, 5, 157 (1984).

279. K. Hyodo and A. G. MacDiarmid, Synthetic Met., 11, 167 (1985).

280. X. Bi, Y. Yao, M. Wan, P. Wang, K. Xiao, W. Yang, and R. Qian, Makromol. Chem., 186, 1101 (1985).

281. M. Satoh, K. Kaneto, and Y. Inuishi, Jpn. J. Appl. Phys., 24, L423 (1985).

282. M. Satoh, K. Kaneto, and K. Yoshino, Synthetic Met., 14, 289 (1986).

283. R. Qian, J. Qiu, and D. Shen, Synthetic Met., 18, 13 (1987).

284. B. Kaye and A. E. Underhill, Synthetic Met., 18, 31 (1987).

285. M. Takakubo, Synthetic Met., 18, 53 (1987).

286. Y. Shen, K. Carneiro, C. Jacobsen, R. Qian, and J. Qiu, Synthetic Met., 18, 77 (1987).

287. S. Kuwabata, K. Okamoto, O. Ikeda, and H. Yoneyama, Synthetic Met., 18, 101 (1987).

288. S. Dong and J. Ding, Synthetic Met., 20, 119 (1987).

289. A. F. Diaz and J. I. Castillo, J. Chem. Soc., Chem. Commun., 397 (1980).

290. O. Inganäs, R. Erlandsson, C. Nylander, and I. Lundström, J. Phys. Chem. Solids, 45, 427 (1984).

291. A. F. Diaz, J. Castillo, K. K. Kanazawa, J. A. Logan, M. Salmon, and O. Fajardo, J. Electroanal. Ch. Inf., 133, 233 (1982).

292. P. Auderbert and G. Bidan, Mol. Cryst. Liq. Cryst., 118, 187 (1985).

293. H. Lindenberger, D. Schäfer-Siebert, S. Roth, and M. Hanack, Synthetic Met., 18, 37 (1987).

294. P. Kovacic, I. Khoury, and R. L. Elsenbaumer, Synthetic Met., 6, 31 (1983).

295. O. Niwa and T. Tamamura, J. Chem. Soc., Chem. Commun., 817 (1984).

296. M.-A. De Paoli, R. J. Waltman, A. F. Diaz, and J. Bargon, J. Chem. Soc., Chem. Commun., 1015 (1984).

297. M.-A. De Paoli, R. J. Waltman, A. F. Diaz, and J. Bargon, J. Polym. Sci. Pol. Lett., 23, 1687 (1985).

298. S. E. Lindsey and G. B. Street, Synthetic Met., 10, 67 (1984/1985).

299. O. Niwa, M. Hikita, and T. Tamamura, Makromol. Chem.-Rapid, 6, 375 (1985).

300. S. J. Jasne and C. K. Chiklis, Synthetic Met., 15, 175 (1986).

301. A. I. Nazzal and G. B. Street, J. Chem. Soc., Chem. Commun., 83 (1984).

302. A. I. Nazzal, G. B. Street, and K. J. Wynne, Mol. Cryst. Liq. Cryst., 125, 303 (1985).

303. G. B. Street, S. E. Lindsey, A. I. Nazzal, and K. J. Wynne, Mol. Cryst. Liq. Cryst., 118, 137 (1985).

304. Y. Furukawa, S. Tazawa, Y. Fujii, and I. Harada, Synthetic Met., 24, 329 (1988).

305. A. F. Diaz, J. Crowley, J. Bargon, G. P. Gardini, and J. B. Torrance, J. Electroanal. Ch. Inf., 121, 355 (1981).

306. K. Yakushi, L. J. Lauchlan, T. C. Clarke, and G. B. Street, J. Chem. Phys., 79, 4774 (1983).

307. K. Yakushi, L. J. Lauchlan, G. B. Street, and J. L. Brédas, J. Chem. Phys., 81, 4133 (1984).

308. P. Pfluger, M. Krounbi, G. B. Street, and G. Weiser, J. Chem. Phys., 78, 3212 (1983).

309. J. L. Brédas, J. C. Scott, K. Yakushi, and G. B. Street, Phys. Rev. B, 30, 1023 (1984).

310. J. H. Kaufman, N. Colaneri, J. C. Scott, and G. B. Street, Phys. Rev. Lett., 53, 1005 (1984).

311. J. C. Scott, J. L. Brédas, K. Yakushi, P. Pfluger, and G. B. Street, Synthetic Met., 9, 165 (1984).

312. E. M. Genies and J.-M. Pernaut, J. Electroanal. Ch. Inf., 191, 111 (1985).

313. J. C. Scott, P. Pfluger, M. T. Krounbi, and G. B. Street, Phys. Rev. B, 28, 2140 (1983).

314. F. Genoud, M. Guglielmi, M. Nechtschein, E. Genies, and M. Salmon, Phys. Rev. Lett., 55, 118 (1985).

315. M. Nechtschein, F. Devreux, F. Genoud, E. Vieil, J. M. Pernaut, and E. Genies, Synthetic Met., 15, 59 (1986).

316. F. Devreux, F. Genoud, M. Nechtschein, and B. Villeret, Synthetic Met., 18, 89 (1987).

317. L. Oddi, R. Capelletti, R. Fieschi, M. P. Fontana, G. Ruani, V. Bocchi, and G. P. Gardini, Mol. Cryst. Liq. Cryst., 118, 179 (1985).

318. S. J. Hahn, W. J. Gajda, P. O. Vogelhut, and M. V. Zeller, Synthetic Met., 14, 89 (1986).

319. K. M. Chenung, B. J. E. Smith, D. N. Batchelder, and D. Bloor, Synthetic Met., 21, 249 (1987).

320. T. Inoue, I. Hosoya, and T. Yamase, Chem. Lett., 563 (1987).

321. J. L. Brédas, B. Thémans, and J. M. André, Phys. Rev. B, 27, 7827 (1983).

322. J. L. Brédas, B. Thémans, J. M. André, R. R. Chance, and R. Silbey, Synthetic Met., 9, 265 (1984).

323. R. de Surville, M. Jozefowicz, L. T. Yu, J. Perichon, and R. Buvet, Electrochim. Acta, 13, 1451 (1968).

324. M. Jozefowicz, L. T. Yu, J. Perichon, and R. Buret, J. Polym. Sci. C, 22, 1187 (1969).

325. M. Doriomedoff, F. Hautière-Cristofini, R. de Surville, M. Jozefowicz, L. T. Yu, and R. Buvet, J. Chim. Phys., 68, 1055 (1971).

326. A. Kitani, J. Izumi, J. Yano, Y. Hiromoto, and K. Sasaki, Bull. Chem. Soc. Jpn., 57, 2254 (1984).

327. A. G. MacDiarmid, J.-C. Chiang, M. Halpern, W.-S. Huang, S.-L. Mu, N. L. D. Somasiri, W. Wu, and S. I. Yaniger, Mol. Cryst. Liq. Cryst., 121, 173 (1985).

328. W. R. Salaneck, B. Liedberg, O. Inganäs, R. Erlandsson, I. Lundström, A. G. MacDiarmid, M. Halpern, and N. L. D. Somasiri, Mol. Cryst. Liq. Cryst., 121, 191 (1985).

329. J. P. Travers, J. Chroboczek, F. Devreux, F. Genoud, M. Nechtschein, A. Syed, E. M. Genies, and C. Tsintavis, Mol. Cryst. Liq. Cryst., 121, 195 (1985).

330. A. G. MacDiarmid, J.-C. Chiang, W. Huang, B. D. Humphrey, and N. L. D. Somasiri, Mol. Cryst. Liq. Cryst., 125, 309 (1985).

331. E. W. Paul, A. J. Ricco and M. S. Wrighton, J. Phys. Chem., 89, 1441 (1985).

332. P. M. McManus, S. C. Yang, and R. J. Cushman, J. Chem. Soc., Chem. Commun., 1556 (1985).

333. J.-C. Chiang and A. G. MacDiarmid, Synthetic Met., 13, 193 (1986).

334. Y. Furukawa, T. Hara, Y. Hyodo, and I. Harada, Synthetic Met., 16, 189 (1986).

335. Y. Cao, S. Li, Z. Xue, and D. Guo, Synthetic Met., 16, 305 (1986).

336. S. K. Brahma, Solid State Commun., 57, 673 (1986).

337. A. G. MacDiarmid, J. C. Chiang, A. F. Richter, and A. J. Epstein, Synthetic Met. 18, 285 (1987).

338. A. J. Epstein, J. M. Ginder, F. Zuo, R. W. Bigelow, H.-S. Woo, D. B. Tanner, A. F. Richter, W.-S. Huang, and A. G. MacDiarmid, Synthetic Met., 18, 303 (1987).

339. M. Nechtschein, C. Santier, J. P. Travers, J. Chroboczek, A. Alix, and M. Ripert, Synthetic Met., 18, 311 (1987).

340. T. Hagiwara, T. Demura, and K. Iwata, Synthetic Met., 18, 317 (1987).

341. M. Angelopoulos, A. Ray, A. G. MacDiarmid, and A. J. Epstein, Synthetic Met., 21, 21 (1987).

342. A. J. Epstein, J. M. Ginder, F. Zuo, H.-S. Woo, D. B. Tanner, A. F. Richter, M. Angelopoulos, W.-S. Huang, and A. G. MacDiarmid, Synthetic Met., 21, 63 (1987).

343. J. P. Travers and N. Nechtschein, Synthetic Met., 21, 135 (1987).

344. B. Lundberg, W. R. Salaneck, and I. Lundström, Synthetic Met., 21, 143 (1987).

345. Ph. Snauwaert, R. Lazzaroni, J. Riga, and J. J. Verbist, Synthetic Met., 21, 181 (1987).

346. F. Wudl, R. O. Angus, Jr., F. L. Lu, P. M. Allemand, D. J. Vachon, M. Nowak, Z. X. Liu, and A. J. Heeger, J. Am. Chem. Soc., 109, 3677 (1987).

347. W. W. Focke, G. E. Wnek, and Y. Wei, J. Phys. Chem., 91, 5813 (1987).

348. J. M. Ginder, A. F. Richter, A. G. MacDiarmid, and A. J. Epstein, Solid State Commun., 63, 97 (1987).

349. Y. W. Park, Y. S. Lee, C. Park, L. W. Shacklette, and R. H. Baughman, Solid State Commun., 1063 (1987).

350. Y. Furukawa, F. Ueda, Y. Hyodo, I. Harada, T. Nakajima, and T. Kawagoe, Macromolecules, 21, 1297 (1988).

351. W. R. Salaneck, I. Lundström, W.-S. Huang, and A. G. MacDiarmid, Synthetic Met., 13, 291 (1986).

352. K. Okabayashi, F. Goto, K. Abe, and T. Yoshida, Synthetic Met., 18, 365 (1987).

353. A. G. MacDiarmid, S.-L. Mu, N. L. D. Somasiri, and W. Wu, Mol. Cryst. Liq. Cryst., 121, 187 (1985).

354. E. M. Genies, A. A. Syed, and C. Tsintavis, Mol. Cryst. Liq. Cryst., 121, 181 (1985).

355. E. M. Genies, J.-M. Pernaut, C. Santier, A. A. Syed, and C. Tsintavis, Springer Series Solid-State Science, 63, 211 (1985).

356. M. Ogawa, T. Fuse, T. Kita, T. Kawagoe and T. Matsunaga, Proceedings of the 27th Battery Symposium in Japan, Ohsaka, 197 (1986).

357. T. Nakajima, S. Toyosawa, K. Suzuki, T. Miyazaki, T. Kitamura, T. Kawagoe, Jpn. Patent Pub. No. 62-149724 (1987).

358. A. G. MacDiarmid, L. S. Yang, W. S. Huang, and B. D. Humphrey, Synthetic Met., 18, 393 (1987).

359. A. F. Diaz and J. A. Logan, J. Electroanal. Ch. Inf., 111, 111 (1980).

360. B. Wang, J. Tang, and F. Wang, Synthetic Met., 13, 329 (1986).

361. W.-S. Huang, B. D. Humphrey, and A. G. MacDiarmid, J. Chem. Soc. Farad., 1, 82

362. B. Wang, J. Tang, and F. Wang, Synthetic Met., 18, 323 (1987).

363. S.-A. Chen and T.-S. Lee, J. Polym. Sci., Pol. Lett., 25, 455 (1987).

364. T. Ohsaka, Y. Ohnuki, N. Oyama, G. Katagiri, and K. Kamisako, J. Electroanal. Ch. Int., 161, 399 (1984).

365. H. Kuzmany, E. M. Genies, and A. Syed, Springer Series Solid-State Science, 63, 223 (1985).

366. T. Nakajima, S. Toyosawa, T. Kawagoe, T. Kita, and T. Matsunaga, Proceedings of the 27th Battery Symposium in Japan, Ohsaka, 193 (1986).

367. M. Ohira, T. Sakai, M. Takeuchi, Y. Kobayashi, and M. Tsuji, Synthetic Met., 18, 347 (1987).

368. H. Kuzmany and N. S. Sariciftci, Synthetic Met., 18, 353 (1987).

369. R. Holze, J. Electroanal. Ch. Int., 224, 253 (1987).

370. N. S. Sariciftci and H. Kuzmany, Synthetic Met., 21, 157 (1987).

371. D. Bloor and A. Monkman, Synthetic Met., 21, 175 (1987).

372. T. Kobayashi, H. Yoneyama, and H. Tamura, J. Electroanal. Ch. Inf., 161, 419 (1984).

373. T. Kobayashi, H. Yoneyama, and H. Tamura, J. Electroanal. Inf., 177, 281 (1984).

374. T. Kobayashi, H. Yoneyama, and H. Tamura, J. Electroanal. Ch. Inf., 177, 293 (1984).

375. W. R. Salaneck, I. Lundström, B. Liedberg, M. A. Hasan, R. Erlandsson, P. Konradsson, A. G. MacDiarmid, and N. L. D. Somasiri, Springer Series Solid-State Science, 63, 218 (1985).

376. E. M. Genies and M. Lapkowski, J. Electroanal. Ch. Inf., 220, 67 (1987).

377. E. M. Genies and M. Lapkowski, Synthetic Met., 21, 117 (1987).

378. F. Devreux, G. Bidan, A. A. Syed, and C. Tsintavis, J. Phys., 46, 1595 (1985).

379. T. Hjertberg, W. R. Salaneck, I. Lundstrom, N. L. D. Somasiri, and A. G. MacDiarmid, J. Polym. Sci., Pol. Lett., 23, 503 (1985).

380. T. Hjertberg, M. Sandberg, O. Wennerström, and I. Lagerstedt, Synthetic Met., 21, 31 (1987).

381. S. H. Glarum and J. H. Marshall, J. Phys. Chem., 90, 6076 (1986).

382. M. Kaya, A. Kitani, and K. Sasaki, Chem. Lett., 147 (1986).

383. P. Snauwaert, R. Lazzaroni, J. Riga, and J. J. Verbist, Synthetic Met., 16, 245 (1986).

384. W. R. Salaneck, I. Lundström, T. Hjertberg, C. B. Duke, E. Conwell, A. Paton, A. G. MacDiarmid, N. L. D. Somasiri, W. S. Huang, and A. F. Richter, Synthetic Met., 18, 291 (1987).

385. P. Snauwaert, R. Lazzaroni, J. Riga, and J. J. Verbist, Synthetic Met., 18, 335 (1987).

386. T. Nakajima and T. Kawagoe, Proceedings of Symposium on Molecular Structure, Kanazawa, 354 (1987).

387. E. M. Genies and C. Tsintavis, J. Electroanal. Ch. Inf., 195, 109 (1985).

388. E. M. Genies and C. Tsintavis, J. Electroanal. Ch. Inf., 200, 127 (1986).

389. A. Kitani, M. Kaya, J. Yano, K. Yoshikawa, and K. Sasaki, Synthetic Met., 18, 341 (1987).

390. N. Mermilliod, J. Tanguy, M. Hoclet, and A. A. Syed, Synthetic Met., 18, 359 (1987).

391. J. Heinze, J. Mortensen, and K. Hinkelmann, Synthetic Met., 21, 209 (1987).

392. G. E. Wnek, Synthetic Met., 15, 213 (1986).

393. D. Vachon, R. O. Angus, Jr., F. L. Lu, M. Nowak, Z. X. Liu, H. Schaffer, F. Wudl, and A. J. Heeger, Synthetic Met., 18, 297 (1987).

394. K. Nakanishi and P. H. Solomon, Infrared Absorption Spectroscpy, 2nd ed., Holden-Day, San Francisco, 1977.

395. A. Perrier-Datin and J.-M. Lebas, J. Chim. Phys. PCB, 69, 591 (1972).

396. F.-L. Lu, F. Wudl, M. Nowak, and A. J. Heeger, J. Am. Chem. Soc., 108, 8311 (1986).

397. J. R. Platt, J. Chem. Phys., 17, 484 (1949).

398. L. D. Ziegler and B. S. Hudson, J. Chem. Phys., 79, 1134 (1983).

399. R. P. Rava and T. G. Spiro, J. Phys. Chem., 89, 1856 (1985).

400. K. Machida, H. Lee, and A. Kuwae, J. Raman Spectrosc., 9, 198 (1980).

401. H. Linschitz, J. Rennert, and T. M. Korn, J. Am. Chem. Soc., 76, 5839 (1954).

402. G. E. Wnek, Synthetic Met., 15, 213 (1986).

403. P. Kovacic and A. Kyriakis, J. Am. Chem. Soc., 85, 454 (1963).

404. P. Kovacic and J. Oziomek, J. Org. Chem., 29, 100 (1964).

405. P. Kovacic and J. Oziomek, Macromol. Synth., 2, 23 (1966).

406. T. Yamamoto and A. Yamamoto, Chem. Lett., 353 (1977).

407. T. Yamamoto, Y. Hayashi, and A. Yamamoto, Bull. Chem. Soc., Jpn., 51, 2091 (1978).

408. M. Satoh, K. Kaneto, and K. Yoshino, J. Chem. Soc., Chem. Commun., 1629 (1985).

409. M. Satoh, M. Tabata, F. Uesugi, K. Kaneto, and K. Yoshino, Synthetic Met., 17, 595 (1987).

410. D. M. Ivory, G. G. Miller, J. M. Sowa, L. W. Shaklette, R. R. Chance, and R. H. Baughman, J. Chem. Phys., 71, 1506 (1979).

411. L. W. Shaklette, R. R. Chance, D. M. Ivory, G. G. Miller, and R. H. Baughman, Synthetic Met., 1, 307 (1979).

412. L. W. Shacklette, H. Eckhardt, R. R. Chance, G. G. Miller, D. M. Ivory, and R. H. Baughman, J. Chem. Phys., 73, 4098 (1980).

413. P. Kovacic, M. B. Feldman, J. P. Kovacic, and J. B. Lando, J. Appl. Polym. Sci., 12, 1735 (1968).

414. P. Pradere, A. Boudet, J.-Y. Goblot, G. Froyer, and F. Maurice, Mol. Cryst. Liq. Cryst., 118, 277 (1985).

415. B. Tieke, Ch. Bubeck, and G. Lieser, Makromol. Chem.-Rapid, 3, 261 (1982).

416. B. Tieke, Ch. Bubeck, and G. Lieser, J. Phys. Colloq., 44, C3-753 (1983).

417. G. Froyer, J. Y. Goblot, J. L. Guilbert, F. Maurice, and Y. Pelous, J. Phys. Collow., 44, C3-745 (1983).

418. S. Krichene, S. Lefrant, G. Froyer, F. Maurice, and Y. Pelous, J. Phys. Collow., 44, C3-733 (1983).

419. Z. Iqbal, H. Bill, and R. H. Baughman, J. Phys. Collow., 44, C3-761 (1983).

420. Y. Soma, M. Soma, and I. Harada, Chem. Phys. Lett., 99, 153 (1983).

421. Y. Soma, M. Soma, and I. Harada, J. Phys. Chem., 88, 3034 (1984).

422. S. Krichene, J. P. Buisson, and S. Lefrant, Synthetic Met., 17, 589 (1987).

423. S. Krichene, S. Lefrant, Y. Pelous, G. Froyer, M. Petit, A. Digua, and J. F. Fauvarque, Synthetic Met., 17, 607 (1987).

424. J. P. Buisson, S. Krichene, and S. Lefrant, Synthetic Met., 21, 229 (1987).

425. D. Raković, I. Božović, S. A. Stepanyan, and L. A. Gribov, Solid State Commun., 43, 127 (1982).

426. G. Zannoni and G. Zerbi, J. Chem. Phys., 82, 31 (1985).

427. I. Božović and D. Raković, Phys. Rev. B, 32, 4235 (1985).

428. D. Raković, I. Božović, L. A. Gribov, S. A. Stepanyan, and V. A. Dementiev, Synthetic Met., 17, 613 (1987).

429. M. Peo, S. Roth, K. Dransfeld, B. Tieke, J. Hocker, H. Gross, A. Grupp, and H. Sixl, Solid State Commun., 35, 119 (1980).

430. L. D. Kispert, J. Joseph, G. G. Miller, and R. H. Baughman, Mol. Cryst., Liq. Cryst., 118, 313 (1985).

431. J. F. Rabolt, T. C. Clarke, K. K. Kanazawa, J. R. Reynolds, and G. B. Street, J. Chem. Soc., Chem. Commun., 347 (1980).

432. R. R. Chance, L. W. Shacklette, G. G. Miller, D. M. Ivory, J. M. Sowa, R. L. Elsenbaumer, and R. H. Baughman, J. Chem. Soc., Chem. Commun., 348 (1980).

433. L. W. Shacklette, R. L. Elsenbaumer, R. R. Chance, H. Eckhardt, J. E. Frommer, and R. H. Baughman, J. Chem. Phys., 75, 1919 (1981).

434. R. L. Elsenbaumer, L. W. Shacklette, J. W. Sowa, and R. H. Baughman, Mol. Cryst. Liq. Cryst., 83, 229 (1982).

435. T. C. Clarke, K. K. Kanazawa, V. Y. Lee, J. F. Rabolt, J. R. Reynolds, and G. B. Street, J. Polym. Sci., Pol. Phys., 20, 117 (1982).

436. L. D. Kispert, L. A. Files, J. E. Frommer, L. W. Shacklette, and R. R. Chance, J. Chem. Phys., 78, 4858 (1983).

437. I. Murase, T. Ohnishi, T. Noguchi, and M. Hirooka, Polym. Commun., 25, 327 (1984).

438. I. Murase, T. Ohnishi, T. Noguchi, and M. Hirooka, and S. Murakami, Mol. Cryst. Liq. Cryst., 118, 333 (1985).

439. D. D. C. Bradley, G. P. Evans, and R. H. Friend, Synthetic Met., 17, 651 (1987).

440. I. Murase, T. Ohnishi, T. Noguchi, and M. Hirooka, Synthetic Met., 17, 639 (1987).

441. D. D. C. Bradley, R. H. Friend, and W. J. Feast, Synthetic Met., 17, 645 (1987).

442. A. J. Heeger, S. Kivelson, J. R. Schriefer, and W.-P. Su, Rev. Mod. Phys., 60, 781 (1988).

443. G. Zerbi, Adv. Appl. FTIR Spectrosc., (M. W. Mackenzie, ed.), Wiley, New York, 1988, pp. 247-322.

444. D. N. Batchelder, Optical Techniques to Characterize Polymer Systems, (H. Bässler, ed.), Elsevier, Amsterdam, 1989, pp. 393-427.

445. Proceedings of the International Conference on Science and Technology of Synthetic Metals (ICSM 1988), Vols. A-F, published in Synthetic Met., 27-29, (1989).